Controlling the Mechanical and Transport Properties of Layer-by-Layer Films and Electrospun Mat Composite Membranes for Fuel Cell Applications

by

David ShinRen Liu

B.S. Chemical Engineering
California Institute of Technology (2007)

SUBMITTED TO THE DEPARTMENT OF CHEMICAL ENGINEERING IN PARTIAL FULFILLMENT OF THE REQUIREMENTS FOR THE DEGREE OF

DOCTOR OF PHILOSOPHY IN CHEMICAL ENGINEERING
AT THE
MASSACHUSETTS INSTITUTE OF TECHNOLOGY
[JUNE 2014]
MAY 2014

Signature redacted

Signature of Author .....
David S. Liu
Department of Chemical Engineering
May 27, 2014

Signature redacted

Certified by: .....
Paula T. Hammond
David H. Koch (1962) Professor in Engineering
Thesis Supervisor

Signature redacted

Accepted by.....
Patrick S. Doyle
Professor of Chemical Engineering
Chairman, Committee for Graduate Students

Controlling the Mechanical and Transport Properties of Layer-by-Layer Films and Electrospun Mat Composite Membranes for Fuel Cell Applications

by

David ShinRen Liu

Submitted to the Department of Chemical Engineering on May 27, 2014,
in partial fulfillment of the requirements for the degree of
Doctor of Philosophy in Chemical Engineering

Abstract

There is an ever increasing need for clean, portable energy devices, such as fuel cells and high energy batteries to replace or reduce the world's dependence on fossil fuels. The continued development of thin-film solid polymer electrolytes with improved mechanical and ion transport properties is critical for the further advancement of such electrochemical energy devices. For hydrogen and methanol fuel cells, the proton exchange membrane (PEM) has to have high protonic conductivity, low fuel crossover, and be mechanically and chemically stable. In particular, for direct methanol fuel cells and for high temperature (>100 °C), low relative humidity (< 60% RH) hydrogen fuel cells, the current industrial standard PEM, Nafion®, does not have all the required attributes.

Layer-by-Layer (LbL) assembly allows for the controlled deposition of alternating polyelectrolytes at the nanometer scale. This technique can be used with highly proton conductive water soluble polymers as well as doped polymers. In addition, LbL assembly can be used to coat a variety of substrates of various shapes and sizes. An LbL system composed of poly(diallyl dimethyl ammonium chloride) (PDAC) and sulfonated poly(2,6-dimethyl 1,4-phenylene oxide) (sPPO) has shown to have relatively high proton conductivity and very low methanol permeability compared to that of Nafion®, but lacking in mechanical strength when hydrated and losing significant proton conductivity at lower RH conditions.

Herein this thesis work describes the selection, optimization, and utilization of multilayer systems and system composites as the PEM in hydrogen and methanol fuel cells, focusing on improving and understanding the improvements to the properties of layer-by-layer films and composite membranes for fuel cell applications by targeting two main areas: the mechanical properties and the conductive properties. In addition, characterization and film analysis work was done to correlate and explain how the changing of the LbL system and fabrication techniques impacted the membrane's mechanical and conductive properties.

First, the mechanical strength and stability were greatly improved by spray-assembling the films on an electrospun fiber mat to form a composite membrane. Spray-LbL assembly was performed both with and without vacuum assistance, which had complementary effects on the film properties. By combining these techniques, composite membranes with methanol permeability twenty times lower than Nafion® and through-plane proton selectivity five times greater than Nafion® were fabricated. In addition, the planar swelling of the composite membranes in water was significantly reduced. This large reduction in swelling is hypothesized to be due to the electrostatic interaction of the LbL system with the underlying electrospun fibers and would not occur in a typical polymer blend.

Second, to improve the conductivity of the LbL films overall and specifically at lower RH conditions, two approaches were used. In the first approach, divalent salts were added to the polyanion solution to provide a stronger shielding effect than monovalent salts. The divalent salts allowed for ion bridging and increased both the number and the mobility of protons associated with sulfonic acid groups in the LbL film; thus increasing the film's conductivity. Through optimization of salt type and concentration, the protonic conductivity of PDAC/sPPO films was increased fourfold, and the humidity dependence of the conductivity was decreased.

In the second approach, PDAC was replaced with a phosphoric-acid-doped polymer, poly(2-vinyl pyridine) (P2VP). The phosphoric acid concentration in the LbL film and the number of free sulfonic acid groups could be controlled post film fabrication by changing the concentration of the phosphoric acid dopant. The resulting P2VP/sPPO films exhibited greater conductivity than similarly doped P2VP films and under stronger doping conditions (0.4 M – 1.0 M phosphoric acid), the film's conductivity increases seventy-fivefold (110 mS/cm at 50% RH at room temperature), resulting in a conductivity an order of magnitude greater than Nafion®. The large increases in conductivity, particularly at low RH conditions further support a recently reported and very promising proton transport mechanism that utilizes both phosphoric and sulfonic acid groups.

Thesis Supervisor: Paula T. Hammond

Title: David H. Koch (1962) Professor in Engineering

Dedicated to my loving parents:

Isaac and Hannah Liu

Acknowledgements

"Life is a journey, not a destination." - Ralph Waldo Emerson. I would like to humbly augment Emerson and say that life is a journey with some landmarks that mark that journey. It is at this time I find myself at one such landmark – the completion of my doctorate – and in looking back, would like to take a moment to thank all the people that helped me along this journey without whom I would not be at such a destination.

First, I would like to thank Prof. Paula Hammond, my thesis advisor, for choosing me, many years ago, to work on this research project and to join her diverse research group and who, throughout these years, has supported and guided me through both the success and failures of research and has been the best advisor I could have hoped for. I also would like to thank my thesis committee members, Prof. Greg Rutledge and Dean Mary Boyce, for their guidance and encouragement over the last five years.

I'd also like to thank Prof. Rutledge specifically for the guidance provided during the composite membrane work and the opportunity to collaborate with a graduate student in his lab (since graduated), Matthew Mannarino. It was Matthew who made and characterized the electruspun mats that were then spray-LbL assembled by me. He also took many of the SEM images of the composite membrane mats and helped me characterize the composite mats – particularly their mechanical and swelling properties. In addition, many ideas of ways to further characterize and analyze the composite membranes came out of the discussions with Matthew. The composite work would not be possible without his contributions.

From the Hammond lab, I'd like to thank Avni and Nathan for their work in the sPPO/PDAC system as well as their mentorship to me early on teaching me many of the basics to LbL assembly and the sulfonation of PPO. I especially would like to thank Nicole Davis who was a co-synthesizer and co-user of sPPO with whom I shared many of the challenges and successes of my research and who has been a constant source of information and help. I would also like to thank the current and former members of the electrochemistry and solar subgroup – Jonathan Harding, Chibueze Amanchukwu, Noemie Dorval, Dr. Nasim Hyder, Po-Yen Chen, Jason Kovacs, Dr. Mariya Khiterer, Dr. Junying Liu, Dr. Brian Aitken, Dr. Julio D'Arcy, and Dr. Sun Hwa Lee – for their insights, advice, guidance, and help. I have been very fortunate to work with such a diverse, intelligent group of people. I would also like to thank my UROPs who were responsible for collecting many of the data used in this thesis – Sarah Rumbley, Marie Burkland, Brian Chmielowiec, Maya Hubbard, Diego Giraldez, and Clarissa Towle – and with whom I've been fortunate to work with and learn from.

Finally, I would like to thank the many friends and family who have supported me throughout my time at MIT. I would not have been able to finish my thesis without the constant and unwavering support of these ones. Specifically I'd like to make mention of the brothers in the brother's house where I've lived during my time at MIT, Peter and Rebecca Tsui who took me in for many weeks while I was writing my thesis, and the members of the Christians on Campus Club at MIT with whom I've shared many a meal and necessary breaks. Lastly, I'd like to thank my parents for their support throughout my entire education process.

Table of Contents

List of Figures

List of Tables

1. Introduction

1.1 Introductory Remarks - Motivation

In today's economy, energy plays a key role in everything we do and every sector of the economy, and its consumption per capita is directly linked to a country's GDP and wealth.[1] Yet, as it currently stands, this energy use, 85% of which is derived from fossil fuels such as coal, oil, and natural gas, is also the main contributor to climate change and global warming.[1-3] The same fossil fuels that have been cheap and abundant, and the main drivers of global development and prosperity are also the main culprits in increased CO_2 concentrations in the atmosphere in the past 250 years and subsequent warming of the earth.[4-6] Without any reduction in fossil fuel usage or CO_2 emissions, it has been estimated that CO_2 levels could reach 550 ppm by 2050 leading to a warming of at least 2 °C.[7] Subsequent increases in CO_2 levels after that would lead to a warming anywhere between 3 – 7 °C by 2100, resulting in the melting of the ice cap, rise in sea levels, and huge possible changes in global weather patterns – all of which would be extremely damaging to the world economy. There is therefore great interest in finding ways to reduce and eliminate CO_2 emissions by finding cheap alternative energy sources that don't produce greenhouse gasses or ways to capture and store the CO_2 emissions, preferably at the source.[8]

One of the most difficult and expensive areas to reduce/eliminate CO_2 emissions is in transportation where oil has been the fuel of choice and capturing CO_2 from individual vehicles impractical. One possible solution is the use of electric vehicles, with the electricity coming from a carbon neutral source: nuclear energy, renewable energy, or carbon sequestered coal or natural gas power plants. The main issue with using electric vehicles is its lack of range, slow rate of

charge, and high cost, all of which are fundamental limitations of batteries that are likely to stay even as technological improvements alleviate some of the issues.[9,10] Particularly, for larger vehicles like trucks or busses, purely electric vehicles will most likely never be practical. Thus there is a need to have an alternative to oil that emits no greenhouse gasses and can be produced without emitting greenhouse gasses. A very promising fuel alternative is hydrogen.[11]

Hydrogen is one of the most common elements on earth, though it is rarely in its pure state, and thus needs to be produced from other hydrogen containing compounds. It has a higher energy densitiy by mass (120 to 44.4 MJ/kg) compared to gasoline but a lower energy density by volume (89,960 to 31,170 MJ/m^3).[9] When used in a fuel cell, the amount of hydrogen, as measured in energy consumed, needed to travel a set distance is less than the amount of gasoline needed because fuel cells (40 – 60% energy efficient) are 1.6 – 2.4 times more efficient than internal combustion engines (~25% energy efficient).[9] In addition, any improvements in efficiency of cars by utilizing a battery hybrid can also be applied to hydrogen fuel cell cars.

For smaller devices where portability, long device life, and quiet operation is desired, a promising fuel alternative is methanol which when used in a fuel cell can provide over eight times the effective energy density of Li-ion rechargeable batteries. In addition, rechargeable batteries lose charge capacity over time and must never be fully discharged to preserve cycle longevity, further lowering its effective energy density. Thus the practical efficiency of rechargeable batteries, after taking into account the cycle constraints and the device space of all the internal components as well as loss of energy stored over time, is around 30% - 40% effective. For fuel cells, the practical efficiency is around 70% [12]. Thus in situations where recharging would be difficult and device weight an issue, for example during hiking or in a battlefield, direct methanol fuel cells (DMFCs) are considered a strong alternative to Li-ion

batteries in laptops and other portable energy devices. Even considering energy losses due to lack of optimization (compared with batteries that have been around for over 20 years), a first generation commercial DMFC should last over six times as long as current Li-ion batteries of the same size and weight.

1.2 Types and Components of a Fuel cell

A fuel cell is an electrochemical device that can convert the chemical energy of a fuel (i.e. hydrogen or methanol) directly into electricity with the use of a catalyst. There are five major types of fuel cells, as classified by the type of electrolyte they use: alkaline fuel cell, polymer electrolyte fuel cell (PEMFC), phosphoric acid fuel cell, molten carbonate fuel cell, and solid oxide fuel cell. The type of electrolyte also dictates the temperature range at which the associated fuel cell is ran: alkaline at room temp to 80 °C, PEMFC at 60-90 °C, phosphoric acid at 150- 200 °C, molten carbonate at 550 °C, and solid oxide at 900 °C. Despite the different electrolyte used, fuel cells typically have four main components, from the outside in: a charge collector on both the anode and cathode side, a fuel diffusion layer for both sides, a catalyst for the anode and cathode, and the electrolyte in the middle that connects the anode and cathode side. The different temperature range and type of electrolyte used also dictates the type of application each fuel cell is most suited for, with the lower temperature fuel cells more suited for smaller, more portable devices and the higher temperature fuel cells suited for large scale stationary devices.

Of particular interest for use in transportation and small devices is the PEMFC. It can be designed for either hydrogen gas (hydrogen fuel cell) or methanol liquid or gas (direct methanol

fuel cell (DMFC)) (see figure 1-1). The electrolyte for both the hydrogen fuel cells and the direct methanol fuel cell is the proton exchange membrane (PEM) and the catalyst used is typically platinum. The two main challenges that prevent PEMFCs from being commercialized are the catalyst and the PEM. Both play a crucial role in determining the power output from a fuel cell and the cost per watt and are also the two most active areas of research for fuel cells. The PEM must be chemically stable, have a high proton conductivity, low fuel permeability, and good mechanical stability, capable of sustaining hundreds to thousands of cycles. For the hydrogen fuel cells, there is a considerable interest in running the fuel cell at higher temperatures (100 -120 °C) to take advantage of improved catalyst kinetics at the higher temperature, minimize catalyst poisoning, and allow the use of less pure fuel streams.

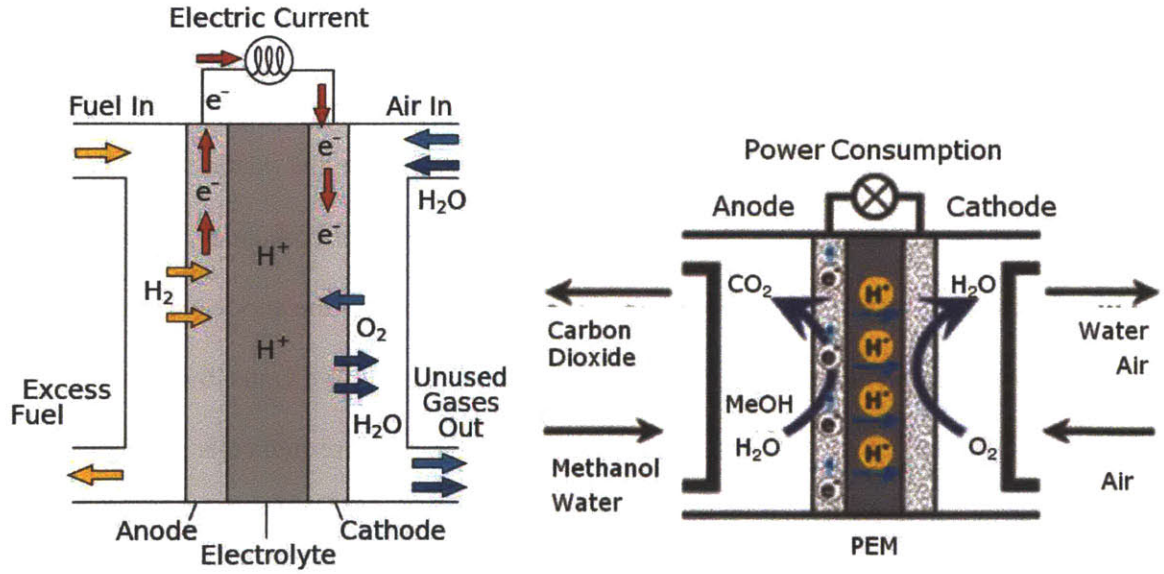

Figure 1-1. Schematic of a hydrogen fuel cell (left) and a direct methanol fuel cell (right) (http://en.wikipedia.org/wiki/File:Solid_oxide_fuel_cell_protonic.svg, http://www.nfcrc.uci.edu/3/FUEL_CELL_INFORMATION/FCexplained/FC_Types.aspx). The

fuel cell is composed of two charge collectors, two fuel diffusion layers, two catalyst layers and a PEM. The fuel diffusion layers, the catalyst layers, and the PEM together make up the membrane electrode assembly (MEA). The fuel (hydrogen or methanol) is oxidized at the anode, protons are transported across the PEM to the cathode, electrons are collected by the charge collectors and travel through the external circuit, and oxygen is reduced at the cathode generating water.

The current industrial standard for polymer electrolyte membranes operated between 25 °C – 80 °C is Dupont's Nafion, a copolymer of tetrafluoroethylene and perfluoro (4-methyl-3,6-dioxa-7-octene-1-sulfonic acid) (see figure 1-2). Nafion has been widely studied for its high conductivity (100 mS/cm at 25C at 100% relative humidity) combined with exceptional chemical and mechanical stability.[13] It benefits from a unique nanoporous channel structure that is lined with sulfate groups that provide the conducting pathways for protons. The channels are ~10 – 50 angstroms wide.[14] However, these same channels of Nafion that makes Nafion such a good conductor for protons also allows methanol to permeate through (Permeability = $2.8*10^{-6}$ cm^2/s) the membrane, thus poisoning the catalyst by competing with the oxygen on the cathode side and reducing the overall fuel cell performance. In addition, Nafion begins to deform and lose its mechanical stability above 100 °C.

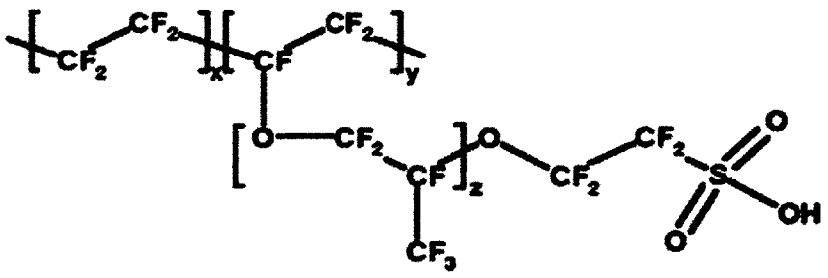

Figure 1-2. General chemical structure of Nafion (x~5-13.5, y~1000, z~1-3). The perfluorinated backbone and side chains give the polymer excellent stability while the sulfonic acid groups form nanoscale channels for rapid ion transport.

1.3 LbL assembly

Layer-by layer assembly (LbL) is a versatile thin-film processing technique that consists of the repeated, sequential electrostatic deposition of the complementary functionalized materials on a substrate [15,16]. Figure 1-3 shows a depiction of the layer-by-layer process. An inherently charged substrate is sequentially exposed to solutions of oppositely charged polymers, which adsorb to the existing film at rates that enable nanometer-scale control of film thickness [17]. As well, by adjusting assembly parameters such as pH and ionic strength, the composition, morphology, and bulk properties of the LbL film can be controlled. This technique has been adapted to many other platforms such as spraying, spin-assisted assembly, and roll-to-roll processing from the traditional dipping process.

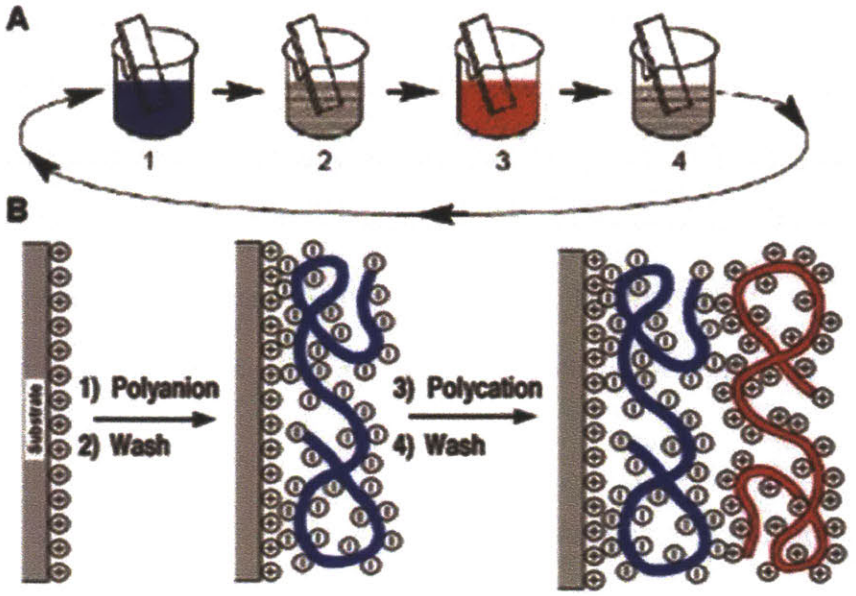

Figure 1-3. Depiction of layber-by-layer film deposition, adapted from Decher.[15] (A) Depicts the dip layer-by-layer process by which a charged substrate is alternatively dipped into negatively and positively charged polymer solutions. (B) Depicts the adsorption and charge reversal process of a polyelectrolyte being deposited onto an LbL film.

One advantage to the LbL technique is its ability to incorporate water soluble polymers into stable homogeneous films. This allows the use of highly sulfonated, high performance, aromatic polymers like sulfonated poly-p-phenylene (sPPP), sulfonated polyphenylene sulfide (sPPS), and sulfonated polyphenyleneoxide (sPPO) that would normally be soluble in water as components in our membranes. In their most conducting states (often greater than the 100 mS/cm of Nafion), the bulk versions of these polymers become highly water swollen and ultimately water soluble, making them unusable as membranes by themselves despite their great ionic properties. Other research groups have avoided this problem by using low degrees of sulfonation (~30%), but by doing so the conductivity of their membranes are compromised.[18] However, with the LbL technique we can utilize those highly sulfonated polymers (in fact it is

desirable to maximize their degrees of sulfonation) with its high conductivity as one of the two components in our LbL films. Because the LbL films are really homogeneous blends and not actually one distinct layer followed by another, just having one component being conductive is enough for the entire film to be conductive. In addition, because these are homogenous films, they have fairly low methanol permeation - on order of $1*10^{-8}$ cm^2/s which is approximately 100 times better than Nafion.[19] This make LbL a very promising and unique technique to use for making PEMs.

1.5 Thesis Objectives and Overview

In looking to the future, there is a need for robust PEMs that can block methanol while selectively allowing proton transport for DMFCs, and for PEMS to be sufficiently proton conducting at low RH conditions for more efficient hydrogen fuel cells. This thesis seeks to address that need by describing methods to improve the properties, mainly proton conductivity and mechanical robustness, of layer-by-layer films and composite membranes for fuel cell applications. The specific objectives in this work is as follows:

1) To mechanically strengthen the LbL films through the use of a supporting substrate – in this case an electrospun mat – and to make a functioning DMFC with the composite membrane.
2) To increase the proton conductivity of the PDAC/sPPO system through increasing the number of free protons in the LbL film and to explore the effect multivalent cation salts have when introduced in the polyanion solution during the LbL process.
3) To increase the proton conductivity of an LbL system at low relative humidity (50% RH) through the incorporation of an additional proton conducting group, phosphoric acid

doped pyridine, and to explore and utilize a proton conducting mechanism that is less susceptible to relative humidity than sulfonic acid based PEM's proton conducting mechanism.

Chapters 2 and 3 describe mechanically strengthening LbL films through the use of a supporting substrate,and the function of the resulting composite membranes in DMFCs. The PDAC/sPPO system, which has high conductivity and low methanol permeability, has been shown to be mechanically deficient when hydrated, preventing the use of the LbL film by itself as a PEM in a DMFC. This work utilizes various LbL-spray assembly techniques to fabricate an electrospun composite mat that is conductive to protons through the membrane that has reduced methanol permeability compared to Nafion, that is significantly more mechanically robust than the LbL film by itself, and that results in a viable fuel cell when used as a PEM in an electrode membrane assembly.

Chapter 4 explores the use of multivalent cation salts during LbL assembly to increase the proton conductivity of the PDAC/sPPO system by increasing the number of free protons present in the LbL films. Lab synthesized pristine sPPO at 90% degree of sulfonation has a conductivity of 600 mS/cm, but in an LbL system, the conductivity is more than an order of magnitude lower as a significant portion of the sulfonate groups in the sPPO are ionically crosslinked to the quaternary amine groups in the PDAC. NaCl has been used previously to shield the charged groups during the LbL assembly process, to change the film growth characteristics of the system, and to increase the conductivity of the PDAC/sPPO system. Multivalent salts can also cause the charge shielding effects of monovalent salts, but in addition, the multivalent salts have the ability to form ion-bridges between charged groups. Also

described is the use of a new depth profiling technique to determine the chemical composition of the LbL films as a result of the use of multivalent salts.

Chapter 5 describes a method to increase the proton conductivity of an LbL system at low relative humidity (50% RH) through the incorporation of an additional proton conducting group, phosphoric acid doped pyridine, and explores the proton conducting mechanism of this new membrane material. Sulfonic acid based PEMs (like PDAC/sPPO) lose a significant portion of their conductivity as the RH in the air decreases (loss of conductivity over two orders of magnitude for hydrocarbon based PEMs and over one order of magnitude for fluorocarbon based PEMs when RH is reduced by 40%). The new hydrocarbon based LbL system described herein loses just half an order of magnitude in conductivity when RH is reduced by 40% and demonstrates conductivity above 100 mS/cm at 50% RH.

1.6 References

[1] Bozoglan, E., Midilli, A., Hepbasli, A., *Energy*, **2012**, *46*, 85-93.

[2] Balta, M.T., Dincer, I., Hepbasli, A., *Int. J. Hydrogen Energy*, **2009**, *34*, 2925-2939.

[3] Dincer, I., *Renew. Sus. Energy Reviews*, **2000**, *4*, 157-175.

[4] Wang, H.Z., Leung, D.Y.C., Leung, M.K.H., Ni, M., *Renew. Sus. Energy Reviews*, **2009**, *13*, 845-853.

[5] Brouwer, J., *Current Applied Physics*, **2009**, *10*, S9-S17.

[6] Elder, R., Allen, R., *Progress in Nuclear Energy*, **2009**, *51*, 500-525.

[7] Haszeldine, R.S., *Science*, **2009**, *325*, 1647-1652.

[8] Orhan, M.F., Dincer, I., Rosen, M.A., Kanoglu, M., *Renew. Sus. Energy Reviews*, **2012**, *16*, 6059-6082.

[9] Armaroli, N., Balzani, V., *ChemSusChem*, **2011**, *4*, 21-36.

[10] Petri, M.C., Yildiz, B., Klickman, A.E., *Int. J. of Nuc. Hydrogen Prod.*, **2006**, *1*, 79-91.

[11] Marban, G., Valdes-Solis, T., *Int. J. of Hydrogen Energy*, **2007**, *32*, 1625-1637.

[12] Winter, M., Brodd, R.J., *Chem. Rev.* **2004**, *104*, 4245-4269

[13] Banerjee, S, Curtin, D.E., *J Flourine Chem*, **2004**, *125*, 1211

[14] Moore, R. B., Mauritz, K. A., *Chem Rev.*, **2004**, *104*, 4535-4585

[15] Dercher, *Science*, **1997**, *277*, 1232-1237.

[16] Lutkenhaus, J.T., Hammond, P. T., *Soft Matter*, **2007**, *3*, 804

[17] Hammond, P.T., *Adv. Mater.*, **2004**, *16*, 1271-1293.

[18] Xu, T., Wu D., Wu., L., *Progress in Polymer Science*, **2008**, *33*, 894-915.

[19] Argun, A.A., Ashcraft, J.N., Hammond, P.T., *Adv. Mater.*, **2008**, *20*, 1539-1543.

2. Spray Layer-by-Layer Electrospun Composite Proton Exchange Membranes

Portions of this chapter are reproduced from David S. Liu, J. Nathan Ashcraft, Matthew M. Mannarino, Meredith N. Silberstein, Avni A. Argun, Gregory C. Rutledge, Mary C. Boyce, and Paula T. Hammond, *Advanced Functional Materials*. **2013**, *23*, 3087-3095.

Abstract

Polymer electrolyte films are deposited onto highly porous electrospun mats using layer-by-layer (LbL) processing to fabricate composite proton conducting membranes. By simply changing the assembly conditions for generation of the LbL film on the nanofiber mat substrate, we can achieve three different and unique composite film morphologies in which the electrospun mats provide mechanical support; the LbL assembly produces highly conductive films that coat the mats in a controlled fashion, separately providing the ionic conductivity and fuel blocking characteristics of the composite membrane. Coating an electrospun mat with the LbL dipping process produces composite membranes with "webbed" morphologies that link the fibers in-plane and give the composite membrane in-plane proton conductivities similar to that of the pristine LbL system. In contrast, coating an electrospun mat using the spray-LbL process without vacuum produces a uniform film that bridges across all of the pores of the mat. These membranes have methanol permeability similar to free-standing poly(diallyl dimethyl ammonium chloride)/sulfonated poly(2,6-dimethyl 1,4-phenylene oxide) (PDAC/sPPO) thin

films. Coating an electrospun mat with the vacuum-assisted spray-LbL process produces composite membranes with conformally coated fibers throughout the bulk of the mat with nanometer control of the coating thickness on each fiber. The mechanical properties of the LbL-coated mats display composite properties, exhibiting the strength of the glassy PDAC/sPPO films when dry and the properties of the underlying electrospun polyamide mat when hydrated. By combining the different spray-LbL fabrication techniques with electrospun fiber supports and tuning the parameters, mechanically stable membranes with high selectivity can be produced, potentially for use in fuel cell applications.

2.1 Introduction

The development of thin solid polymer electrolytes with improved performance is critical for the advancement of electrochemical energy devices.[1] In recent years, considerable interest has been focused on designing chemically and mechanically stable membranes while maintaining high ionic conductivity with low fuel cross-over.[2] For hydrogen and direct-methanol fuel cells, membranes comprising perfluorosulfonic acid polymers such as Nafion have been used because they exhibit superior protonic conductivity with relatively high mechanical integrity and chemical stability, despite their high cost.[3] However, even the perfluorosulfonic acid polymers have shown limited device lifetimes due to chemical and mechanical degradation.[4-8] One of the main causes of membrane failure is the poor dimensional stability, caused by repeated swelling/deswelling of the membrane in a fuel cell from the cycling of temperature and humidity, which has been shown to mechanically weaken the membrane after only a few hundred cycles.[9-12] Typically, to improve the membrane's mechanical properties,

the ionomer (Nafion) is incorporated into dimensionally stable supporting matrices such as expanded polytetrafluoroethylene (ePTFE).[4,13-16] Other researchers have tried incorporating carbon nanotubes, metal oxides, and zirconium phosphates into Nafion matrices to improve lifetime or cell performance.[17-19]

The difficulty with these bulk composites is the lack of control of composition on the micron scale and the continued reliance on Nafion, with its high cost and relatively high fuel crossover, in particular for methanol. A promising approach is to combine two relatively new processing techniques, layer-by-layer (LbL) assembly of polymer thin films and electrospinning of fiber mats. LbL assembly is an extremely versatile nano-scale fabrication technique that allows for the conformal coating of any wettable substrate with a combination of two or more polymers possessing complementary interactions, e.g. oppositely charged functional groups.[20-22] The films are generated through the alternating adsorption of polyanions and polycations, and can be further tuned by adjusting the pH or adding salt to the polymer solutions during assembly, with typical thickness per bilayer ranging from a few nanometers to over a hundred nanometers. Argun, Ashcraft et al. recently reported LbL-based proton exchange membranes (PEMs) with high performance in hydrogen and direct methanol fuel cells.[23,24] In particular, the LbL system composed of poly(diallyl dimethyl ammonium chloride) (PDAC) and sulfonated poly(2,6-dimethyl 1,4-phenylene oxide) (sPPO), structures shown in Figure 1a, yielded the highest protonic conductivity of any LbL assembled system, as high as 70 mS cm^{-1}, which is on the order of Nafion's conductivity, with methanol permeability values less than one hundredth that of Nafion;[25] However, these LbL-based PEMs are not sufficiently strong when hydrated and require a reinforcing mechanical substrate.

An interesting class of materials for reinforcing LbL membranes is the electrospun fiber mat. Electrospun mats are non-woven, highly porous materials with high surface-to-volume ratios and small pore sizes relative to other fibrous materials.[26-29] A wide range of polymers can be formed into electrospun mats, and the fiber diameters can be varied during fabrication over a wide range (0.1 – 10 μm).[29] Electrospinning has been used to produce high proton conductivity fibers from perfluorosulfonic acid (PFSA) and polyethylene oxide (PEO) into mechanically robust membranes;[30] however, a non-swelling, mechanically stable nanofiber mat could also serve as a porous scaffold for deposition of a conducting medium. Figure 2-1b shows a diagram illustrating the steps by which a composite membrane can be fabricated by either dip-LbL or spray-LbL application of polyelectrolytes to an electrospun nanofiber mat. The spray-assisted LbL process enables the coating of complex and porous surfaces, while also significantly reducing the cycle times for multilayer assembly from several minutes to a few seconds, thus making the LbL approach commercially viable.[31] In a recent publication we demonstrated that the spray-LbL process can be used to generate LbL-coated electrospun mats.[32] The fibers were shown to be individually coated throughout the interior of the mat when assembled with the assistance of a vacuum to control flow through the mat. In the absence of a vacuum, a condensed thin film was found to form at the surface of the mat, resulting in asymmetric composite membranes. This work demonstrated the versatility of combining the spray-LbL assembly process with electrospun mats.

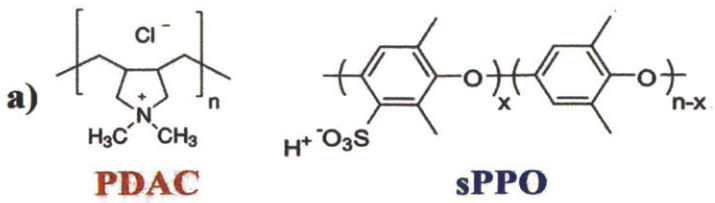

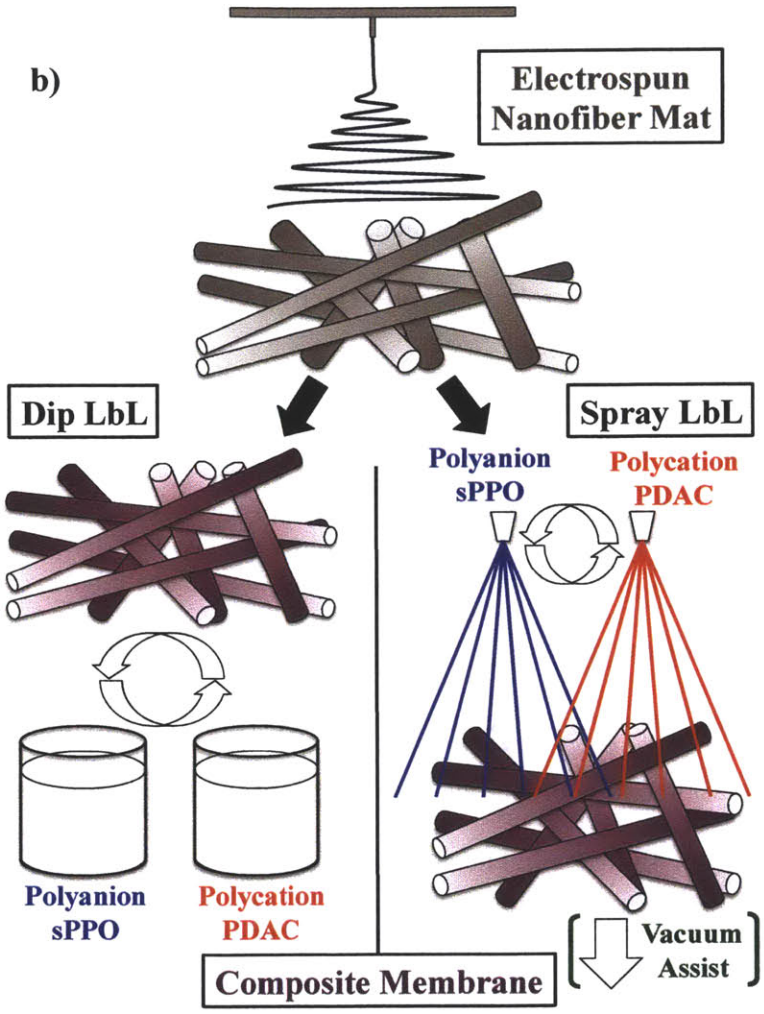

Figure 2-1. (a) Chemical structures of PDAC and sPPO. These two polymers are combined in the LbL assembly process to yield highly conductive PEMs. (b) Schematic diagram showing the fabrication process of LbL-fiber composite membranes by both dip and spray processes.

Here we demonstrate the mechanical enhancement of LbL membrane systems with the use of electrospun mats as substrate materials. Specifically, LbL assembly is used to generate selective coatings on and within the electrospun mats, producing thin, mechanically stable composite fuel cell membranes for high power density devices. These material systems can be

modified at the molecular level to alter transport properties, simply by changing the relative compositions of each adsorbed bilayer of polymer, while the mechanical and chemical stability can be modified by altering the nature or composition of the underlying electrospun network; the systems are highly controllable and the architectures of the films are modified across the thickness to achieve mechanically robust, highly selective and readily processable ultrathin fuel cell membranes, with the goal of rivaling or exceeding the performance of Nafion. To demonstrate this, we explore in this report three different LbL assembly techniques: traditional dip-LbL, which involves directly dipping into alternate polyelectrolyte solutions, spray-LbL, and vacuum-assisted spray-LbL. We observe that each of these three techniques create distinctively different nanometer to micron scale morphologies on the fiber scaffold, each contributing different membrane characteristics. The mechanical properties of the composites are investigated, as well as other key properties for a methanol PEM: protonic conductivity and methanol permeability. Poly(trimethyl hexamethylene terephthalamide) (PA 6(3)T) and polycaprolactone (PCL) electrospun mats are used for their range of fiber sizes (200nm – 10 μm). The dip-LbL electrospun composite membranes are shown to yield morphologies with less controlled bridging and linking of fibers together. The spray-LbL electrospun composite membranes consist of surface top-coatings that do not penetrate into the bulk of the mat. On the other hand, when a vacuum is pulled across the electrospun mat during spray-LbL assembly, the process yields conformal coatings of the individual fibers with minimal bridging throughout the bulk of the mat. The mechanical properties of the spray-LbL electrospun mats are shown to be superior to the pristine LbL free-standing films previously studied.

2.2 Experimental Section

Chemicals. Poly(2,6-dimethyl 1,4-phenylene oxide) (PPO) (Mw = 23,000) and polycaprolactone (PCL) (Mw = 80,000) were obtained from Sigma-Aldrich, Inc. poly(diallyl dimethyl ammonium chloride) (PDAC) (Mw = 240,000) was obtained from Polysciences, Inc. The amorphous polyamide poly(trimethyl hexamethylene terephthalamide), denoted PA 6(3)T, was obtained from Scientific Polymer Products, Inc. It has a glass transition temperature of 153°C. N,N-dimethylformamide (DMF) was purchased from Sigma-Aldrich and used as received for creating polymeric solutions. Sodium chloride salt was purchased from VWR and used as received. PPO was sulfonated as previously reported to yield highly sulfonated sPPO [24].

Electrospun Mats. The electrospinning apparatus, similar to that previously reported, consisted of two aluminum disks 10 cm in diameter oriented parallel to each other and separated by distance of 35 cm.[27] A 30 vol% solution of PA 6(3)T was delivered with a syringe pump (Harvard Apparatus PHD 2000) at a rate of 0.01 mL min-1 to a 1.0 mm ID needle in the top aluminum disk. A high voltage power supply (Gamma High Voltage Research, ES40P) provided a 34 kV potential to the upper aluminum disk in contact with the solution. Under these conditions, an electrospun mat about 100 μm thick could be produced in 2 hours. PCL electrospun mats were made using the same setup from a 10% solution of polymer in chloroform and methanol (3:1 by weight). The PCL mats had an average fiber diameter of 8.6 ± 0.8 μm, while the PA 6(3)T mats had an average fiber diameter of 1.24 ± 0.17 μm. Similar fibers and mats have been produced and characterized previously [35-37].

LbL Dip Assembly (Dip-LbL). Electrospun mats about 1" x 2" in size were placed into home-built plastic sample holders to ensure the sample remained planar during assembly. LbL assembly utilized a programmable ZEISS DS50 slide stainer. The mats were immersed in PDAC

solution for 15 minutes, followed by three two minute rinses in water, and then placed in sPPO solution for 15 minutes, followed by three two minute rinses in water; the process was repeated numerous times to yield thick coatings. The PDAC and sPPO solutions were both 10 mM based on the molecular weight of repeat units. All polymer and rinse solutions for dip-LbL had pH 1. The composite membranes were rinsed in deionized water after assembly to remove excess ions from the films. Various concentrations of sodium chloride were added to polyelectrolyte and rinse solutions to control the growth characteristics and transport properties of the LbL film.

LbL Spray Assembly (Spray-LbL). Electrospun mats about 4" x 4" in size were placed onto a 3" diameter plastic funnel fitted with a steel mesh for support. Sprayed films were fabricated using the same polymer and rinse solutions described above. The mats were plasma-etched in oxygen for 45 seconds and soaked in the PDAC solution for 5 minutes before spraying. A home-built automated spraying setup, as previously detailed, was used to coat the mats [31]. An automated program run by a logic relay controlled the apparatus, spraying the PDAC and sPPO solutions for 3 seconds each, with 5 seconds of rinse water spray in between the polymer sprays. The process was repeated for the desired number of bilayers. For some samples, a vacuum was applied to the back of the electrospun mat using a venturi pump supplied with nitrogen at 50 psi (vacuum-assisted spray-LbL). Free-standing LbL films were assembled on Teflon substrates or polystyrene-coated silicon wafers and gently peeled off after assembly, similar to a previous report [38].

Characterization. SEM images were obtained on a JEOL JSM-6060 scanning electron microscope after coating the composite membranes with 5 nm of Au/Pd. Cross-sectional images were obtained by cryofracturing composite membranes in liquid nitrogen. Protonic conductivity measurements of the coated electrospun mats were made by cutting 1 cm x 2 cm samples,

soaking them in pH 2 water and then rinsing with deionized water so that only protons associated with the sulfonic acid groups are available to contribute to the measured conductivity, and placing them in a conductivity cell with two platinum wires 1 cm apart as the electrodes. Temperature and humidity were controlled using a chamber from Electro-tech Systems, Inc. Impedance values were determined by electrochemical impedance spectroscopy with a Solartron 1260 impedance analyzer, measuring from 100 kHz down to 10 Hz. The thickness of the composite membrane was measured using cross-sectional imaging on an optical microscope and confirmed by a micrometer with 0.5 N applied force. Methanol permeability values were determined by using a dual chamber apparatus, where the membrane sample is the separator between pure methanol and water. The chambers were stirred, and the increase in methanol concentration of the water as a function of time was determined by the changes in the refractive index of the solution using a Waters 2414 Refractive Index Detector. Uniaxial tensile tests were conducted on 100 mm X 25 mm rectangular specimens of coated electrospun mats, at ambient conditions and constant engineering strain rate, with an EnduraTEC Electroforce 3200 in displacement control mode. "Wet" state experiments were conducted by saturating the specimens with deionized water once they were in the tensile fixture and testing immediately. Axial and transverse strains were measured with a Qimaging Retiga 1300 video camera in conjunction with Vic2D video extensometer software. The force-displacement data as taken from the Electroforce and the video extensometer, respectively, were reduced to true stress-true strain results assuming isotropic incompressible behavior. True stress is defined as the ratio of force to current (deformed) cross-sectional area and true strain is defined as the natural logarithm of the ratio of current length to original length (length being the axial distance between video-imaged marks).

2.3 Results and Discussion

2.3.1 Mechanical Properties of Dipped Layer-by-Layer Films

Stress-strain curves of free-standing PDAC/sPPO films are shown in Figure 2 for both ambient (dry) and fully hydrated (wet) conditions. It has previously been shown that dry PDAC/sPPO films have higher elastic moduli and strain-to-break than dry pristine sPPO, an indication that the LbL polyelectrolyte complex films are more mechanically durable than sPPO alone.[25] The dry, free-standing PDAC/sPPO films exhibit elastic-plastic behavior with elastic modulus values ranging from 250-1100 MPa and yield stress values ranging from 4-40 MPa depending on the processing conditions. LbL assembly at higher salt concentrations forms a more compliant network due to ionic shielding and a lower effective ionic crosslink density, resulting in films with lower elastic modulus and higher yield stress values than films assembled with lower or no salt concentrations, which form highly cross-linked, rigid materials. Overall, under dry conditions, the elastic modulus and yield stress values of PDAC/sPPO compare well with those of Nafion, which has an elastic modulus of 300 MPa and a yield stress of 12 MPa.[33] However, the layer-by-layer films become brittle when dry and tear at small strains. The average true strain-to-break of free-standing PDAC/sPPO films is 0.07, which compares unfavorably to a true strain-to-break greater than 1.0 for Nafion under dry conditions. Under hydrated conditions the PDAC/sPPO free-standing films become almost gel-like, and the mechanical strength is lower than the detection threshold of the extensometer. At the hydrated operating conditions of a fuel cell, these mechanical values would lead to very short MEA lifetimes due to mechanical failure of the membrane. These results motivated the development of electrospun mats as reinforcing substrates in this work.

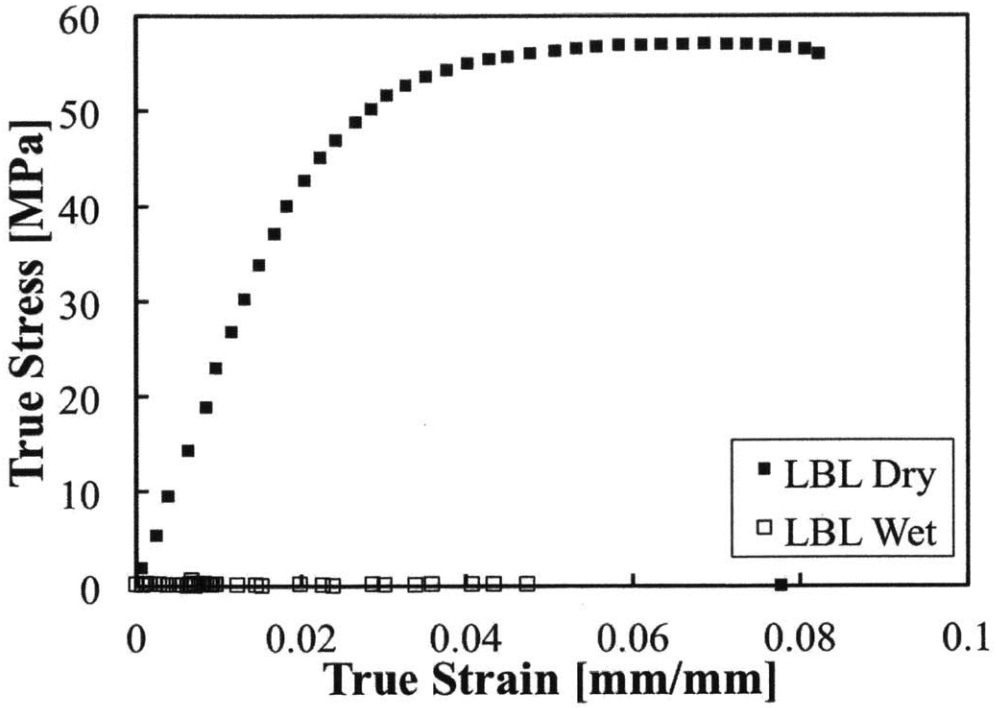

Figure 2-2. Typical stress-strain curves for free-standing PDAC/sPPO films at ambient (dry) and fully humidified (wet) conditions. The PDAC/sPPO films were assembled at pH = 1.0 with 0.5 M NaCl in the sPPO assembly solution. The films were sprayed onto a polystyrene coated silicon wafer and gently removed after assembly.

2.3.2 Dipped Layer-by-Layer Electrospun Composite Films

Figure 3 shows SEM images of PCL electrospun mats coated through the dip-LbL assembly process; electrospun mats with 0, 50, 125, and 250 bilayers (BL) of PDAC/sPPO film are shown. The uncoated PCL electrospun mats have mean fiber diameter of 8.6 μm as shown in Figure 3a. Figure 3b-d show that the fibers become coated as more bilayers of PDAC/sPPO are applied to the PCL mats, but the multilayers form webbed thin films that bridge across the various fibers even at low numbers of bilayers. This webbed morphology is unique to dip-LbL

assembly. It is believed to be the result of full water immersion followed by long vertical drain times associated with dipping, which permits the formation of a polymer film joining two fibers starting at their intersection but not bridging across all the fibers in one uniform film. Meanwhile, the fibers that aren't webbed continue to be coated with PDAC/sPPO film and grow thicker until webbing eventually occurs. The result is a surface coating that has a propensity to bridge at fiber intersections and yields a non-uniform, partially-bridged morphology. LbL films of PDAC/sPPO fabricated at the same assembly conditions on a planar glass substrate grow at a rate of 24.0 nm/BL; therefore, a 50 BL deposition of PDAC/sPPO corresponds nominally to a 1.2 μm film thickness, and a 250 BL deposition of PDAC/sPPO corresponds nominally to 6 μm in thickness. From Figure 3b (50 BL coating) and Figure 3d (250 BL), the fibers, particularly those on the top layers, appear to grow in diameter by about 2.4 μm and 12 μm, respectively, while the bridging films connect more fibers with additional layers. A continuous coating that prevents fuel crossover could be achieved with a sufficient number of bilayers; however, the processing time for such a composite membrane would be on the order of weeks with this dip-LbL method. In addition it was observed by cross-sectional SEM that the multilayer film did not fully penetrate into the interior of the electrospun mat. This results in a gradient in coating across the thickness of the membrane, which is expected to lead to anisotropy in the ionic conductivity of the composite membrane.

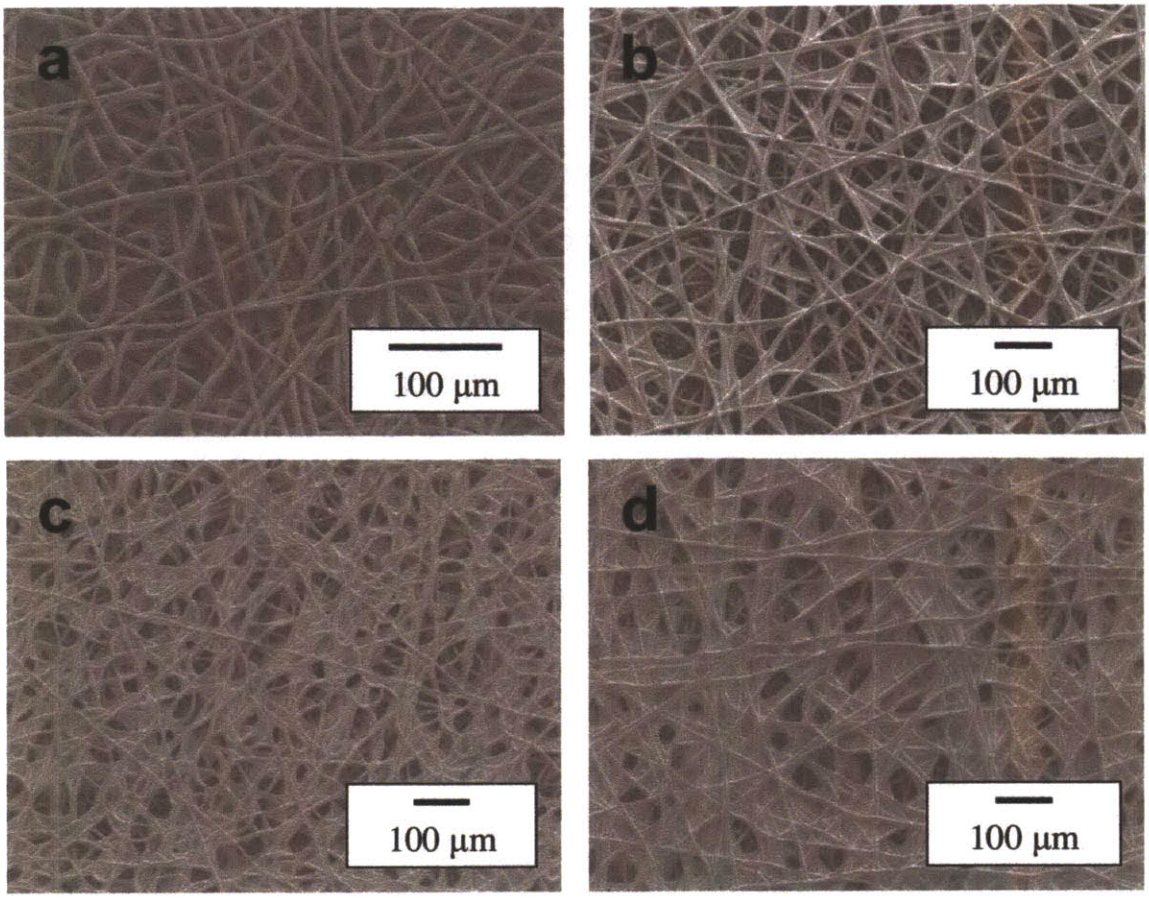

Figure 2-3. SEM images of PCL electrospun mats coated using dip-LbL with (a) 0 BL, (b) 50 BL, (c) 125 BL, and (d) 250 BL of PDAC/sPPO. PCL electrospun mats have mean fiber diameter of 8.6 μm. PDAC/sPPO deposition conditions are pH = 1.0, 0.5 M NaCl in sPPO, and no salt in PDAC or any rinse solutions. Scale bar for each SEM micrograph is 100 μm.

The in-plane protonic conductivity values of PCL electrospun mats coated with 125 and 250 BL of PDAC/sPPO are shown in Figure 4, along with a PDAC/sPPO film assembled on a glass slide. As the number of bilayers deposited on the electrospun mat increases, the number of webbed bridges increases and the total in-plane protonic conductivity of the composite

membrane increases. It appears that by 250 BLs, all of the coated fibers have been connected and the protonic conductivity of the composite approaches that of PDAC/sPPO; however, due to the lack of penetration into the electrospun mat, the void space in the center of the mat is not completely filled. The slope of the composite membrane conductivity with humidity, particularly of the 125BL dipped electrospun mat, is the same as that of the PDAC/sPPO-only film, indicating the same mechanism of ion transport through the composite.

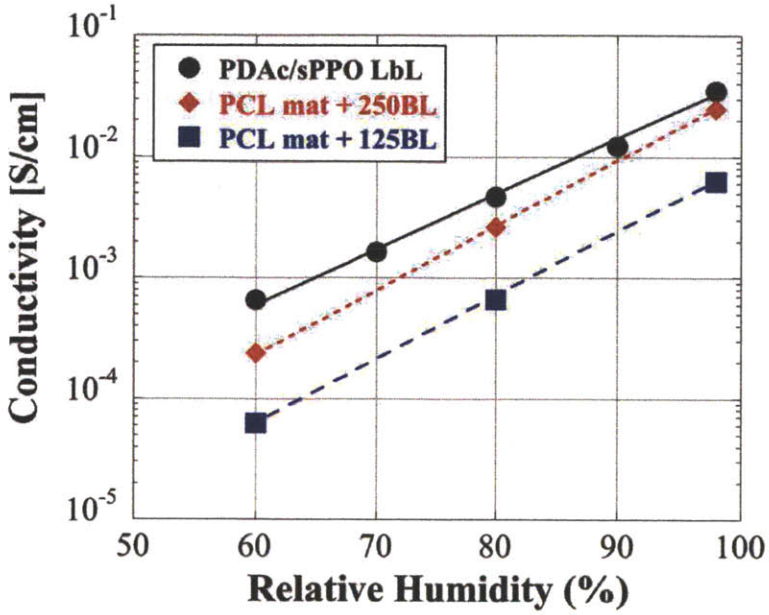

Figure 2-4. Relative humidity dependence of in-plane protonic conductivity of PDAC/sPPO films coated on PCL electrospun mats. PDAC/sPPO deposition conditions are pH = 1.0, 0.5 M NaCl in sPPO, and no salt in PDAC or any rinse solutions. As the number of bilayers deposited on the electrospun mat increases, the webbing of the PDAC/sPPO helps link all the coated fibers and a large increase in conductivity is observed.

2.3.3 Spray-LbL Electrospun Composite Films

To further investigate the potential to achieve highly conductive composite membranes, an improved methodology was adopted. PCL is biodegradable and hydrolytically unstable, so the more durable, hydrolytically stable PA 6(3)T was selected for producing electrospun mats for the remaining studies. PA 6(3)T fiber diameters can be varied from 2 μm down to 0.2 μm. With spray-LbL, it is possible to achieve both pore filling and covering of pores at the surface by using two different spray conditions. Pore filling is achieved when a vacuum is drawn on the downstream side of the electrospun mat during the vacuum-assisted spray-LbL process, effectively coating each fiber through the entirety of the mat. By contrast, a superficial film on both sides of the mat is achieved by simply turning off the vacuum during the spraying process and flipping over the mat to cover both sides of the membrane. Figure 5 shows the electrospun mats used prior to any spray coating process; the mean fiber diameter is 1.24 μm.

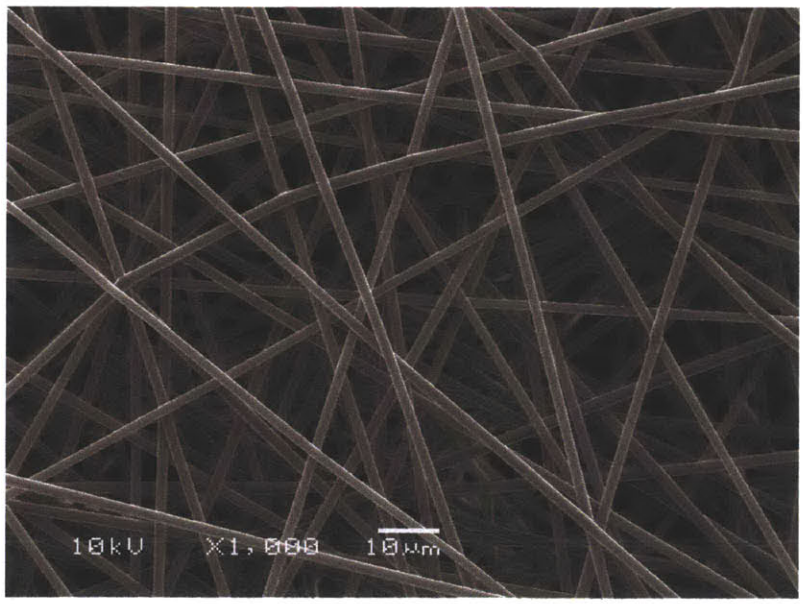

Figure 2-5. SEM micrograph of a PA 6(3)T electrospun mat having mean fiber diameter of 1.24 μm, scale bar for the micrograph is 10 μm.

To fill the electrospun mat uniformly and improve through-plane conductivity, a vacuum was applied to the downstream side of the mat during assembly, allowing a highly conductive matrix to be electrostatically connected to the supporting mat. Representative SEM images of the spray-coated electrospun PA 6(3)T mats with and without vacuum are shown in Figure 6. Figures 6a and 6b show images at two different magnifications of an electrospun mat coated with 250 bilayers of PDAC/sPPO with a vacuum applied to the back of the mat. When sprayed under vacuum, the individual fibers of the mat are coated conformally, as the deposition occurs below the critical Reynolds number for flow separation from the downstream side of a cylinder[34] using conditions similar to those previously reported.[30] As can be seen in Figure 6a, the vacuum-assisted spray-LbL process produces fibers that are smoothly, uniformly, and individually coated with minimal pore blockage. The polyelectrolyte solution is pulled across the entire thickness of the electrospun mat and thus all the fibers, not just those near the surface, are coated. The charged surface of the PA 6(3)T fibers caused by plasma-treatment increases the wettability of the mat and providing an anionic substrate for LbL adhesion. The result is that the LbL penetrates through the void spaces and conformally deposits smooth and uniform LbL films around each fiber. From Figure 6b, it is observed that the growth of the multilayer film on the fibers (5.6 ± 0.4 nm/BL) is almost identical to the growth of the film on glass (6.1 nm/BL) under the salt conditions, indicating a similar growth mechanism. The vacuum-assisted spray-LbL process enables uniform coating by eliminating webbing that would hinder the flow of the polymer solution droplets through the electrospun mat. The vacuum-assisted spray-LbL process allows the precise control of LbL film thickness on each fiber as well as the functional surface area and the degree of porosity of the composite film.

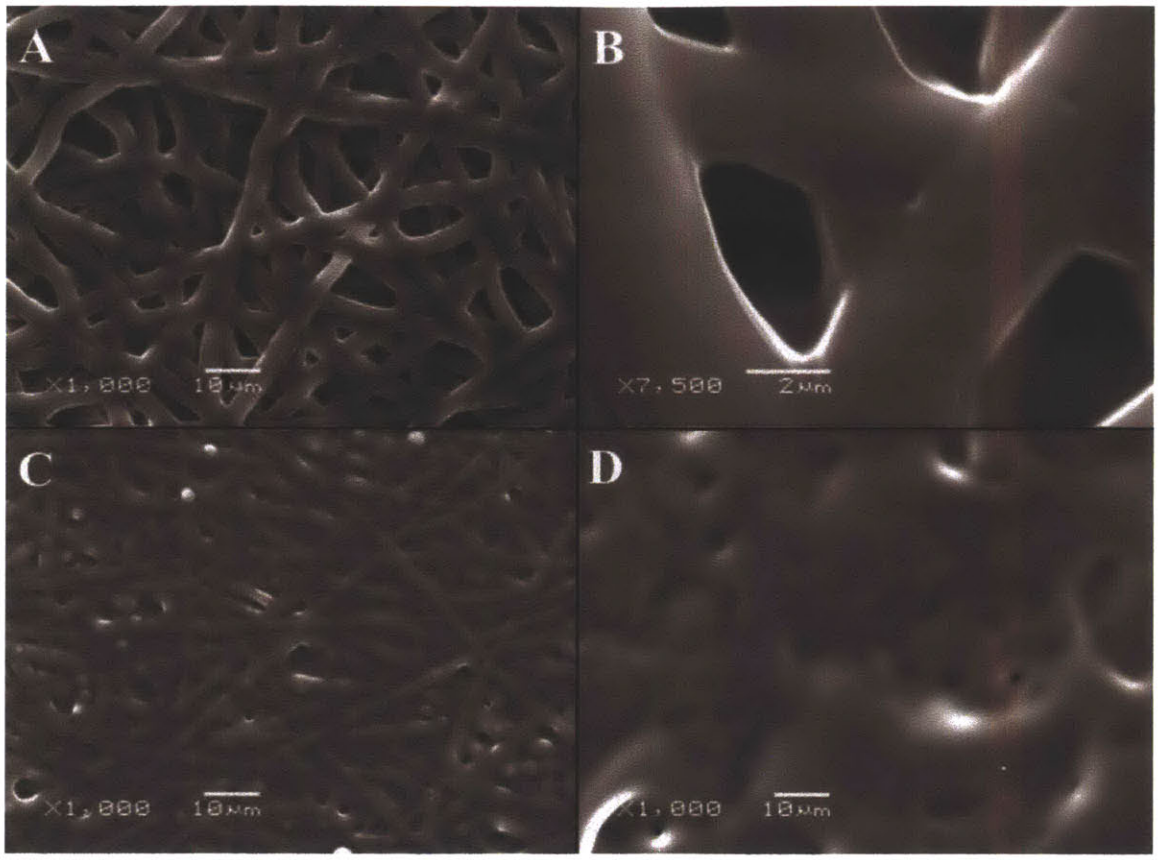

Figure 2-6. SEM images of PA 6(3)T electrospun mat (a – front-side, b – zoomed in) spray-LbL coated with 250 BL of PDAC/sPPO, at pH2 with 0.5M NaCl in the sPPO solution, when a vacuum is applied. The spray coatings provide a uniform coating on the fibers individually without webbing or pore covering. When there is no vacuum applied during the spray deposition, a pore-bridging film is observed after just 100BL (2.0 μm equivalent on glass) is sprayed (c) at pH2 with 1.0 M NaCl in all solutions. After 300 BL (6.0 μm equivalent on glass) are deposited, the films have formed such a thick covering that it obscures the fibers underneath (d).

To create a film that covers all the pores in the supporting electrospun mat and drastically reduce the methanol permeability of the composite membrane, spray-LbL assembly without

vacuum was applied to plasma-treated electrospun mats. When there is no vacuum applied during the spray deposition, the polymer solution droplets do not penetrate through the membrane and instead, form a pore-bridging film that spans across all the fibers along the top surface of the membrane. Figures 6c and 6d show images of an electrospun mat after spraying 100BL (2 μm) and 300 BL (6 μm) with no vacuum, respectively. As can be seen in Figure 6c, with 100BLs, the pores are covered, although the underlying PA 6(3)T fiber structure can still be seen. At 300BLs, see Figure 6d, the LbL coating is so thick that the fibers (1.24 μm mean diameter) underneath are not visible anymore.

To probe the interior of the spray-coated electrospun mats, cross-sectional SEM images were obtained by cryofracturing the composite membranes in liquid nitrogen. Figure 7a shows the cross-section of a PA 6(3)T electrospun mat spray-coated with 175 BL of PDAC/sPPO without vacuum. There is no penetration of the polymer solution into the electrospun mat, while the fibers underneath appear to be unaffected in any way. Figure 7b shows an electrospun mat spray-coated with 150 BL of PDAC/sPPO with vacuum. For composite membranes prepared without vacuum, the LbL film starts growing at the surface, bridging across all the pores, and grows outward. For samples prepared with vacuum, Figure 7b shows that the individual fibers of the electrospun mat are coated throughout the film. The enlarged inset shows the conformal nature of the coating and how the LbL film on two adjacent fibers can merge. Because the LbL film grows on each fiber throughout the mat, just 150 BL (0.5 μm) were enough to fill the majority of the void spaces of an 80 μm thick membrane, reducing membrane porosity from 80% to 30% as measured gravimetrically based on the apparent density of the membrane and bulk density of the polymer. With further optimization, LbL electrospun composite membranes could be produced with even lower void space. However, an electrospun mat coated only with the

vacuum-assisted spray-LbL process can never be completely filled with polyelectrolyte, and will be highly methanol permeable due to the remaining void space needed for the flow of air to be accommodated through the fiber mat. An improved composite membrane that conducts protons but rejects methanol can be formed by combining both types of spray-LbL techniques: the vacuum-assisted spray-LbL technique to fill the PA 6(3)T mat with conductive PDAC/sPPO, and the spray-LbL technique without vacuum to form a methanol barrier across the surface of the membrane.

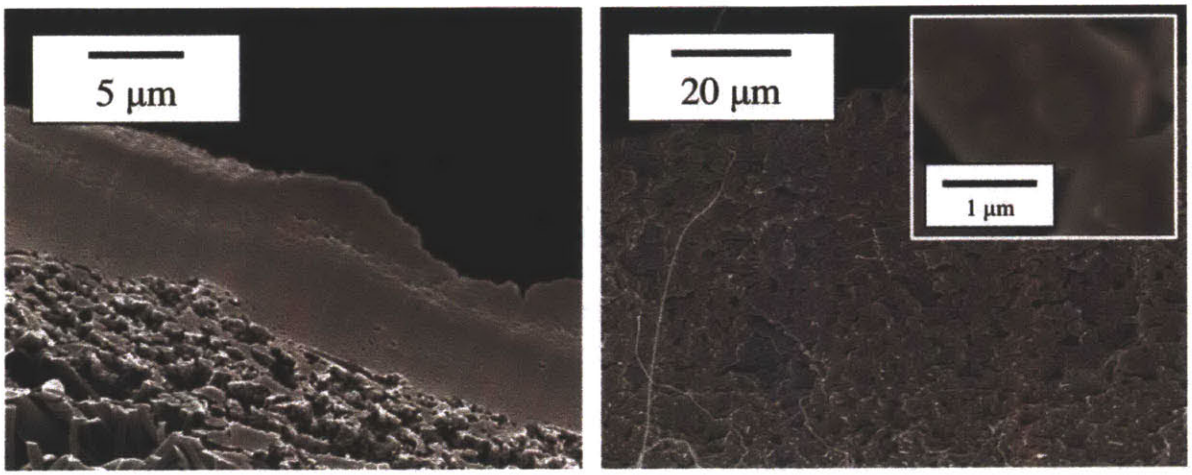

Figure 2-7. Cross-sectional SEM images of PA 6(3)T electrospun mats (mean fiber diameter of 0.46 ± 0.06 μm) spray coated with 175 BL (6 μm) of PDAC/sPPO without vacuum (left) and spray coated with 150 BL (0.5 μm) of PDAC/sPPO with vacuum (right and inset). Without vacuum, a pore-spanning film over the surface of the mat is formed, leaving the interior of the mat uncoated. With the application of a vacuum across the electrospun mat, the fibers of the mat are conformally coated throughout the mat. Scale bar for the left micrograph is 5 μm, scale bar for the right micrograph is 20 μm, and the scale bar for the inset is 1 μm.

2.3.4 Methanol Permeability Results

Methanol permeability was measured for spray-LbL electrospun mats to evaluate the effectiveness of the LbL films in reducing methanol crossover. When vacuum was applied during the spray LbL process, the resultant composite membrane, with 30% void space, was highly permeable to methanol. However, when there was no vacuum applied during the spray LbL process, the pore-bridging film was able to significantly reduce methanol permeability. Figure 8 shows the methanol permeability of the composite membrane after a certain number of bilayers have been sprayed onto an electrospun mat without vacuum. With as little as 100 BLs (2 μm) on an 80 μm thick electrospun mat, a fully bridged film is formed and the overall methanol permeability is already lower than that of Nafion. As seen in Figure 8, as the number of bilayers increases, a thicker LbL film is sprayed and the overall methanol permeability decreases. Thus, with the spray LbL fabrication technique, the methanol permeability of the composite membrane may be varied.

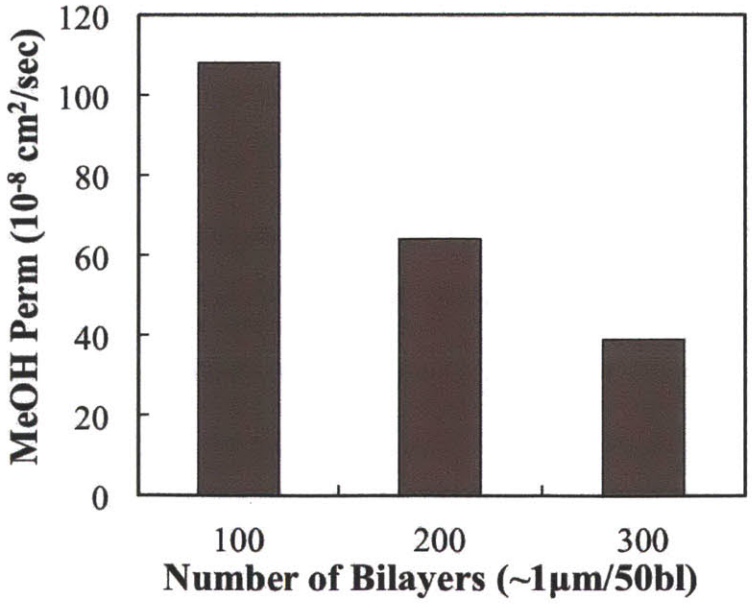

Figure 2-8. Methanol permeability of the composite membrane as a function of LbL film thickness for spray-coated electrospun mats. The spray conditions for the PDAC/sPPO films were pH = 2.0, 1.0 M NaCl in all solutions. As more bilayers are applied, the overall methanol permeability decreases.

To verify that the decrease in methanol permeability comes from the PDAC/sPPO pore-bridging top film on the electrospun mat and not from the bulk membrane, we compared the methanol permeability of the composite membranes with that of PDAC/sPPO supported on track-etched nucleopore membranes, as published previously.[24] Table 2-1 lists the overall permeability of the composite membranes as well as the MeOH permeability of the LbL layer alone, assuming that it provides the sole barrier to MeOH crossover, measured for the composite membranes with different numbers of bilayers. The overall permeability is the measured rate of methanol crossover divided by the methanol concentration gradient (the change in concentration divided by the total thickness of the composite membrane comprising both LbL film and the electrospun mat). The permeability of the LbL layer alone is defined as the crossover divided by the methanol concentration gradient where only the thickness of the blocking LbL coating is used, ignoring the electrospun mat base. The thickness of the LbL coating on the fibers is estimated from the film growth curve as determined on a planar glass substrate and confirmed by cross sectional SEM. As seen in Table 2-1, the overall permeability of the composite membrane drops with increasing number of bilayers; however, the estimated permeability of the LbL layer remains the same indicating, that the inherent transport properties of the LbL film does not change with the number of bilayers. These numbers are similar to what was previously

published on PDAC/sPPO films alone.[24] This proves that the primary blocking component for methanol crossover is a linearly growing PDAC/sPPO film on top of the electrospun mat.

Table 2-1. Methanol permeability of composite membranes with various numbers of bilayers of PDAC/sPPO.

# of Bilayers	Overall Permeability [10-8 cm^2/sec] [a]	Thickness of LbL film [μm]	Estimated Permeability of LbL layer [10-8 cm^2/sec] [b]
100 [c]	108	2.0	2.7
200 [c]	64	4.0	3.2
300 [c]	39	6.0	2.9
PDAC/sPPO film [24]	2.18	On Nucleopore	2.18
Nafion	282	N/A	N/A

[a] Defined as methanol flux multiplied by the total thickness of the membrane divided by the concentration difference across the membrane.

[b] Defined as methanol flu x multiplied by thickness of blocking layer (LbL or Nafion) divided by the concentration difference across the membrane.

[c] Spray conditions: pH=2, 1.0 M NaCl in all solutions without vacuum on a 75μm thick electrospun mat.

2.3.5 Mechanical Behavior of the Composite Membranes

Monotonic and cyclic uniaxial tensile testing was performed on bare PA 6(3)T electrospun mats and vacuum-assisted, PDAC/sPPO spray-coated mats to assess the mechanical behavior of these composite materials (Fig. 9). Free-standing PDAC/sPPO films exhibit brittle elastic behavior with a Young's modulus up to 1100 MPa and a yield stress of 40-50 MPa under dry testing conditions. Uncoated PA 6(3)T electrospun mats exhibit elastic-plastic behavior with

an elastic modulus ranging from 8 - 53 MPa and a yield stress ranging from 0.2 – 2 MPa. In cyclic testing the electrospun mats are seen to unload linearly at the same slope as the initial loading and to reload along nearly the same path, indicating little hysteresis. The electrospun mats are susceptible to necking and exhibit strains at break ranging from 0.3 - 1.0. The mechanical behavior of the PDAC/sPPO vacuum-assisted spray-coated electrospun mats is highly dependent upon the relative humidity, and maintains the characteristics of both the free-standing LbL and the bare mat. When the composite membrane is dry, the mechanical properties of the LbL film give the composite membrane a large elastic modulus with low strain-to-break. At failure, the LbL film component tears first, followed by yielding of the underlying electrospun mat. When the composite membrane is wet, the LbL provides minimal mechanical strength and the coated electrospun mat behaves like the bare PA 6(3)T mat as shown in Figure 9.

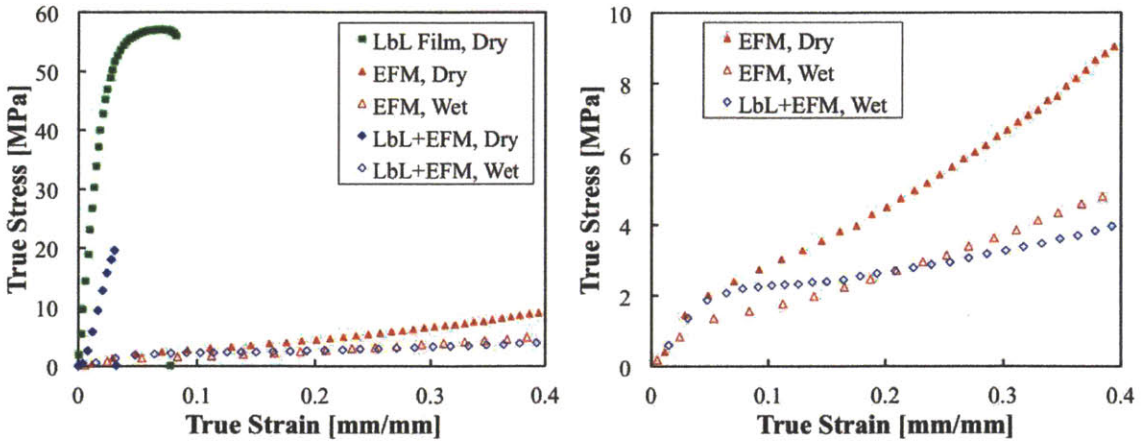

Figure 2-9. Stress-strain curves comparing free-standing LbL film to uncoated and vacuum-assisted spray-coated PA 6(3)T electrospun mats at ambient (dry) and fully humidified (wet) conditions. Shown to the full stress range of the LbL dry film (left). Shown at a lower stress range to better differentiate among the more compliant materials (right). The spray-coated mats

exhibit composite membrane behavior; the LbL strengthens the mat when dry while the mat provides the supporting base when wet.

In observing the failure mechanisms of the coated mats after mechanical testing for both the dry and hydrated cases, it is seen that in the dry case, cracking occurs along the LbL surface, exposing the underlying electrospun mat, whereas in the hydrated case the surface layer is able to deform with the rest of the mat without cracking due to the ductile behavior of the LbL coating under hydrated conditions, as seen in bare film testing. Consequently, the spray coated mats exhibit superior mechanical properties as compared to the bare films, and are comparable to commercial proton exchange membranes. The mechanical properties of the underlying mat may be improved apart from LbL fabrication, thereby improving the structural properties of the composite membrane without affecting the key electrochemical properties of the LbL film, specifically methanol permeability and proton conductivity.

2.4 Conclusion

Composite membranes of highly conductive layer-by-layer (LbL) films and electrospun fiber mats are fabricated and characterized for mechanical strength and selectivity. The mechanical response of highly conducting PDAC/sPPO LbL films are improved by forming the LbL matrix on a highly controllable electrospun fiber scaffold. Free-standing PDAC/sPPO films have elastic moduli up to 1100 MPa and a maximum yield stress of 40 MPa. PDAC/sPPO films assembled with more salt in the assembly baths have better mechanical properties due to the more favorable cross-linked network that is formed. The mechanical properties of PDAC/sPPO

are on par with commercial proton exchange membranes like Nafion at moderate to low relative humidity conditions; however, the PDAC/sPPO films break at extremely low strains (~ 0.07 mm/mm) and become gel-like with low elastic modulus values when wet. Coating a PCL electrospun mat with the LbL dipping process produces composite membranes with interesting webbed morphologies that span adjacent fibers. The in-plane protonic conductivity of the composite membrane is similar to the pristine LbL system beyond a critical number of bilayers.

To create a fuel-blocking layer and to fill in more of the void space throughout the electrospun mat, the spray-LbL assembly is utilized as a means for the rapid formation of LbL films. When the spray-LbL technique is used along with an applied pressure gradient across the electrospun mat during assembly, the resulting LbL electrospun mat composites have conformal coatings on the individual fibers throughout the bulk of the mat. When the spray-LbL technique is used without vacuum, the resulting LbL film bridges across the pores of the electrospun mat, forming a continuous fuel-blocking layer with properties similar to the free-standing LbL film by itself. The mechanical properties of the spray coated electrospun mats are shown to be superior to the LbL-only system, particularly at hydrated conditions. This shows the versatility of the spray-LbL system to fabricate composite membranes with finely tuned morphology and properties. Future studies are underway to model the mechanical behavior of the LbL electrospun composite membranes, and to develop future systems with increased mechanical durability as well as test the composite membrane in an operational direct methanol fuel cell.

2.5 References

[1] F. de Bruijn, *Green Chemistry* **2005**, *7*, 132.

[2] S. G. Chalk, J. F. Miller, *J. Power Sources* **2006**, *159*, 73.

[3] M. Doyle, G. Rajendran, in *Handbook of Fuel Cells: Fundamentals, Technology and Applications*, Vol. 1 (Eds: W. Vielstich, A. Lamm, H. A. Gasteiger), John Wiley & Sons Ltd., Chichester, England **2003**, 351.

[4] J. Wu, X. Z. Yuan, J. J. Martin, H. Wang, J. Zhang, J. Shen, S. Wu, W. Merida, *J. Power Sources* **2008**, *184*, 104.

[5] M. Inaba, T. Kinumoto, M. Kiriake, R. Umebayashi, A. Tasaka, Z. Ogumi, *Electrochim. Acta* **2006**, *51*, 5746.

[6] R. Borup, J. Meyers, B. Pivovar, Y. S. Kim, R. Mukundan, N. Garland, D. Myers, M. Wilson, F. Garzon, D. Wood, P. Zelenay, K. More, K. Stroh, T. Zawodzinski, J. Boncella, J. E. McGrath, M. Inaba, K. Miyatake, M. Hori, K. Ota, Z. Ogumi, S. Miyata, A. Nishikata, Z. Siroma, Y. Uchimoto, K. Yasuda, K. I. Kimijima, N. Iwashita, *Chem. Rev.* **2007**, *107*, 3904.

[7] Y.-H. Lai, C. K. Mittelsteadt, C. S. Gittleman, D. A. Dillard, *J.Fuel Cell Sci. Tech.* **2009**, *6*, 021002.

[8] F. Bauer, S. Denneler, M. Willert-Porada, *J. Polym. Sci., B Polym. Phys.* **2005**, *43*, 786.

[9] R. Solasi, Y. Zou, X. Huang, K. Reifsnider, D. Condit, *J. Power Sources* **2007**, *167*, 366.

[10] A. Kusoglu, A. M. Karlsson, M. H. Santare, S. Cleghorn, W. B. Johnson, *J. Power Sources* **2006**, *161*, 987.

[11] X. Huang, R. Solasi, Y. Zou, M. Feshler, K. Reifsnider, D. Condit, S. Burlatsky, T. Madden, *J. Polym. Sci., B Polym. Phys.* **2006**, *44*, 2346.

[12] R. C. McDonald, C. K. Mittelsteadt, E. L. Thompson, *Fuel Cells* **2004**, *4*, 208.

[13] F. Liu, B. Yi, D. Xing, J. Yu, H. Zhang, *J. Membr. Sci.* **2003**, *212*, 213.

[14] K. M. Nouel, P. S. Fedkiw, *Electrochim. Acta* **1998**, *43*, 2381.

[15] T. L. Yu, H. L. Lin, K. S. Shen, L. N. Huang, Y. C. Chang, G. B. Jung, J. C. Huang, *J. Polym. Res.* **2004**, *11*, 217.

[16] J. J. Shi, B. Jang, *J. Fuel Cell Sci. Technol.* **2011**, *8*, 014501.

[17] Y.-H. Liu, B. Yi, Z.-G. Shao, D. Xing, H. Zhang, *Electrochem. Solid-State Lett.* **2006**, *9*, A356.

[18] E. Chalkova, M. V. Fedkin, D. J. Wesolowski, S. N. Lvov, *J. Electrochem. Soc.* **2005**, *152*, A1742.

[19] C. Yang, P. Costamagna, S. Srinivasan, J. Benziger, A. B. Bocarsly, *J. Power Sources* **2001**, *103*, 1.

[20] G. Decher, *Science* **1997**, *277*, 1232.

[21] G. Decher, J. D. Hong, J. Schmitt, *Thin Solid Films* **1992**, *210*, 831.

[22] P. T. Hammond, *Adv. Mater.* **2004**, *16*, 1271.

[23] T. R. Farhat, P. T. Hammond, *Adv. Funct. Mater.* **2005**, *15*, 945.

[24] A. A. Argun, J. N. Ashcraft, P. T. Hammond, *Adv. Mater.* **2008**, *20*, 1539.

[25] J. N. Ashcraft, A. A. Argun, P. T. Hammond, *J. Mater. Chem.* **2010**, *20*, 6250.

[26] J. Doshi, D. H. Reneker, *Journal of Electrostatics* **1995**, *35*, 151.

[27] Y. M. Shin, M. M. Hohman, M. P. Brenner, G. C. Rutledge, *Polymer* **2001**, *42*, 09955.

[28] G. C. Rutledge, S. V. Fridrikh, Advanced Drug Delivery Reviews **2007**, *59*, 1384.

[29] S. V. Fridrikh, J. H. Yu, M. P. Brenner, G. C. Rutledge, *Phys. Rev. Lett.* **2003**, *90*, 144502.

[30] J. Choi, K. M. Lee, R. Wycisk, P. N. Pintauro, P. T. Mather, *J. Mater. Chem.* **2010**, *20*, 6282.

[31] K. C. Krogman, N. S. Zacharia, S. Schroeder, P. T. Hammond, Langmuir **2007**, *23*, 3137.

[32] K. C. Krogman, J. L. Lowery, N. S. Zacharia, G. C. Rutledge, P. T. Hammond, *Nat. Mater.* **2009**, *8*, 512.

[33] S. Kundu, L. C. Simon, M. Fowler, S. Grot, *Polymer* **2005**, *46*, 11707.

[34] W. M. Deen, *Analysis of Transport Phenomena*, Oxford Univeristy Press, **1998**.

[35] J. L. Lowery, N. Datta, G. C. Rutledge, Biomaterials **2010**, *31*, 491.

[36] C.-L. Pai, M. C. Boyce, G. C. Rutledge, Polymer **2011**, *52*, 2295.

[37] M. M. Mannarino, G. C. Rutledge, Polymer **2012**, *53*, 3017.

[38] J. L. Lutkenhaus, K. D. Hrabak, K. McEnnis, P. T. Hammond, *J. Am. Chem. Soc.* **2005**, *127*, 17228.

3. Mechanical and Transport Properties of Layer-by-Layer Electrospun Composite Proton Exchange Membranes for Fuel Cell Applications

Portions of this chapter are reproduced from Matthew M. Mannarino*, David S. Liu*, Paula T. Hammond, and Gregory C. Rutledge, *ACS Applied Materials and Interfaces*, **2013**, *5 (16)*, 8155-8164.

Abstract

Composite membranes composed of highly conductive and selective layer-by-layer (LbL) films and electrospun fiber mats were fabricated and characterized for mechanical strength and electrochemical selectivity. The LbL component consists of a proton-conducting, methanol-blocking poly(diallyl dimethyl ammonium chloride)/sulfonated poly(2,6-dimethyl 1,4-phenylene oxide) (PDAC/sPPO) thin film. The electrospun fiber component consists of poly(trimethyl hexamethylene terephthalamide) (PA 6(3)T) fibers in a nonwoven mat of 60-90% porosity. The bare mats were annealed to improve their mechanical properties, which improvements are shown to be retained in the composite membranes. Spray LbL assembly was used as a means for the rapid formation of proton-conducting films that fill the void space throughout the porous electrospun matrix and create a fuel-blocking layer. Coated mats as thin as 15 μm were fabricated, and viable composite membranes with methanol permeabilities twenty times lower than Nafion, and through-plane proton selectivity five and a half times greater than Nafion, are demonstrated. The mechanical properties of the spray coated electrospun mats are shown to be

superior to the LbL-only system, and possess intrinsically greater dimensional stability and lower mechanical hysteresis than Nafion under hydrated conditions. The composite proton exchange membranes fabricated here were tested in an operational direct methanol fuel cell. The results show the potential for higher open circuit voltages (OCV) and comparable cell resistances when compared to fuel cells based on Nafion.

3.1 Introduction

Improvements to the performance of thin-film solid polymer electrolytes are critical for the advancement of electrochemical energy devices.[1] In recent years, there has been considerable interest in designing more chemically stable and mechanically robust membranes while maintaining high ionic conductivity and low fuel crossover.[2,3] For current state-of-the-art hydrogen and methanol fuel cells, proton exchange membranes (PEMs) comprising perfluorosulfonic acid polymers such as Nafion are the material of choice, primarily because they exhibit superior protonic conductivity, relatively high mechanical integrity, and chemical stability; however, even perfluorosulfonic acid polymers have shown limited device lifetimes due to mechanical degradation.[4,5] One of the main causes of membrane failure is the repeated swelling/deswelling of the membrane during fuel cell operation due to the cycling of temperature and humidity. This cyclic fatigue stress has been shown to weaken the membrane mechanically after as few as a hundred cycles.[6,7] The hydro-thermal mechanical behavior of Nafion during swelling has been extensively studied;[5,8,9] there is a significant need to improve upon the current membrane's durability. Many methods have been proposed to improve the mechanical properties of PEMs, such as incorporating Nafion into a polytetrafluoroethylene (PTFE)

supporting matrix.[10,11] Other methods of mechanical reinforcement include the incorporation of metal oxides,[12] zirconium phosphates,[13] and carbon nanotubes[14] into Nafion matrices in order to improve PEM lifetime or the overall fuel cell performance.

The continued reliance on Nafion, with its high cost and relatively high fuel crossover, has proven to be a limiting factor for development of direct methanol fuel cells (DMFCs). In recent years, alternative composite polyelectrolyte membranes have been investigated as substitutes for Nafion in PEMs, such as semi-interpenetrating polymer networks (IPNs),[15] sulfonated poly(ether ether ketone)/phenoxy resin (SPEEK/PHR) composites,[16] poly(vinyl alcohol)/sulfonated polyhedral oligosilsesquioxane (PVA/sPOSS) hybrid membranes,[17] and sulfonated polystyrene/poly(vinylidene fluoride) blends compatibilized with block copolymers.[18] More recently, researchers have attempted to fabricate a composite membrane based on sulfonated poly(2,6-dimethyl 1,4-phenylene oxide) (sPPO) reinforced by electrospun and cross-linked bromomethylated poly(2,6-dimetyl-1,4-phenylene oxide) (cBPPO), for a hydrogen fuel cell.[19] While many of these alternative composite PEMs have shown promising results, there are still concerns regarding their mechanical durability, chemical stability, and/or transport properties that prevent them from widespread use in DMFCs.

In recent reports, we have produced layer-by-layer (LbL)-based PEMs that perform well in hydrogen and direct methanol fuel cells.[20,21] LbL assembly is a versatile nanoscale fabrication technique that allows for the coating of any wettable substrate with a combination of two or more polymers possessing complementary interactions, such as oppositely charged functional groups.[22,23] The films can be tuned by adjusting the pH or salt content of the polymer solutions; the thickness per bilayer of films constructed by the LbL method ranges from as small as a few nanometers to over one hundred nanometers. An LbL system composed of

poly(diallyl dimethyl ammonium chloride) (PDAC) and sulfonated poly(2,6-dimethyl 1,4-phenylene oxide) (sPPO) has shown particular promise for use in a DMFC. It has the highest ionic conductivity of any LbL assembled system to date, at 70 mS cm^{-1}, comparable to that of Nafion, while possessing methanol permeability values less than one hundredth that of Nafion. A key weakness of this promising system is that it is mechanically deficient when hydrated.[21,24,25] In fact, many electrostatically assembled polymer membrane systems present the same issues with regard to mechanical integrity.

Electrospun fiber (EF) mats are non-woven materials with high porosities and high specific surface areas (~1-10 m^2/g).[26,27] A wide range of polymers can be formed into electrospun mats, and it has been shown that the resulting fiber diameters can be controlled during fabrication in the range of 0.1–10 μm, depending on the solution and processing parameters.[28] In addition, we have previously shown that significant improvements in the mechanical response of EF mats can be achieved by thermal annealing, with only modest decreases in porosity of the mats.[29] The spray-assisted LbL process can be used to coat fibers individually throughout the interior of the electrospun mat with the assistance of a vacuum to control the convection of the spray through the mat; in the absence of a vacuum, the spray-assisted LbL process creates a film that can bridge the pores at the surface of the mat, resulting in an asymmetric composite membrane.[25,30] This versatility in fabrication through the combination of LbL assembly and electrospinning allows for the manufacture of PEMs with controllable transport properties. Previously, we demonstrated that the highly selective PDAC/sPPO LbL system could be conformally coated onto electrospun fiber mats and successfully blocks pores, thus producing a stronger membrane with superior methanol resistance when compared to Nafion.[25]

In this work we manipulate the structure of the underlying electrospun nanofiber scaffold to investigate the effects on the mechanical and functional performance of the composite proton exchange membrane. Thermal annealing of the electrospun fiber mats at temperatures near the glass transition was found to improve the mechanical response and dimensional stability of the coated PEMs. The mechanical durability and hysteretic cycling of the composite membranes were investigated as well as the key transport properties (protonic conductivity and methanol permeability) for a PEM to be used in a methanol fuel cell. The transport properties of the composite systems are controllable by manipulation of the fiber mat thickness and LbL deposition parameters. Complete Membrane Electrode Assemblies (MEAs) were constructed and used to evaluate composite PEM performance in an operational DMFC for comparison to Nafion.

3.2 Experimental Section

Chemicals. PPO (Mw = 23,000) was obtained from Sigma-Aldrich, Inc. PDAC (Mw = 240,000) was obtained from Polysciences, Inc. Poly(trimethyl hexamethylene terephthalamide) [PA 6(3)T] was purchased from Scientific Polymer Products, Inc. N,N-dimethyl formamide (DMF) was purchased from Sigma-Aldrich and used as received for creating polymeric solutions. PPO was sulfonated as previously reported[21] to yield highly sulfonated sPPO. Magnesium nitrate salt was purchased from Sigma-Aldrich and used as received. An E-Tek gas diffusion layer (GDL) comprising 4.0 mg/cm^2 of 60 wt.% HP Pt catalyst on Vulcan XC-72 was used for the cathode side of the membrane electrode assembly (MEA) and an E-Tek GDL comprising 4.0 mg/cm^2 of 80 wt.% Pt/Ru catalyst on Vulcan XC-72 was used for the anode side. For the custom ink and wet deposition, 80 wt.% Pt/Ru on Vulcan carbon was purchased from the Fuel Cell Store. Nafion DE2020 solution was purchased from Ion Power, Inc. and used as the

catalyst binder at 0.8:1 wt. ratio to carbon. Catalyst ink slurry using a 1:1 mixture by volume of isopropanol:water as solvent was sonicated for five minutes before application. The target catalyst loading was 4.0 mg/cm^2 and the gas diffusion layer was ELAT carbon cloth from the Fuel Cell Store.

Electrospinning Fiber Mats. As described in a previous report,[29] the electrospinning apparatus consisted of two aluminum disks 10 cm in diameter oriented parallel to each other and separated by a distance of 30 cm. A 22 wt.% solution of PA 6(3)T in DMF was pumped through a Teflon tube with a syringe pump (Harvard Apparatus PHD 2000) at a rate of 0.01 mL/min through a 0.040" ID needle in the top aluminum disk. A high voltage power supply (Gamma High Voltage Research, ES40P) provided 20-24 kV potential to the upper aluminum disk, and the polymer solution jet emitted from the needle was drawn to the bottom grounded disk, where ultrafine fibers of approximately 400 nm diameter were collected. The thickness of the mat (from ~10 μm to 80 μm) was controlled by the time allowed for deposition. The EF mats were (optionally) annealed in an oven at a specified temperature between 130-170 °C for 2 hours prior to coating by the spray-LbL method as previously reported.[29]

LbL Spray Assembly. Samples of EF mats about 100 mm in diameter were first plasma treated in an oxygen atmosphere for 1 minute to make the EF mats hydrophilic and to impart an initial negative charge to the fibers (forming carboxylates on the surface).[31] The mats were then placed onto a 75 mm diameter plastic funnel fitted with a steel mesh (2 mm grating) to support the membrane. Sprayed films were fabricated using the same polymer and rinse solutions described previously.[25] For all ES mats 25 μm or thicker, halfway through the desired number of bilayers, the coated mat was flipped over on the steel mesh such that the vacuum was drawn through the opposite side; this is done to provide a more even coating throughout the fiber

matrix. The coated fiber mats were then hydrated in deionized water and consolidated in a Carver Hot Press (15 cm x 15 cm platens) at 100 °C and 50 kN for 30 minutes in order to reduce the remaining pore spaces within the composite membrane. A "capping layer" of LbL film (typically 1 μm thick) was then applied to the composite membrane on both sides by spraying without the vacuum assist, to further inhibit methanol crossover. Free-standing LbL films were also assembled on Teflon substrates or polystyrene-coated silicon wafers and gently peeled off after assembly, similar to a previous report.[24]

Composite Membrane Characterization. Scanning electron microscopy (SEM) images were obtained on a JEOL JSM-6060 scanning electron microscope after coating the composite membranes with roughly 5 nm of Au/Pd. Cross-sectional images were obtained by cryo-fracturing the composite membranes in liquid nitrogen. Porosities of the fiber mats were determined gravimetrically by cutting out rectangular specimens and measuring the mass and dimensions of the mat sample and converting to porosity. Sample thickness was measured with a Mitutoyo digital micrometer with a constant measuring force of 0.5 N. Lateral sample dimensions were determined using a digital caliper. The volume and mass of the specimen were then converted to a porosity using the bulk density. The bulk density was estimated as the average value for the polymers used: PA 6(3)T (1.12 g/cm^3), sPPO (1.06 g/cm^3), PDAC (1.04 g/cm^3).

Mechanical Testing. Uniaxial tensile testing of dry and fully hydrated electrospun fiber mats and composite membranes was performed with a Zwick Roell Z2.5 tensile testing machine using a 2.5 kN load cell. Rectangular specimens were cut to 100 mm x 12.5 mm and extended at a constant crosshead speed of 0.50 mm/s with a 50 mm gauge length (corresponding to a constant strain rate of 0.01 s^{-1}). The thickness of each specimen was determined from the average

of three measurements taken along the gauge length with a Mitutoyo digital micrometer at a constant force of 0.5 N. The force–displacement data were converted to engineering stress versus engineering strain using the initial cross-sectional area and gauge length of the test specimen, respectively. Samples defined as "dry" were tested at ambient conditions of 25 °C and approximately 40-45% RH, while samples defined as "hydrated" were conditioned overnight in water and tested while fully saturated with water. Tensile testing under specific humidity conditions was conducted in an EnduraTEC Electroforce 3200 (ELF) with an environmental control chamber. Samples were cut to 4 mm x 30 mm and tested at a constant crosshead speed of 0.12 mm/s with a 0.12 mm gauge length (corresponding to a constant strain rate of 0.01 s^{-1}). The ELF testing grips were completely enclosed in a stainless steel chamber, which was controlled at 25 °C and 50% RH with a magnesium nitrate salt solution, as confirmed by a humidity gauge. Samples were equilibrated in a humidity chamber before being transferred to the testing chamber, and the chamber allowed to re-equilibrate for 1 min after reaching the desired relative humidity prior to being tested.

Swelling measurements were performed by cutting out approximately 10 mm x 10 mm specimens and measuring the precise length and width using a Mitutoyo digital caliper with 0.01 mm precision. Specimens were then placed in boiling water (maintained at 100 °C) for 2 hours, following the specifications set by MacKinnon et al.,[7] before being removed and re-measured using the digital calipers. The linear swelling was then defined as: swelling %=100% x $(L_s - L_0)/L_0$, where L_0 is the longer of the original length or width (at ambient humidity, 50% RH), and L_s is the corresponding swollen length or width of the specimen.

Transport Properties. Proton conductivity, unless otherwise noted, was measured in-plane using a custom machined poly(ether ether ketone) (PEEK) electrode with two platinum

wires spaced 1 cm apart. The samples were immersed in 18.2 MΩ deionized water before drying to ensure the removal of excess ions, and then dried and cut into approximately 1.5 cm x 2 cm rectangles and placed on top of a glass slide. The electrode was placed above the PEM specimen and clamped down to ensure good continuous connection between the wires and the sample membrane. Humidity was controlled using a chamber from Electro-tech Systems, Inc. Impedance values were determined by electrochemical impedance spectroscopy with a Solartron 1260 impedance analyzer, measuring from 1 MHz down to 1 Hz at room temperature.

Through-plane proton conductivity measurements were made using a two electrode Swagelok cell with two 12 mm diameter aluminum plates as electrodes.[32] The composite membrane testing specimens were soaked in deionized water and cut into 12 mm diameter disks. Excess water was removed from each sample with a laboratory tissue, and the specimen was placed between two 10 mm diameter fine wire meshes to decrease the contact resistance. Impedance values were determined using a Solartron 1260 impedance analyzer as described earlier; the membrane resistance was calculated as the total resistance minus the resistance contribution of the Swagelok cell and the two wire meshes.

Methanol permeability values were determined by using a dual chamber apparatus, where the membrane sample is the separator between pure methanol and water, as described previously.[21] The liquids in both chambers were stirred, and the increase in methanol concentration of the water as a function of time was determined by the changes in the refractive index of the solution using a Waters 2414 Refractive Index Detector.

Direct Methanol Fuel Cell Testing. The membrane electrode assemblies (MEA) were fabricated by sandwiching a 16 mm diameter circular cut-out composite PEM between two 12 mm diameter GDLs containing catalyst coating and hot-pressing at 135 °C and a force of 5 kN

for 5 minutes using a Carver Hot Press. Two 8 cm x 8 cm square gasket layers (250 μm thick PTFE-coated fiberglass sheets, VWR) were used to align the positions of the PEM and GDL during hot-pressing and to transfer the assembly to the DMFC. The MEAs were then tested using DMFC hardware obtained from Fuel Cell Technologies, Inc. Methanol (10% v/v in water) was fed to the anode at a flow rate of 4 mL/min using a peristaltic pump, and humidified air was supplied to the cathode at 60 mL/min. Polarization curves were generated from a Gamry PCI750 potentiostat connected to the DMFC hardware.

3.3 Results and Discussion

3.3.1 Composite PEM Fabrication

Figure 3-1 shows a diagram illustrating the main steps of composite PEM fabrication (electrospinning, spray-assisted LbL deposition, hot-pressing, and LbL capping), as well as a representative cross-sectional SEM of a completed composite membrane. The membrane solidity (defined as (1-porosity)) was found to increase up to ~70-80 % with 200-250 bilayers, at which point further increases in solidity with additional bilayers were not observed. In order to fill the remaining interstices of the fiber matrix (and thus create a denser composite membrane), the coated membranes were hydrated in deionized water and hot-pressed. This process allows the collapse of the remaining pore space between the hydrated, compliant coatings on fibers, thus increasing the overall PEM solidity.

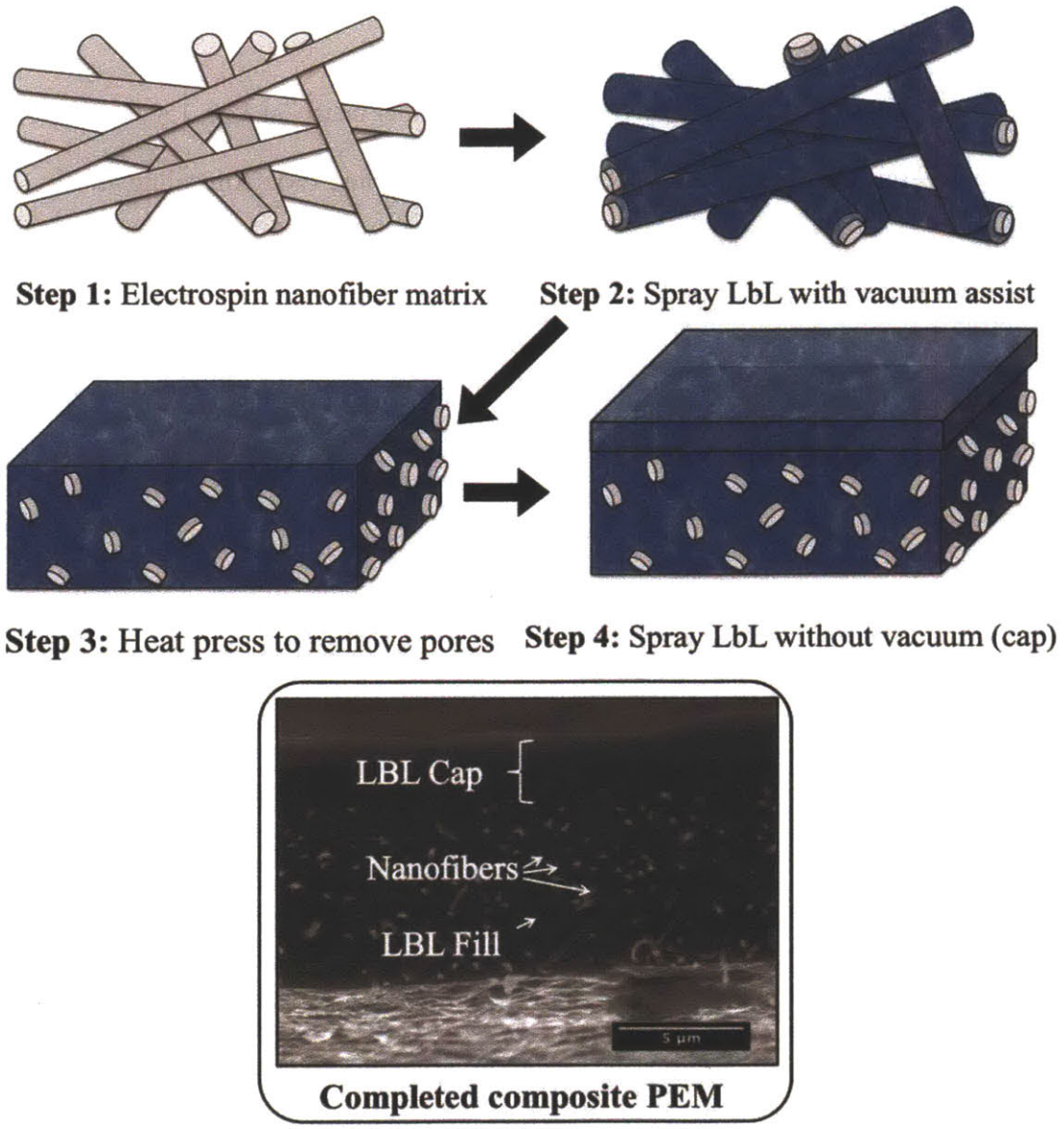

Figure 3-1. Diagram showing the steps used in fabricating the composite PEM: 1) electrospinning of nanofiber matrix (with optional thermal annealing); 2) spray-coat fibers with LbL polyelectrolytes using a vacuum assist; 3) heat press membrane to remove voids; 4) continue coating LbL without vacuum to provide a capping layer to top of PEM. The SEM micrograph is a cross-section of a typical composite PEM. The scale bar of the SEM micrograph is 5 µm.

Thermal annealing of the underlying electrospun fiber matrix at 130, 150, and 170 °C was used to improve the mechanical properties of the composite PEM. Annealing at temperatures close to the glass transition (T_g) of PA 6(3)T was found to increase the mechanical strength while increasing the solidity of uncoated EF mats from about 11-14%, for mats annealed below 150 °C, up to 35% for mats annealed at 170 °C.[29] After coating 200 bilayers of PDAC/sPPO using vacuum-assisted spray-LbL, all membranes plateaued at 68-76% solidity. We hypothesize that the residual porosity was due to closing off of unfilled pores prematurely ("bottle-necking") and non-uniformity of pressure drop through the entirety of the membrane. Hot-pressing of the hydrated membranes was used to push the membrane solidity up to 88-93%, with the EF mats originally annealed at 130 °C and 150 °C exhibiting the highest overall solidities after fabrication. Data for the solidity of the composite membranes after each step in the fabrication process, as a function of the annealing temperature of the EF mat prior to LbL deposition can be found in the Supporting Information (Figure 3-2). Although all of the composite membranes exhibit comparable solidities after hot-pressing, the ratio of LbL:EF for the 170 °C thermally annealed fiber mats is much lower than that of the other membranes.

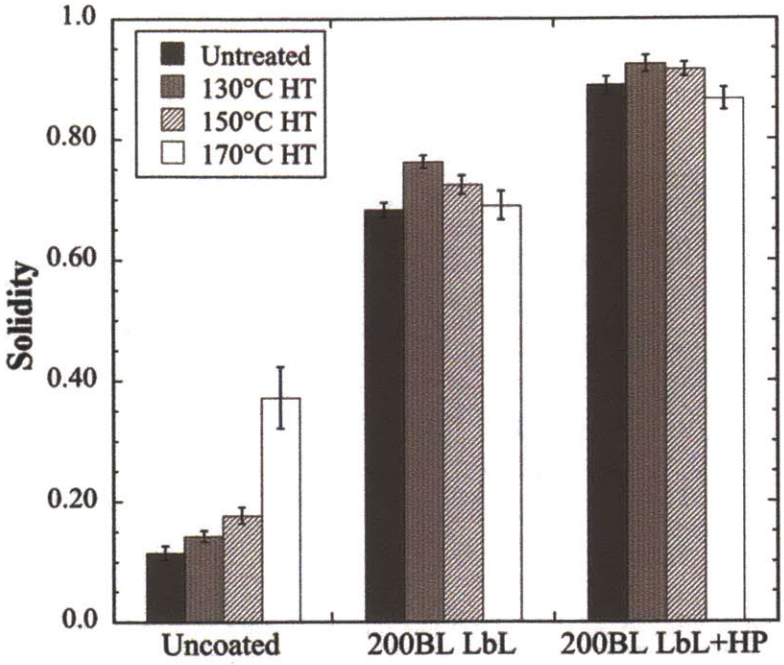

Figure 3-2. Histogram of solidity of PA 6(3)T EFMs annealed at various temperatures, after each step of the fabrication process: thermal treatment of uncoated EFM, after deposition of 200 bilayers (BL) of PDAC/sPPO, and after hot pressing (HP) of the hydrated composite membranes. Average fiber diameter was 463±[64] nm.

Representative SEM images of the composite PEM at different stages of fabrication are shown in Figure 3-3. PA 6(3)T nanofibers that have been conformally coated with 50 bilayers of PDAC/sPPO are shown in Figure 3-3a,b; there remains a significant amount of pore space between the coated fibers. SEM micrographs of a cross-section of the hot-pressed composite membranes with 250 bilayers of PDAC/sPPO sprayed with vacuum assist are shown in Figure 3-3c,d; the LbL film can be seen filling the interstices between the PA 6(3)T fibers due to compression of the hydrated LbL system into the void space during pressing. Before hot-

pressing, the composite membrane was an opaque, whitish color; after hydrating and hot-pressing, it turns clear, as a result of the elimination of residual air pockets that scatter light.

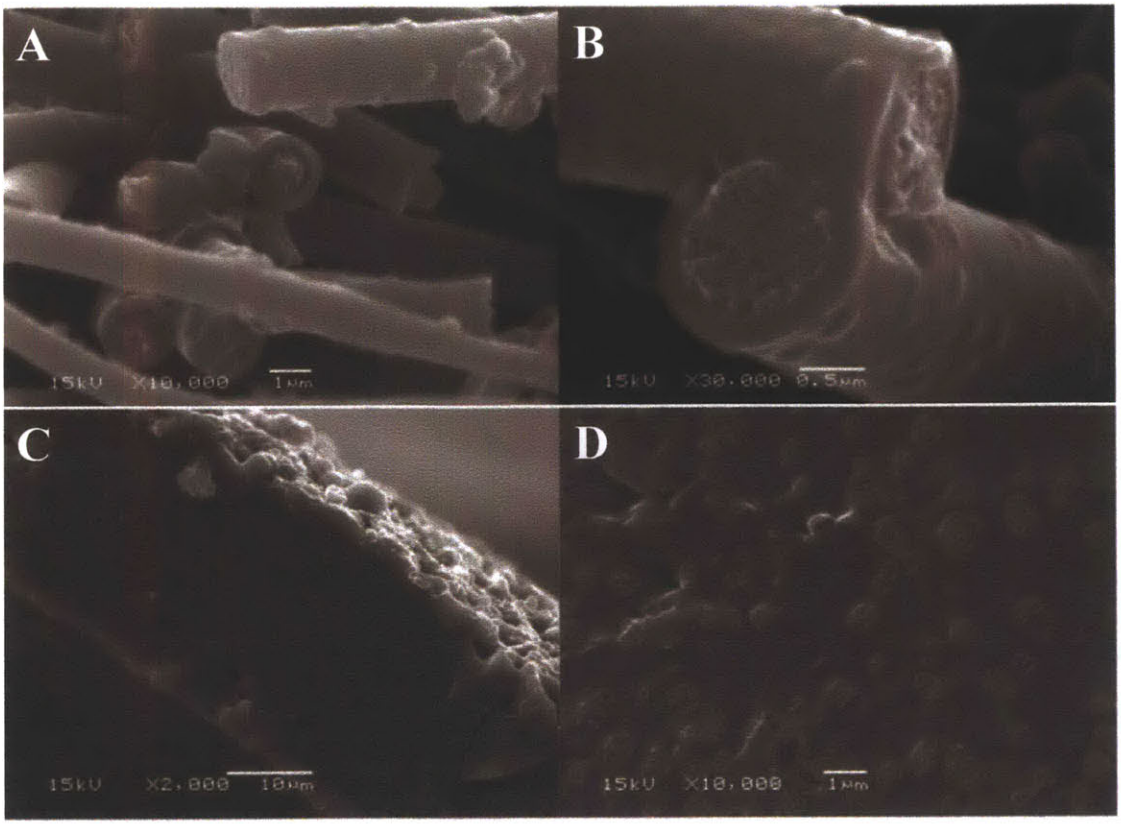

Figure 3-3. SEM micrograph of ~800 nm diameter PA 6(3)T fibers coated with 50 bilayers of PDAC/sPPO (A & B). SEM micrograph of composite PEM, consisting of PA 6(3)T fibers whose interstices are completely filled with PDAC/sPPO (250 BLs with vacuum assist) after being hot-pressed while hydrated. Scale bars for A & D are 1 μm; scale bar for B is 0.5 μm; scale bar for C is 10μm.

3.3.2 Mechanical Properties

We have previously shown that the mechanical properties of the composite LbL-EF membranes in the hydrated state depend primarily on the nonwoven fiber "endoskeleton", while

those of the composite membranes in the dry state are stiff and brittle, like the LbL film itself.[25] The mechanical properties of uncoated nanofiber mats have also been investigated extensively, and can be controlled by various post-spin treatments.[29,33,34] Annealing of the PA 6(3)T nanofiber mats, in particular, improves the mechanical properties of the EF mats by a factor of 5-6 fold over the as-spun mats. Here we show that these improvements survive hydration and are reflected in the composite PEMs as well.

Under dry conditions, the Young's moduli of the composite membranes range from 383 ± 43 MPa, for the composite PEM based on the unannealed PA 6(3)T EF mat, up to 482 ± 71 MPa, for the composite PEM based on the EF mat annealed at 150 °C. Yield stresses range from 8.9 ± 3.5 MPa to 12.3 ± 3.3 MPa for these same composite PEMs. The values for Young's modulus and yield stress are comparable to the values for the free-standing PDAC/sPPO film, at 610 ± 113 MPa and 12.8 ± 4.5 MPa, respectively. Even though the Young's moduli and yield stresses of the composite PEMs are greater than those of Nafion, all of the LbL systems exhibit brittle behavior at 25 °C and 50 %RH.

In an operational DMFC, the composite PEMs are in a hydrated state; therefore, tensile testing was also conducted on membranes that have been pre-conditioned in water for 24 hours and tested while hydrated. A summary of the improvements to the Young's moduli and yield stresses of the composite PEMs when hydrated as a function of the annealing temperature of the EF mat is shown in Table 3-1. An increase of up to 5-6 fold in the Young's modulus and yield stress of the hydrated composite PEM can be observed for the composite PEMs as a result of annealing the underlying PA 6(3)T fiber mat. The mechanical properties of the fully hydrated composite LbL-EF PEMs with various temperatures of heat treatment match that of the uncoated PA 6(3)T fibers mats under the same conditions, confirming that the mechanical response of the

composite PEM is controlled by the underlying electrospun mat. At 150 °C heat-treatment, the mechanical properties of the hydrated composite PEM are comparable to that of hydrated Nafion N112, with Young's moduli of 80.2 ± 9.9 and 74.3 ± 5.7 MPa, and yield stresses of 3.39 ± 0.37 and 5.56 ± 0.22 MPa, respectively.

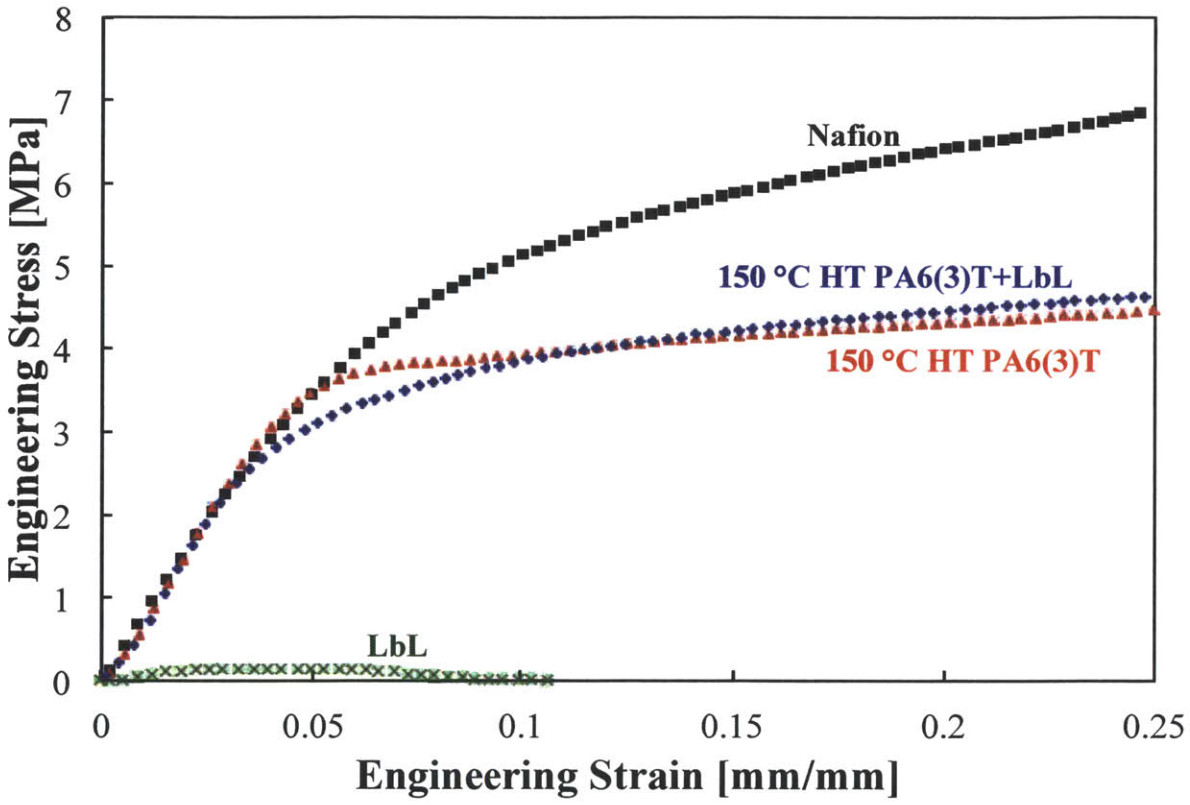

Figure 3-4. Representative stress-strain plots for hydrated membranes of: Nafion (black squares), 150 °C heat-treated PA 6(3)T nanofiber mat (red triangles), free-standing LbL film (green x's), and the composites of PA 6(3)T and using 150 °C heat-treated electrospun mat (blue diamonds).

Figure 3-4 compares the data for engineering stress vs. engineering strain for a typical composite membrane annealed at 150°C vs. Nafion in the hydrated state; included as well, for reference, are curves for a hydrated uncoated 150 °C heat-treated PA 6(3)T fiber mat and for a

free-standing LbL film. When hydrated, the free-standing LbL film becomes plasticized and pliable, thus losing most of its mechanical integrity. The yield stress drops to ~0.1 MPa and the Young's modulus drops to 1-2 MPa. Figure 3-4 shows that when coated onto the heat-treated PA 6(3)T electrospun fiber scaffold, the composite membrane exhibits the superior mechanical response of the underlying thermally treated EF mat. At low strains (<0.05 mm/mm), the mechanical response of the composite membrane is nearly identical to that of the hydrated Nafion membrane, and maintains its integrity through the plastic deformation region (>0.05 mm/mm).

The failure mechanisms of the coated fiber mats in both the dry and hydrated cases were observed during mechanical testing. In the dry case, cracking occurs along the LbL surface, exposing the underlying electrospun mat. In the hydrated case, the polyelectrolyte coating is able to deform with the rest of the mat without cracking, due to the ductile behavior of the LbL films when hydrated; this ductility was also observed in bare film testing. SEM micrographs of the fracture plane for composite membranes after tensile testing in both "dry" conditions and "wet" conditions are presented in Figure 3-5. The breaking mechanism for the dry samples is brittle fracture, as indicated by the minimal plastic deformation of the specimen before breaking and the very smooth conchoidal fracture (normal to the applied tension) (Figure 3-5a). The breaking mechanism for the wet samples is ductile rupture; the wet membrane exhibits significant necking and the fiber matrix deforms plastically before rupture, yielding a very rough fracture surface (Figure 3-5b). Consequently, the spray coated fiber mats exhibit greater toughness in the hydrated state relative to the free-standing PDAC/sPPO films, and are comparable to commercial proton exchange membranes such as Nafion.

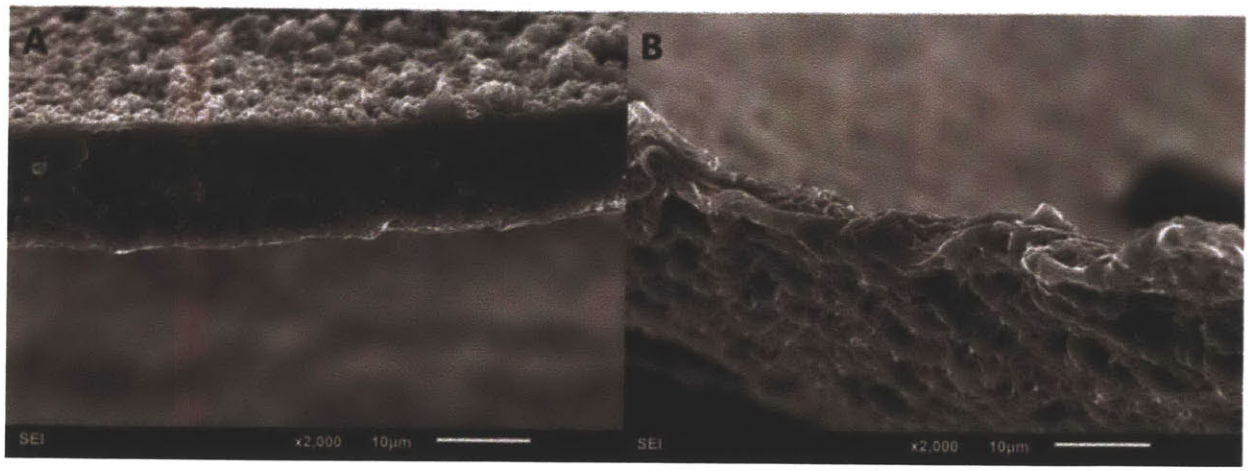

Figure 3-5. Representative SEM micrographs of composite LbL-electrospun fiber membrane fracture surfaces: A) "dry" membrane fracture plane indicating brittle fracture mechanism, B) "wet" membrane fracture plane showing thinning & plastic deformation during ductile rupture. The scale bar for each image is 10 μm.

3.3.3 Swelling Behavior

In an operational fuel cell, the PEM undergoes repeated swelling and de-swelling cycles, which can decrease significantly the lifetime of the membrane.[9,35] Perfluorosulfonic acid (PFSA)-based proton exchange membranes, such as Nafion, exhibit substantial swelling in water. Repeated hydration cycling often leads to mechanical failure and fracture, as a result of membrane thinning and pinhole formation;[9,36] therefore, PEMs that swell less offer some advantages in a fuel cell due to their potential for increased service lifetime. Figure 3-6 shows that the composite membranes fabricated in this work have significantly greater dimensional stability than both Nafion and the pristine LbL film during a swelling experiment under the same conditions. We hypothesize that the significant decrease in linear swelling for the composite

PEM is due to constraint of the LbL film within the electrospun fiber matrix; the LbL film is electrostatically bound to the fiber surfaces and is unable to expand freely because the film is mechanically weaker than the electrospun fibers. This hypothesis explains why the linear swelling decreases with increasing annealing temperature of the underlying EF mat. Figure 3-6 also shows a comparison of the tensile strain-to-break of the PEMs at 50% RH and 25 °C. The composite membranes exhibited both a moderate increase in the strain to break at 50% RH (0.06 mm/mm for the free-standing LbL to 0.10 mm/mm for the composite system), and a more than three-fold decrease in the linear swelling (from 0.17 mm/mm for the free-standing LbL to 0.03-0.05 mm/mm for the composite PEM), compared to the pristine LbL film. The linear swelling strains of all of the LbL systems were found to be significantly lower than Nafion, which swelled to 0.36 ± 0.04 mm/mm, nearly an order of magnitude larger than the composite PEMs. A summary of the strain to break and linear swelling properties can be found in Table 3-1.

Table 3-1. Summary of Mechanical and Swelling Properties of Composite PEM at 25 °C.

	Young's Modulus (100% RH) [MPa]	**Yield Stress (100% RH) [MPa]**	**Strain at Break (50% RH) [mm/mm]**	**Linear Swelling[a] [mm/mm]**	**Hydration Stability Factor[b] (HSF)**	**Hysteresis[c] (1 Swelling Cycle) (100% RH) [%]**
PDAC/sPPO Film	1.70 ± 0.95	0.11 ± 0.04	0.06 ± 0.02	0.16 ± 0.02	0.34 ± 0.11	N/A
As-spun+LbL	36.1 ± 5.1	1.07 ± 0.14	0.10 ± 0.02	0.05 ± 0.01	1.84 ± 0.35	47.5 ± 6.3
130 °C HT+LbL	52.1 ± 10.8	1.69 ± 0.10	0.09 ± 0.01	0.04 ± 0.01	1.97 ± 0.31	36.8 ± 5.6
150 °C HT+LbL	80.2 ± 9.9	3.39 ± 0.37	0.09 ± 0.01	0.03 ± 0.01	2.76 ± 0.37	37.0 ± 5.2
170 °C HT+LbL	197.7 ± 54.2	6.51 ± 0.63	0.07 ± 0.01	0.03 ± 0.01	2.64 ± 0.37	39.2 ± 5.4
Nafion® N112	74.3 ± 5.7	5.56 ± 0.22	1.56 ± 0.15	0.36 ± 0.04	4.28 ± 0.40	62.9 ± 3.9

[a] Subjected to boiling water (100 °C) for 2 hours

[b] Ratio of strain at break [mm/mm] to linear swelling [mm/mm]

[c] Each sample extended to its corresponding linear swelling strain

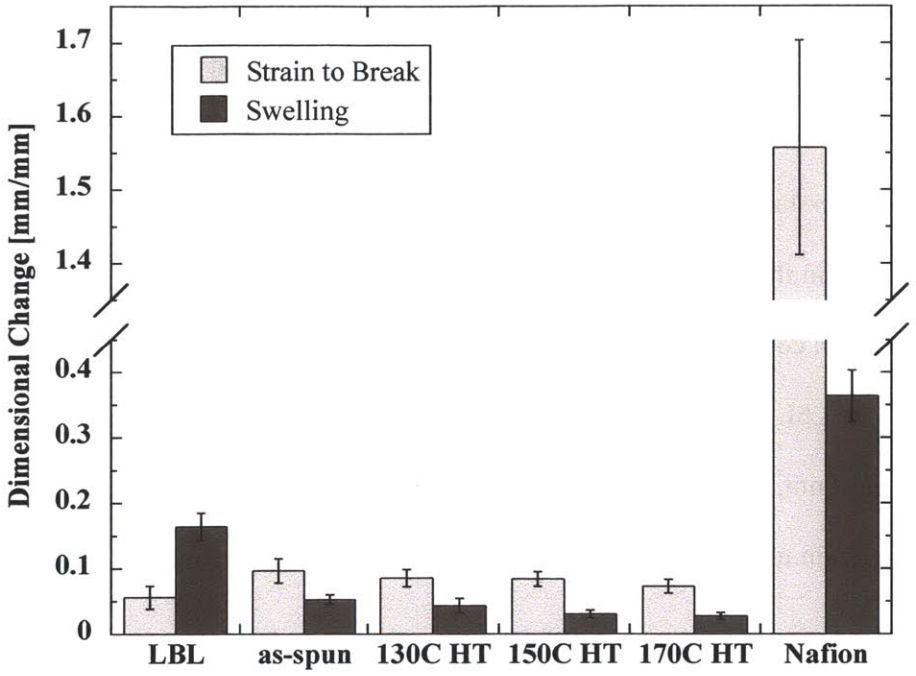

Figure 3-6. Dimensional change in the strain to break (at 50% RH) and linear swelling of composite PEMs and Nafion.

The mechanical durability of a PEM in a hydrated fuel cell is directly linked to its tensile strain to break and its linear swelling in the same direction after exposure to liquid water. Membranes undergo significant swelling when humidified, and may fail mechanically if membrane stresses experienced during hydration cycling exceed the tensile strength of the membrane; therefore, larger membrane breaking strains are desirable. The hydration stability factor is a metric that was proposed recently for characterizing the likelihood that a membrane can withstand repeated humidity cycling;[7] it is defined as:

$$\text{HSF} = \frac{\text{strain at break [mm/mm] (25 °C,50 \%RH)}}{\text{linear swelling [mm/mm] (100 °C in } H_2O\text{)}} \quad (1)$$

This metric has proven to be a convenient measure for assessing various membranes and for predicting their relative durability in the accelerated mechanical humidity cycling test. Figure 3-7a shows the HSF of the composite membranes as well as the HSF of the free-standing LbL film and of Nafion. A value of HSF<1 indicates that the membrane is not robust enough to survive even one humidity cycle, which highlights the weakness of the free-standing PDAC/sPPO film, whose HSF is 0.34 ± 0.11. All of the composite LbL-EF membranes are seen to have HSF values that are 5-6 times larger than that for the free-standing LbL, and only ~30% or so less than Nafion; these results indicate that the composite LbL-EF PEMs possess sufficient mechanical integrity to withstand humidity cycling in an operational fuel cell.

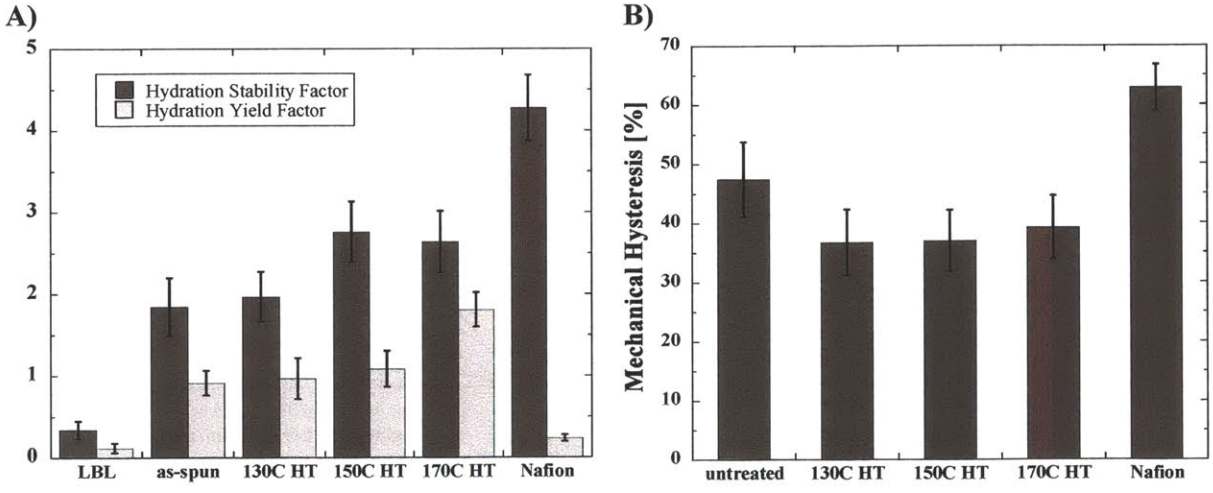

Figure 3-7. (A) Comparison of hydration stability factor and hydration yield factor for the free-standing LbL film, composite PEMs made with EF mats annealed at different temperatures, and Nafion. (B) Comparison of the mechanical hysteresis for composite PEMs made with EF mats annealed at different temperatures and Nafion.

The comparable values of HSF for the composite PEMs and Nafion suggest that the LbL-EF membranes may exhibit humidity fatigue cycling lifetimes similar to Nafion; however, the HSF does not fully capture the significant advantage of the dimensional stability (reduced linear swelling) of the composite PEMs in this work. A comparison of the single load-unload stress-strain curves for Nafion and the composite LbL-EF membrane under extension can be found in Figure 3-8a. The membranes are extended up to a total strain equivalent to its linear swelling deformation in boiling water. It is important to note that the strain reached by Nafion upon swelling (~0.36 mm/mm after 2 hrs in water at 100°C) extends well beyond the yield point (~0.08 mm/mm at 25°C, RH=50%) of Nafion. A membrane that is repeatedly deformed beyond the yield point loses its mechanical integrity irreversibly, increasing the likelihood of mechanical failure within an operational fuel cell.[33]

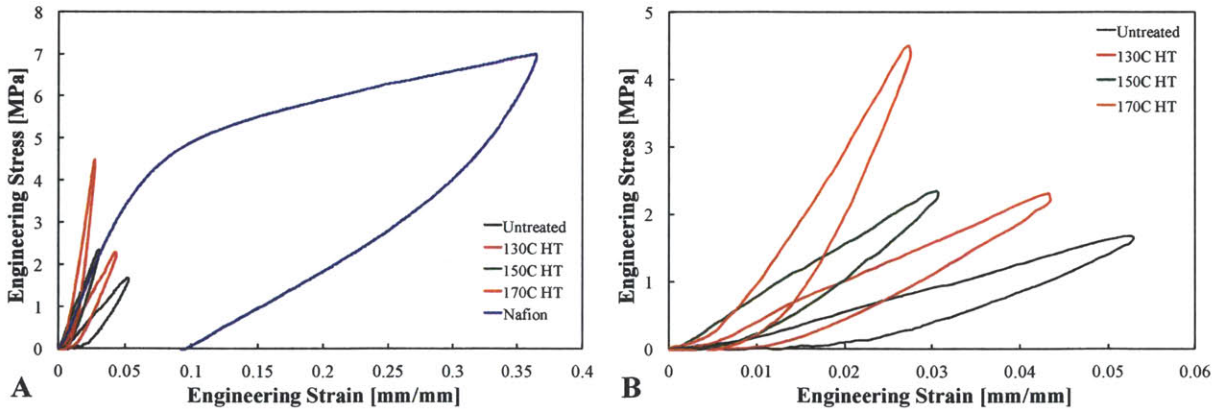

Figure 3-8. Single load-unload mechanical hysteresis stress-strain plots of Nafion and PA6(3)T+LbL (A), and a close-up of the composite PA 6(3)T+LbL membranes (B). Each sample was extended to their respective mean swelling strain. All tests conducted at 100% RH.

To better evaluate the extent of the irreversible deformation a membrane would experience with each swelling cycle, we propose the following "hydration yield factor", which we define as

$$\text{Hydration Yield Factor} = \frac{\text{yield strain [mm/mm](25 °C, 50 \%RH)}}{\text{linear swelling [mm/mm] (100 °C in } H_2O)} \quad (2)$$

If the hydration yield factor is greater than 1, then the swelling occurs mostly within the elastic regime, and strains associated with repeated cycling should be mostly recoverable; however, if the hydration yield factor is less than 1, then the sample deforms plastically during each cycle; the more the ratio is below one, the greater the permanent deformation exhibited by the membrane during hydration cycling. All of the composite PEM's exhibit hydration yield factors of ~1 or higher (1.09 ± 0.22 for the 150 °C annealed sample), indicating that the strains induced in the membranes by swelling are equal to or slightly below the yield point, and thus mostly recoverable, as shown in Figure 3-7b. The hydration yield factor of Nafion is found to be 0.24 ± 0.04, which corresponds to large plastic (unrecoverable) deformation after each swelling cycle.

To quantify the energy loss during a swelling cycle, the mechanical hysteresis for a single cycle of loading and unloading (up to the measured swelling strain) was determined for each sample and compared to that of Nafion (Figure 3-8b). The area contained between the load-unload curves is an indication of the work performed on the membrane with each swelling cycle; Nafion exhibits significantly larger hysteretic losses compared to the LbL-EF membranes. A quantitative comparison of the percent of mechanical hysteresis for each type of PEM is shown in Figure 3-7b. All of the composite LbL-EF membranes exhibit lower percent mechanical hystereses relative to that of Nafion. The composites of 130 °C and 150 °C heat-treated PA 6(3)T

and LbL exhibit the lowest hysteretic losses, at 36.8 ± 5.6 % and 37.0 ± 5.2 %, respectively, compared to 62.9 ± 3.9 % for Nafion. The greater dimensional stability and lower mechanical hysteresis indicate the potential for longer operational lifetimes of the composite LbL-EF proton exchange membranes relative to Nafion.

3.3.4 Transport Properties

In-plane conductivities of the composite PEMs assembled using the various thermally treated PA 6(3)T electrospun scaffolds and of the free-standing LbL-deposited film were measured to quantify their dependence on humidity (see Figure 3-9a). All of the composite PEMs and the pristine LbL film show similar humidity dependence; the proton conductivity improves by approximately an order of magnitude with every 20% increase in the relative humidity, indicating that the proton conduction mechanism of the LbL films is not significantly affected by the assembly method or by the supporting scaffold. The PA 6(3)T electrospun mats (80 μm thick) annealed at 130°C yielded composite PEMs with a protonic conductivity several times higher than those annealed at 150 °C or 170 °C. The slight porosity decrease of the fiber mats is not enough to explain the significant drop in ion transport with the higher annealing temperatures. This difference in the conductivity is most likely due to difficulty in coating mats comprising merged fibers and weld points, which are believed to exacerbate bottle-necking of the spray-LbL before complete filling of pore space. Lower total resistances and a reduction of bottle-necking can be achieved by utilizing thinner proton exchange membranes in DMFCs and in the composite LbL-EF PEMs. Figure 3-9b shows the effect of using electrospun mats of various thicknesses (80, 60, 40, and 25 μm thick before coating and pressing) for fabrication of the composite PEM. All of these PA 6(3)T mats were annealed at 150 °C. The thinner membranes exhibited increased protonic conductivity due to more complete impregnation with

polyelectrolytes; when fully hydrated, the thinnest membrane (25 μm) exhibits protonic conductivity comparable to that of a pure LbL film.

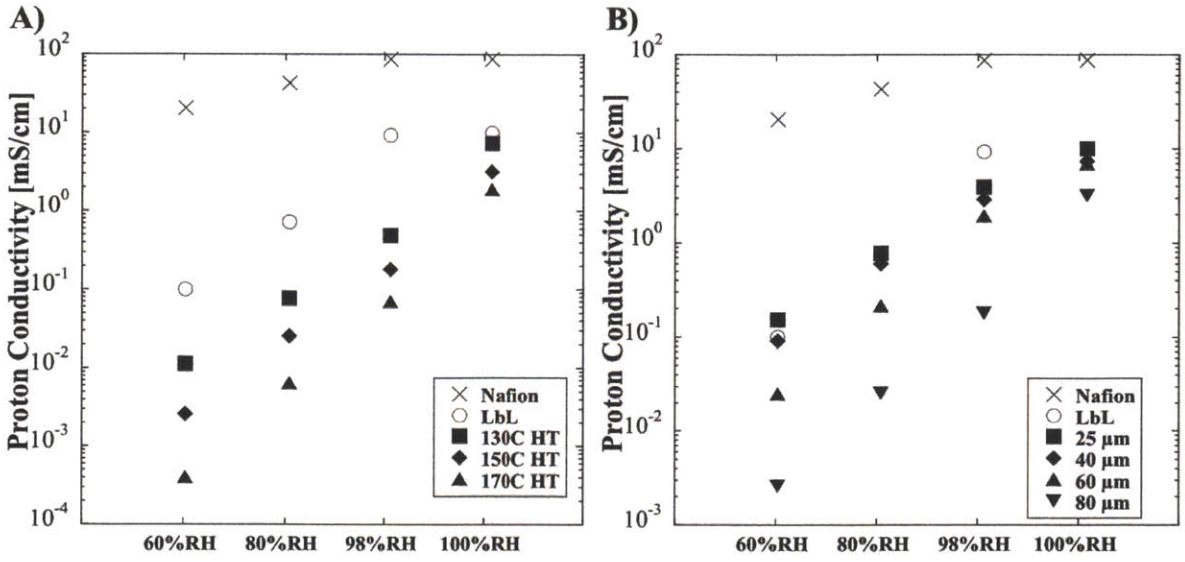

Figure 3-9. Humidity dependence of the in-plane proton conductivity of (A) the composite PEMs assembled on various thermally treated EFMs (80 μm thick before annealing) and free-standing LbL film and (B) the proton conductivity for different composite PEM thickness (150 °C heat-treated samples). The in-plane proton conductivity of Nafion (N112) is included for reference.

To observe the effect of adding the capping layer on conductivity, the through-plane and in-plane conductivities were measured for uncapped and capped PEMs (see Figure 3-10). While the in-plane conductivity of the capped PEM (7.7 ± 0.4 mS/cm) showed a marked, four-fold increase over that of the uncapped PEM (1.6 ± 0.1 mS/cm), the through-plane conductivity of the capped PEM (7.0 ± 0.3 mS/cm) was comparable to that of the uncapped PEM (6.9 ± 0.4 mS/cm). We hypothesize that the uncapped composite PEM had a low in-plane conductivity due to proton transport occurring along the length of the electrospun fibers, which are randomly aligned, and

that the large increase in the in-plane conductivity after the addition of the capping layer was the result of the conduction through the capping LbL film. Conversely, the uncapped composite PEM exhibited a high through-plane conductivity because the LbL films were already well connected through the thickness of the fiber matrix as a result of the vacuum-assisted LbL deposition process and the subsequent hot-pressing. The capping process does not alter significantly the through-plane ionic conductivity of the mat. Note that despite the anisotropic morphology of the capped composite PEM, the conductivity through-plane and in-plane are quite similar. This is in contrast to Nafion membranes, which exhibit through-plane conductivities between 1/3 to 1/4 of their in-plane conductivities.[4]

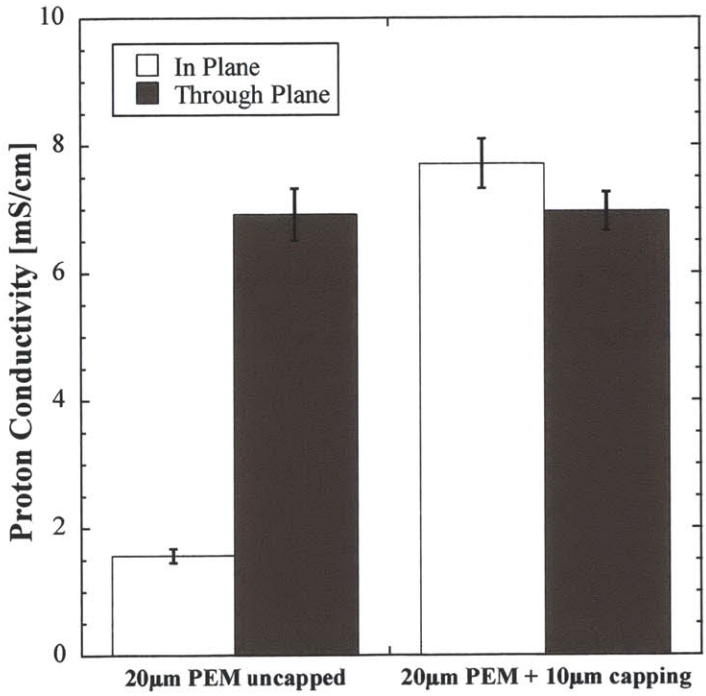

Figure 3-10. Comparison of in-plane and through-plane proton conductivity of uncapped (20 μm thick) and capped (30 μm thick) composite PEMs. Samples tested at 25 °C and 100% RH.

While the through-plane proton conductivity of the composite PEM provides an indication of the membrane's ability to sustain high currents in a fuel cell, its methanol permeability ultimately determines its potential use for DMFC applications. Lower crossover limits fuel loss and permits the use of a higher methanol feed concentration. This in turn leads to a higher overall cell voltage, power density and efficiency. In the context of DMFCs, "selectivity", is defined as the ratio of proton conductivity to methanol permeability, and is a useful metric for predicting the performance of a PEM.[7] Protons and methanol have similar molecular transport mechanisms in sulfonic acid-containing PEMs. As a consequence, it is generally difficult to improve membrane selectivity significantly, even with substantial modifications to the membrane's ion content, water content, or polymer chemistry, architecture or morphology.[4] LbL assembled PDAC/sPPO films exhibit methanol permeabilities two orders of magnitude lower than that of Nafion due to the light cross-linking between PDAC and sPPO. It is therefore possible to decrease the methanol crossover of the composite PEM significantly (by capping), while maintaining a reasonable through-plane conductivity. Table 3-2 shows a summary of the through-plane proton conductivity, methanol permeability and calculated selectivity of the composite PEM from this work, compared with Nafion and highly selective composite PEMs reported in the literature. The capped composite PEM was made from an 18 μm thick EF mat that was thermally treated at 130 °C, coated by the vacuum assisted spray LbL method and subsequently capped with 5 μm of PDAC/sPPO on both sides. The resultant PEM had a through-plane conductivity one fourth that of Nafion (7 vs. 26 mS/cm) and methanol permeability twenty times lower than that of Nafion (9.7 vs. 198 x 10^{-8} cm^2/s). The result is a selectivity five and a half times greater than that of Nafion (7.2 vs. 1.3 x 10^7 $mS \cdot sec/cm^3$) and greater than that of all the highly selective composite PEMs listed in Table 3-2. Taking into

consideration the thickness of the composite membrane (30 μm) relative to that of the Nafion membrane typically used in a DMFC (180 μm), the composite PEM's conductance (conductivity / thickness) is 60% higher than that of Nafion, and its permeance (permeability / thickness) is still 3.4 times lower than that of Nafion.

Table 3-2. Summary of Transport Properties of Composite PEMs.

Membrane	Through-plane Proton Conductivity* (σ) [mS/cm]	MeOH Permeability ($Px10^8$) [cm^2/s]	Selectivity ($S=\sigma/Px10^8$) [$mS \cdot sec/cm^3$]
PA6(3)T+PDAC/sPPO (~10 μm cap/30 μm) [this work]	7.0	9.7	0.72
Nafion N112[4]	26	198	0.13
Sulfonated poly(styrene-b-ethylene-r-butadiene-b-styrene) block copolymer[37]	23	82	0.28
Phosphotungstic acid/poly(vinyl alcohol) composite[38]	6	45.4	0.13
Nafion/poly(vinyl alcohol) blend[39]	20	65	0.31
PVOH/PVP blend[40]	1.4	10	0.14
SPEEK/cyclodextrin[41]	48	76	0.63

* tested at 100 %RH

3.3.5 DMFC Performance

Despite the attractive characteristics of the composite PEM, fabrication of a membrane electrode assembly (MEA) using the composite PEM proved to be a challenge. This difficulty was traced to incomplete bonding of the PEM to the electrode during MEA assembly. The difficulty in determining optimum hot-pressing conditions for adhesion of the PEM to the

catalyst layers was exacerbated by the incompatible thermal expansion and swelling of the composite PEM versus the catalyst, which has a Nafion binder, especially upon drying. The Pt catalyst-coated GDL (cathode side) was found to adhere well to the LbL-EF composite PEM after MEA hot-pressing; however, the Pt/Ru catalyst-coated GDL (anode side) was found to delaminate frequently from the PEM, leading to increased cell resistances and greatly reduced catalyst activation. This problem has been observed previously with other Nafion-free PEMs.[42] Cross-sectional SEM micrographs of the MEA showing the delamination of the Pt-Ru catalyst side can be found in the Figure 3-11.

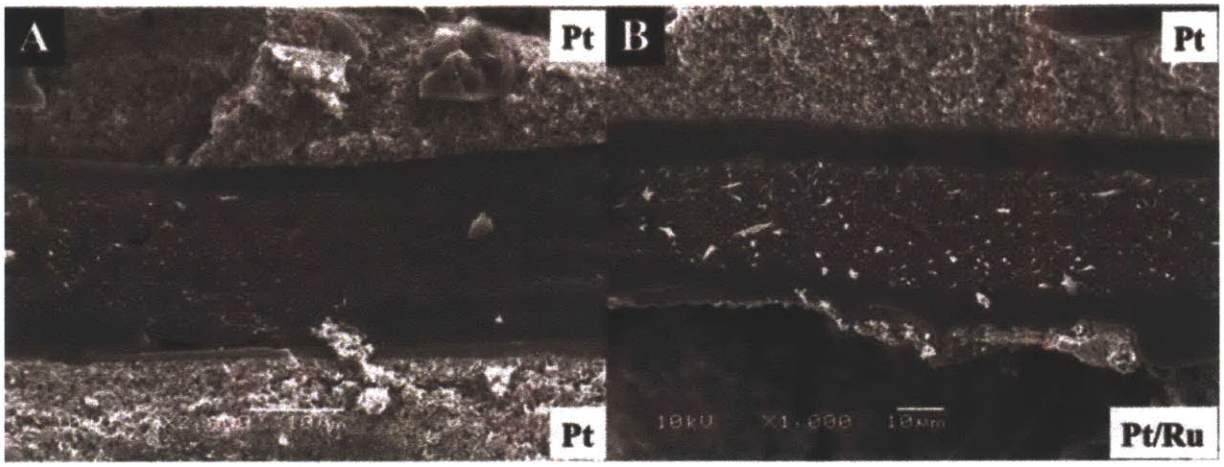

Figure 3-11. Cross-sectional SEM of MEA showing catalyst layer, PEM (with top & bottom capping layers), and Nafion binder. (A) PA 6(3)T+LbL composite PEM sandwiched between two Pt catalyst GDLs exhibiting good adhesion on both sides, (B) PA 6(3)T+LbL sandwiched between a Pt (Cathode) and Pt/Ru (Anode) GDL exhibiting fracture on the anode side leading to poor DMFC performance (scale bar for each micrograph is 10μm).

Several techniques to remedy the MEA delamination were attempted; these included adjusting the hot-pressing conditions (temperature, time, wet or dry PEM), adding a thin layer of Nafion paint as binder, coating catalyst directly onto the PEM, or even synthesizing a custom batch of Pt/Ru catalyst slurry using PDAC/sPPO as the polymer binder. A summary of several of the various MEA construction methods and catalysts used are shown in Table 3-3 along with the resultant cell resistances and comments on whether methanol penetrated through the membrane. In each case, the MEA exhibited higher cell resistances and/or higher methanol crossover than expected. However, some trends were observed to reduce cell resistances. Hot-pressing was observed in all situations to improve contact and, on average, reduced resistances by half. However, hot-pressing while wet led to increased methanol crossover, which we believe was due to failure of the capping layer. Wet assembly of the cell (either by depositing the ink on the membrane or by using wet membranes) further improves contact and prevents delamination (upon drying), but the membranes again tend to exhibit methanol crossover. Use of excess Nafion paint helped reduce the methanol crossover, but not completely. These techniques for improving connection typically have little effect in Nafion based systems, further proof that it is the difference in properties of the composite membrane (i.e. mechanical properties, swelling and flow behavior) versus Nafion that is responsible for the high resistances.

Table 3-3. Summary of MEAs.

Membrane Condition	**Anode Catalyst**[a]	**Hot Press**	**Area-Normalized Cell Resistance**[b] **[$\Omega \cdot cm^2$]**	**Comments**
Wet	None	n/a	0.43	Resistance of membrane alone
Dry flat	Pt/Ru (E-TEK)	No	20.65	Fuel blocking
Dry flat	Pt/Ru (E-TEK)	Yes	12.31	Fuel blocking

Dry flat	Pt/Ru (wet deposit)	No	11.80	Fuel break-through
Dry flat	Pt/Ru (wet deposit)	Yes	6.01	Fuel break-through
Wet	Pt/Ru (E-TEK)	No	7.96	Fuel break-through
Wet	Pt/Ru (custom ink)	No	5.21	Fuel break-through
Wet	Pt/Ru (E-TEK)	Yes	3.47	3x Nafion paint, reduced break-through
Dry flat	Pt (E-TEK)	Yes	3.01	Fuel blocking

[a] Pt (E-TEK) used as cathode catalyst for all MEAs

[b] Defined as the cell resistance times the effective area of the cell (1.13 cm^2)

Since we were not successful in integrating the Pt/Ru catalyst into the MEA containing the composite LbL-EF PEM, an alternative system consisting of Pt-catalyst coated GDL sandwiched around both sides of the PEM was used to obtain a relative measure of the DMFC performance. The activation energy of methanol oxidation with Pt catalyst is higher than that with Pt/Ru catalyst, resulting in lower fuel efficiency; however, the PEM transport should be unaffected. Comparison of the overall performance of this MEA with the composite PEM to that of an MEA constructed using Nafion and the same Pt(anode)/Pt(cathode) catalyst assembly provides a useful measure of the relative operational DMFC performance. Figure 3-12 shows voltage-current polarization curves as well as a power density curve for a 100 μm thick Nafion PEM and a 25 μm thick LbL-EF composite PEM in a DMFC using 10 wt.% methanol in water as the fuel and tested at 25 °C. The MEA with composite PEM exhibits comparable open circuit voltage (OCV) to the MEA with Nafion (270 mV vs. 257 mV), indicating that methanol is blocked as efficiently by the thinner composite PEM. The MEA with composite PEM also draws a current of 5.8 mA at 100 mV, compared to 9.4 mA at 100 mV for the MEA with Nafion. Even with the Pt catalyst, the total cell resistance was greater than expected, based on the sum of the area-normalized resistances in series for the individual components (electrode, PEM, charge collector) (3.01 $\Omega \cdot cm^2$ measured vs. ~0.6 $\Omega \cdot cm^2$ estimated from components alone). From this,

we conclude that the contact resistances between components are high, which we attribute to poor adhesion between the PEM and electrode, indicating that the PEM adhesion to the electrode was still not optimal. It is possible that the DMFC performance of the composite PEM could be further improved with the development of a custom catalyst and binder system for optimized compatibility with the composite PEM, but this is beyond the scope of the current study.

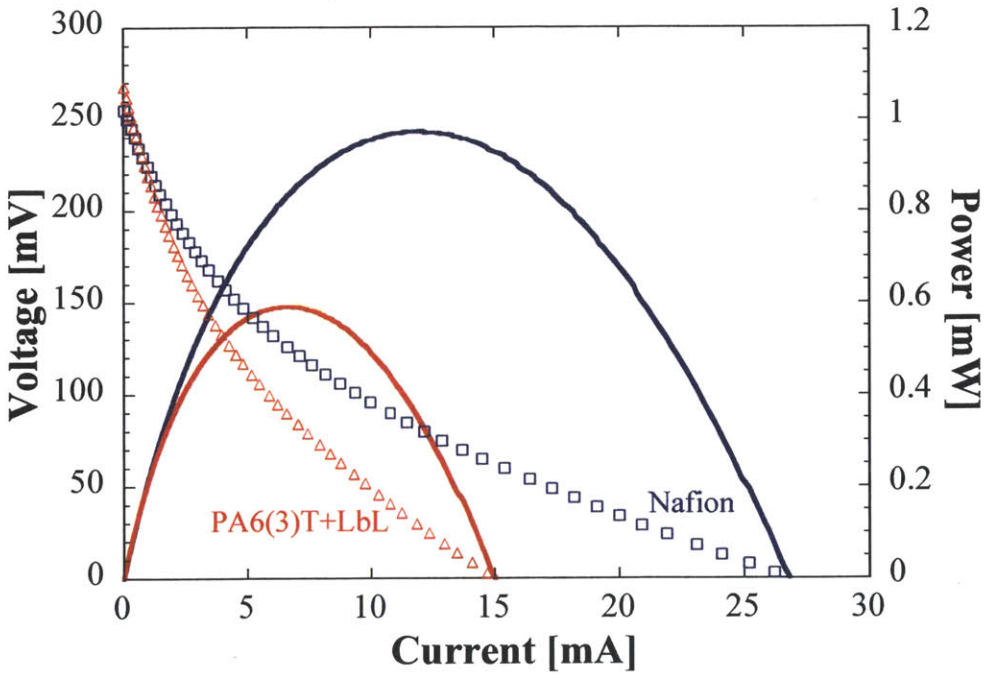

Figure 3-12. V-I polarization curves for Nafion and PA6(3)T+LBL composite membrane using Pt catalyst for both the anode and cathode GDL in 10 wt.% methanol/water mixture.

3.4 Conclusion

Composite membranes of highly conductive LbL films and electrospun fiber mats were fabricated and characterized for mechanical strength and electrochemical selectivity. To create a

proton-conducting, fuel-blocking layer and to fill in the void space throughout the porous electrospun fiber matrix, the spray-LbL assembly method with and without vacuum was used to form LbL films rapidly. These membranes consist of highly selective poly(diallyl dimethyl ammonium chloride)/sulfonated poly(2,6-dimethyl 1,4-phenylene oxide) (PDAC/sPPO) thin films. The mechanical properties of the spray coated electrospun fiber mats are shown to improve with increasing temperature of thermal annealing of the underlying electrospun scaffold. The composite PEMs exhibited a Young's modulus of 80.2 MPa and a yield stress of 3.39 MPa when the EF mat was annealed at 150 °C, comparable to the mechanical properties of Nafion under the same testing conditions. Modifications to the mechanical response of the composite PEM were achieved by thermal treatment of the underlying EF mat. The composite PEMs also swell less than Nafion under hydration cycling; the greater dimensional stability also means lower mechanical hysteresis under hydration cycling, which promises longer operational lifetimes. The composite PEM also exhibited through-plane proton conductivity as high as 7 mS/cm at 100 %RH and methanol permeability as low as 9.7×10^{-8} cm^2/sec, indicating a membrane selectivity of 7.2×10^7 $mS \cdot sec/cm^3$; this is over five times greater than the selectivity of Nafion. The composite proton exchange membranes were also tested in an operational direct methanol fuel cell. These results show the potential for higher OCVs (270 mV vs. 257 mV) and comparable cell resistances when compared to Nafion when using Pt/Pt catalyst for both the anode and the cathode.

3.5 References

[1] De Brujin, F. *Green Chem.* **2005**, *7*, 132-150.

[2] Ulbricht, M. *Polymer* **2006**, *47*, 2217-2262.

[3] Chalk, S. G.; Miller, J. F. *J. Power Sources* **2006,** *159*, 73-80.

[4] Deluca, N. W.; Elabd, Y. A. *J. Polym. Sci., Part B: Polym. Phys.* **2006**, *44*, 2201-2205.

[5] Mauritz, K. A.; Moore, R. B. *Chem. Rev.* **2004**, *104*, 4535-4585.

[6] Lai, Y.-H.; Mittelsteadt, C. K.; Gittleman, C.S.; Dillard, D. A. *J. Fuel Cell Sci. Technol.* **2009,** *6*, 021002.

[7] MacKinnon, S. M.; Fuller, T. J.; Coms, F. D.; Schoenweiss, M. R.; Gittleman, C. S.; Lai, Y.-H.; Jiang, R.; Brenner, A. M. *Encyclopedia of Electrochemical Power Sources* **2009,** 741-754.

[8] Silberstein, M. N.; Pillai, P. V.; Boyce, M. C. *Polymer* **2011,** *52*, 529-539.

[9] Silberstein, M. N.; Boyce, M. C. *J. Power Sources* **2011**, *196*, 3452-3460.

[10] Liu, F. Q.; Yi, B. L.; Xing, D. M.; Yu, J. R.; Zhang, H. M. *J. Membr. Sci.* **2003**, *212*, 213-223.

[11] Nouel, K. M.; Fedkiw, P. S. *Electrochim. Acta* **1998**, *43*, 2381-2387.

[12] Chalkova, E.; Fedkin, M.V.; Wesolowski, D. J.; Lvov, S. N. *J. Electrochem. Soc.* **2005,** *152*, A1742-A1747.

[13] Yang, C.; Costamagna, P.; Srinivasan, S.; Benziger, J.; Bocarsly, A. B. *J. Power Sources* **2001**, *103*, 1-9.

[14] Liu, Y.-H.; Yi, B.; Shao, Z.-G,; Xing, D.; Zhang, H. *Electrochem. Solid-State Lett.* **2006**, *9*, A356-A359.

[15] Chikh, L.; Delhorbe, V.; Fichet, O.; *J. Membr. Sci.* **2011**, *368*, 1-17.

[16] Cai, H.; Shao, K.; Zhong, S.; Zhao, G.; Zhang, G.; Li, X.; Na, H. *J. Membr. Sci.* **2007**, *297*, 162-173.

[17] Chang, Y.-W.; Wang, E.; Shin, G.; Han, J.-E.; Mather, P. T. *Polym. Adv. Technol.* **2007,** *19*, 535-543.

[18] Piboonsatsanasakul, P.; Wootthikanokkhan, J.; Thanawan, S. *J. Appl. Polym. Sci.* **2008**, *107*, 1325-1336.

[19] Yun, S.-H.; Woo, J.-J.; Seo, S.-J.; Wu, L.; Wu, D.; Xu, T.; Moon, S.-H. *J. Membr. Sci.* **2011**, *367*, 296-305.

[20] Farhat, T. R.; Hammond, P. T. *Adv. Funct. Mater.* **2005,** *15*, 945-954.

[21] Argun, A. A.; Ashcraft, J. N.; Hammond, P. T. *Adv. Mater.* **2008,** *20*, 1539-1543.

[22] Decher, G. *Science* **1997,** *277*, 1232-1237.

[23] Hammond, P. T. *Adv. Mater.* **2004,** *16*, 1271-1293.

[24] Ashcraft, J. N.; Argun, A. A.; Hammond, P. T. *J. Mater. Chem.* **2010,** *20*, 6250-6257.

[25] Liu, D. S.; Ashcraft, J. N.; Mannarino, M. M.; Silberstein, M. N.; Argun, A. A.; Rutledge, G. C.; Boyce, M. C.; Hammond, P. T. *Adv. Funct. Mater.* **2013,** *23,* 3087-3095.

[26] Doshi, J.; Reneker, D. H. *J. Electrost.* **1995,** *35*, 151-160.

[27] Rutledge, G. C.; Fridrikh, S. V. *Adv. Drug Delivery Rev.* **2007,** *59*, 1384-1391.

[28] Fridrikh, S. V.; Yu, J. H.; Brenner, M. P.; Rutledge, G. C. *Phys. Rev. Lett.* **2003,** *90*, 144502.

[29] Mannarino, M. M.; Rutledge, G. C. *Polymer* **2012,** *53*, 3017-3025.

[30] Krogman, K. C.; Lowery, J. L.; Zacharia, N. S.; Rutledge, G. C.; Hammond, P. T. *Nat. Mater.* **2008,** *8*, 512-518.

[31] Pappas, D.; Bujanda, A.; Demaree, J. D.; Hirvonen, J. K.; Kosik, W.; Jensen, R.; McKnight, S. *Surf. Coat. Technol.* **2006**, *201*, 4384-4388.

[32] Guyomard, D.; Tarascon, J. M. *J. Electrochem. Soc.* **1992,** *139*, 937-948.

[33] Pai, C.-L.; Boyce, M. C.; Rutledge, G. C. *Polymer* **2011,** *52*, 6126-6133.

[34] Silberstein, M. N.; Pai, C.-L.; Rutledge, G. C.; Boyce, M. C. *J. Mech. Phys. Solids* **2012,** *60*, 295-318.

[35] Silberstein, M. N.; Boyce, M. C. *J. Power Sources* **2010,** *195*, 5692-5706.

[36] Borup, R.; Meyers, J.; Pivovar, B.; Kim, Y. S.; Mukundan, R.; Garland, N.; Myers, D.; Wilson, M.; Garzon, F.; Wood, D.; Zelenay, P.; More, K.; Stroh, K.; Zawodzinski, T.; Boncella, J.; McGrath, J. E.; Inaba, M.; Miyatake, K.; Hori, M.; Ota, K.; Ogumi, Z.; Miyata, S.; Nishikata, A.; Siroma, Z.; Uchimoto, Y.; Yasuda, K.; Kimijima, K. I.; Iwashita, N. *Chem. Rev.* **2007,** *107*, 3904-3951.

[37] Kim, B.; Kim, J.; Jung, B. *J. Membr. Sci.* **2005,** *250*, 175-182.

[38] Li, L.; Xu, L.; Wang, Y. *Mater. Lett.* **2003,** *57*, 1406-1410.

[39] Deluca, N.; Elabd, Y. *J. Power Sources* **2006,** *163*, 386-391.

[40] Huang, Y. F.; Chuang, L .C.; Kannan, A. M.; Lin, C. W. *J. Power Sources* **2009,** *186*, 22-28.

[41] Yang, T.; Liu, C. *Inter. J. Hydrogen Energy* **2011,** *36*, 5666-5674.

[42] Jung, H.-Y.; Cho, K.-Y.; Sung, K. A.; Kim, W.-K.; Park, J.-K. *J. Power Sources* **2006,** *163*, 56-59.

4. Control of Permanently Free Charged Groups Through the Use of Divalent Salts in Layer-by-Layer Proton Exchange Membranes

Abstract

Layer-by-layer (LbL) films composed of poly(diallyl dimethyl ammonium chloride) and sulfonated poly(2,6-dimethyl 1,4-phenylene oxide) (sPPO) (PDAC/sPPO) were studied to determine the effect multivalent salts have on ion conducting LbL films made from two permanently charged polyelectrolytes. Divalent salts added to the polyanion solution increase the resultant film's conductivity because they provide a stronger shielding effect than monovalent salts, allows for ion bridging, and increases the number and mobiliy of the protons associated with sulfonic acid groups in the LbL film. By optimizing for salt type and concentration, the protonic conductivity of PDAC/sPPO films was increased fourfold (from 15 mS/cm with 0.5 M NaCl to 74 mS/cm with 1 M $CaCl_2$) in humidified conditions and over an order of magnitude (from 0.09 mS/cm to 1.9 mS/cm) at 60% relative humidity. Furthermore, the ratio of sPPO to PDAC in the LbL film was accurately measured for the first time through X-ray photoelectron spectroscopy paired with a polymer compatible etching source (C_{60}^+ cluster ion) and was shown to be highly affected by the divalent salt concentrations – a 35% increase in sPPO content in the film from changing the divalent salts concentrations versus a 3.5% increase from changing the monovalent salt concentration equivalently. The energy of activation for proton conductivity was lower for films made with divalent salts indicating that the divalent salt

films not only contained a larger number of free protons due to increased sPPO content, but also had increased proton mobility.

4.1 Introduction

There is an ever increasing need for clean, portable energy devices, such as fuel cells and high energy batteries to replace or reduce the world's dependence on fossil fuels.[1,2] The continued development of thin-film solid polymer electrolytes with improved mechanical and ion transport properties is critical for the further advancement of such electrochemical energy devices.[3-5] For hydrogen and methanol fuel cells, the membrane resistance is typically the largest contributor to the overall cell resistance and can significantly affect the overall efficiency of the cell.[6] Therefore much of the proton exchange membrane (PEM) research has focused on improving membrane's conductivities, either through increasing the number of free ions (by means such as increasing the degree of sulfonation), or by increasing the water content of the membranes.[7-9] But those improvements typically involve chemical modifications, which are costly. There has been renewed interest in improving and furthering the understanding of the ionic conductivity and proton mobility without chemical modifications, usually by aligning the ion conducting pathways through post-treatment steps such as solvent annealing and annealing under applied force.[8,10,11]

LbL assembly is a thermodynamic based self-assembly process that allows for the controlled deposition of alternating polyelectrolytes at the nanometer scale through charge overcompensation at the molecular level.[12,13] It allows for the formation of a singular thin

film from oppositely charged entities (polymeric or colloidal, organic or inorganic) and the coating of said film on any wettable substrate.[14,15] The relative simplicity and tremendous versatility of the LbL assembly technique has allowed for the exploration of LbL assembly in numerous solid state electrolyte and electrochemical energy applications.[16,17] Of particular interest here, an LbL system composed of poly(diallyl dimethyl ammonium chloride) (PDAC) and highly sulfonated poly(2,6-dimethyl 1,4-phenylene oxide) (sPPO) (PDAC/sPPO) has shown promise particularly for a direct methanol fuel cell membranes, having proton conductivity comparable to that of Nafion®, but with methanol permeability two orders of magnitude less than Nafion's (chemical structure in Figure 4-1).[18,19] This LbL system utilized NaCl salt in the anion solution to improve the film's conductivity. In addition the membrane mechanical properties were greatly improved when the film was spray-coated on an electrospun fiber mat to form a composite membrane, with swelling reduced by four times and about an order of magnitude less than Nafion.[20,21] However, due to the electrostatic interaction between the charged sulfonate and amine groups, most of the sulfonate groups are bound and the conductivity of the resultant films is significantly lower than pristine sPPO.[19] This binding of the charged, active groups by the oppositely charged groups – thus deactivating them – poses a challenge for the use of LbL assembly in making highly conducting polymer electrolytes.

Because LbL films are fabricated under a thermodynamic process with rinse steps removing excess polymers, LbL films' composition and characteristics cannot be adjusted conventionally; i.e. increasing concentration of one polymer over the other does not result in an increase of that polymer in the overall LbL film, nor do post-treatment steps not involving charged ions (such as thermal annealing) have much of an effect.[22] Instead, the films can be tuned by adjusting the pH or salt content of the polymer solutions during the assembly process –

changing the thermodynamics of the adsorbed layer.[19,23] Therefore to increase the conductivity of an LbL film one must look at changing the polymer adsorption thermodynamics to increase the incorporation of unbound active charged groups and/or to improve the connectivity between these free charged groups.

There has been considerable interest and research into the effect of monovalent salts on permanently charged polymers like polystyrene sulfonate.[24] However, less research has been done on the effect of multivalent salts on these same polymers: Schlenoff looked at the effect multivalent ions have on the hydration of LbL films, but the films were made only with monovalent salt (NaCl) and the multivalent salts introduced afterwards [25]. Only one group has reported looked at utilizing divalent salts in LbL assembly and they were using large molecular anion salts and never varied the salt's concentration[26]. In recent years, Muthukumar has looked into the theory of competitive adsorption of divalent salts on flexible polyelectrolytes and found divalent counterions replaced monovalent counterions in competitive adsorption and the ion-bridging by divalent counterions leads to a reversal of polymer charge and first-order collapse of the polymers in certain conditions.[27,28] To better quantify and understand the effect salts with different valencies would have on LbL films, a quantitative analytical method that can measure into the depth of the films, like X-ray photoelectron spectroscopy (XPS) with depth-profiling, is desirable. Many depth-profiling techniques use single-atom sputtering sources such as argon, which is applicable to inorganic materials but severely damaging to polymers.[29,30] Cluster ion C60+ sputtering is much less damaging because the energy transfer from the ion to the material occurs primarily at the surface, which is subsequently removed, minimizing the chemical damage deep into the film.[31] It has recently been used to analyze interlayer diffusion in an LbL film.[32]

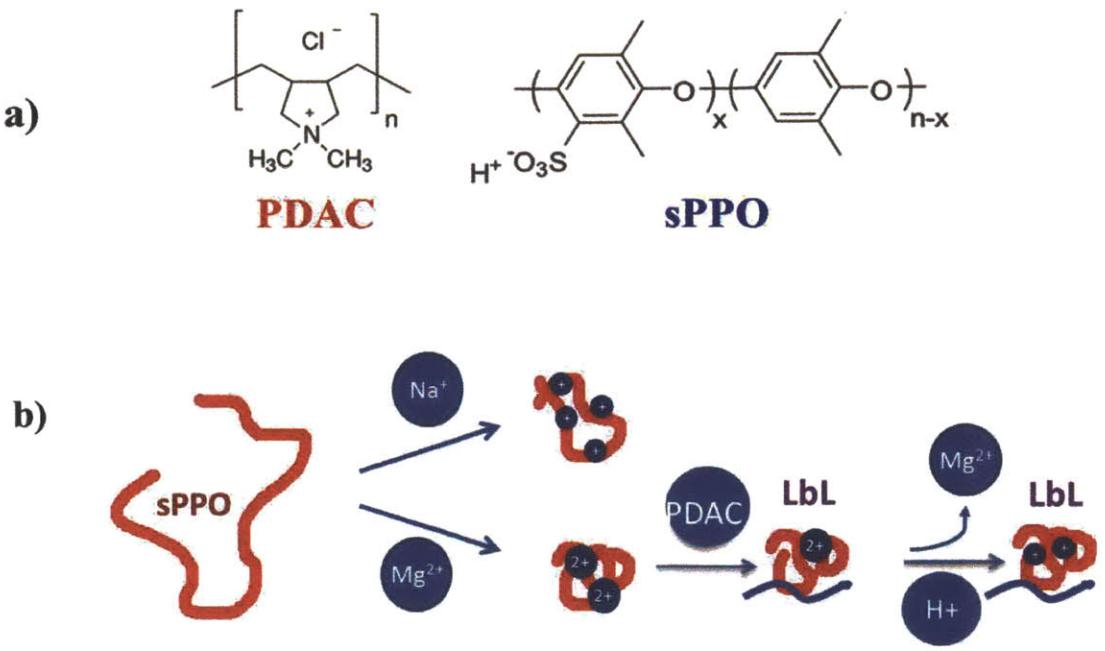

Figure 4-1. Schematic of LbL film formation using divalent salts ($MgCl_2$ in this case) instead of NaCl. The charged sPPO polymer is more shielded in divalent salts. After the LbL film is formed, there is an additional soak step in 1 M HCl to exchange the divalent salt ions for protons followed by a DI rinse to remove all excess ions.

In this report, we manipulate the PDAC/sPPO system by utilizing different concentrations of multivalent salts during the LbL assembly followed by an acid and water rinse to investigate the effect of multivalency of salt on protonic conductivity, bulk film properties, and ion channel morphologies (Figure 4-1b). Previously, only monovalent salt was used to improve the PDAC/sPPO film performance. The solubility of sPPO in various concentrations of $MgCl_2$, $CaCl_2$, and $CeCl_3$ and hydrochloric acid conditions were examined. From the range of soluble solutions, PDAC/sPPO films were made and their conductivities, growth rates, and film

stabilities were measured. PDAC/sPPO films made with $MgCl_2$ and $CaCl_2$ were found to be the most promising and these films were compared with films made with NaCl in terms of their overall protonic conductivities and the conductivities' dependence on salt concentration. EDS and surface XPS of the films were measured to determine that the divalent salts were being fully exchanged from the film in the final rinse steps. XPS with depth profiling was used to quantify the film's anion versus cation composition as a function of the type of salt and its concentration. The energy of activation for proton conductivity was measured for the different films.

4.2 Experimental Section

Chemicals. Poly(2,6-dimethyl 1,4-phenylene oxide) (PPO) (Mw = 23,000), magnesium chloride, and calcium chloride, were obtained from Sigma-Aldrich, Inc with the two salts used as received. Poly(diallyl dimethyl ammonium chloride) (PDAC) (Mw = 240,000) was obtained from Polysciences, Inc. Sodium chloride salt, and reagent grade hydrochloric acid, concentrated, was purchased from VWR and used as received. PPO was sulfonated as previously reported to yield highly sulfonated sPPO.[18] All polymers, sPPO and PDAC, were weighed and diluted to the desired concentration using Millipore MilliQ deionized water (18.2 MΩ cm filtered through a 0.22 μm membrane) and the specified acid and/or salt added. The pH of the solutions were adjusted by adding 1M HCl solution dropwise.

LbL Dip Assembly (Dip-LbL). Assembly of the LbL films was completed by using a programmable ZEISS DS50 slide stainer. To construct LbL films, substrates (glass, silicon wafers) were first cleaned and plasma treated in oxygen to impart an initial negative charge to the substrates. The substrates were then immersed in PDAC solution for 10 minutes, followed by three one minute rinses in water, and then placed in sPPO solution for 10 minutes, followed by

three one minute rinses in water; the process was repeated numerous times to yield the specified number of bilayers. The LbL film was then put in 0.1M HCl solution for at least a couple hours, followed by DI water for another couple hours and then dried. The PDAC, and sPPO solutions were all 10 mM based on the molecular weight of repeat units. The sPPO and PDAC polymer and rinse solutions were adjusted to pH 1 or pH 2 as specified with HCl.

Proton Conductivity. Protonic conductivity was measured in-plane using a custom machined PEEK electrode with two platinum wires spaced 1 cm apart. The electrode was placed above the center of the LbL film and clamped down to ensure good continuous connection between the wires and the film. Humidity was controlled using a chamber from electro-tech Systems, Inc. Impedance values were determined by electrochemical impedance spectroscopy with a Solartron 1260 impedance analyzer, measuring from 1 MHz down to 1 Hz at room temperature. The films were allowed to come to equilibrium at each relative humidity (RH) point. Since the films have been rinsed in DI water before dried, the only ions present in the film is protons. The thickness of the films was measured by scoring the films with a razor blade and measuring the step change in the height between the film and the substrate with a Dektak 150 profilometer.

X-ray Photoelectron Spectroscopy (XPS). Chemical composition of the surface was characterized using a PHI VersaProbe II X-ray photoelectron spectrometer with a scanning monochromated AI source (1,486.6 eV; 50 W; spot size, 200 μm). The takeoff angle between the sample surface and analyzer was 45°, and the X-ray beam collected C1s, N1s, O1s, and S2p and one or more of the following Na1s, Cl2p, Mg2p, and Ca2p elemental information while rastering over a 200x700 μm area depending on which samples were being tested. Depth profiling was

accomplished using the instrument's C_{60}^+ ion source operated at 10 kV, 10 nA, and rastered over a 3x3 mm area at an angle of 70° to the surface normal. Sputtering occurred in 10 minute intervals while the sample was moved using concentric Zalar rotation at 1rpm. The sputter rate was determined by measuring the time it took to etch a 200 nm thick film. In-depth elemental scans were taken following each sputter cycle. Atomic composition was determined based on photoelectron peak areas and the relative sensitivity factors provided in PHI's MultiPak processing software.

Bulk Film or Solution Characterization. Bulk chemical composition was roughly characterized using the energy-dispersive X-ray spectroscopy (EDS) function of a JEOL scanning electron microscope. The samples were made on Si wafers or over 1 μm in thickness to avoid having the substrate affect the analysis of the measurements. Bulk film water update at different relative humidities was taken by a Masscal G1 (quartz crystal microbalance/heat conduction calorimeter) which had two mass flow controllers that supplied nitrogen streams to the G1 sample chamber.[33] One nitrogen stream was kept dry, while the other was humified to 100% RH. Varying the ratio of these two streams allowed fine control (± 2%) of the sample chamber RH. The actual RH of the streams was determined by a Sable Systems R300 water vapor analyzer. The size of the charged polymer in solutions of various salt concentrations and acidities was measured by dynamic light scattering with a Beckman Delsa-Nano C Particle Analyzer.

Ion-exchange capacity (IEC). LbL films were deposited on polystyrene substrates to aid in the removal of the film. Films consisting of 150 bilayers (BLs) were made and the film rinsed and dried. Membranes were weighed and 1.5 mL of 0.1M LiCl was added and the film was

allowed to exchange its ions overnight. The solution was then pipetted as carefully as possible (so as to remove as little of the membrane as possible) and titrated with NaOH.

4.3 Results and Discussion

4.3.1 Solution Properties of sPPO

To test the feasibility of making LbL films with multivalent salts, the solubility of sPPO in pH 1 and pH 2 solutions with different salts was examined. Three representative salts were used, two divalent and one trivalent: $MgCl_2$, $CaCl_2$, and $CeCl_3$, at low to moderate concentrations. For divalent salts, magnesium and calcium chloride were examined, keeping the anion the same. For trivalent salts, cerium chloride was chosen for its water and acid stability and solubility. sPPO is a highly sulfonated, hydrophilic, water soluble polymer and does not precipitate with the addition of monovalent salts but does with both the divalent and trivalent salts. When salt was added to a more acidic sPPO solution (pH 1 versus pH 2), it was observed that more salt could be added before onset of cloudiness (formation of micron sized aggregates that are suspended in the solution) and precipitation (polymer crashing out of solution). $CeCl_3$ caused the precipitation of sPPO at pH 2 when even a small amount was added; at pH 1 the onset of sPPO precipitation was at 0.25 M. For $MgCl_2$, at pH 2, the onset of sPPO precipitation was at 0.75 M; at pH 1 the onset was at 1.25 M. For $CaCl_2$, at pH 2, the onset of sPPO precipitation was at 1.5 M; at pH 1 the onset was at 2.5 M. Before sPPO precipitation, the solutions became visibly cloudy, typically at half the critical salt concentration and got increasingly cloudy until the polymer precipitated.

We hypothesize that this salting out phenomenon is due to the multivalent salt's ability to form ion bridges between charged groups (sulfonate groups in sPPO) of different polymer chains, thus linking multiple polymer chains together, forming larger and larger aggregates until the polymer precipitates from the solution. This would explain why the trivalent salt caused precipitation of sPPO at much lower concentrations. Comparing salts with the same valency, it appears the ability to salt out the charged polymer follows the Hoffmeister series with Mg destabilizing the polymer in water more than Ca does. In addition, the hydrochloric acid helps keep sPPO in the solution, by competing with the multivalent salt's adsoption onto the charge sites. Dynamic light scattering experiments on the polymer/salt solutions showed that aggregates started to form as early as 0.25 M for $MgCl_2$ and $CaCl_2$ in pH 1 and above 0.125 M for $MgCl_2$ and $CaCl_2$ in pH 2, before the films became visibly cloudy. This is in contrast to sPPO in NaCl solutions where no aggregation was observed up to 2.0 M NaCl in pH 1 or pH 2, again highlighting the difference between monovalent and multivalent salts.

4.3.2 Layer-by-Layer Film Growth

LbL assembly of the polymers PDAC and sPPO is performed by utilizing the electrostatic charge interaction between the positively charged PDAC and the negatively charged sPPO, with the presence of salt in the sPPO solution affecting its solution morphology and adsorption characteristics. LbL films made with $MgCl_2$, $CaCl_2$, and $CeCl_3$ in the sPPO solution were assembled and tested. Only salt conditions under which sPPO was soluble were tested. One challenge in making LbL films with solutions that aggregate strongly is that the resultant films are highly irregular, and less stable as the charged polymers are no longer being deposited chain by chain but rather aggregate by aggregate, with the aggregates in the solution getting

larger after each bilayer and the LbL growth no longer linear. Thus for pH 2 solutions with divalent salts and pH 1 solution with trivalent salts, while LbL films did form for all the solutions tested, the films formed with high concentrations of salt were very rough and highly unstable in water – the films lost thickness upon immersion in a stirred rinse bath overnight (the films made with trivalent salts at pH 1 behaved similarly to films made with divalent salts at pH 2). The use of pH 1 solutions resulted in much more stable films. At the higher divalent salt concentrations ($\geq$ 0.5 M) the resultant films were often visually cloudy (these films are generally transparent), but the films grew linearly (indicating controlled polymer adsorption and not aggregate growth) and the roughness (except for the 1.0 M $MgCl_2$ film) never exceeded 10% of the film's thickness (figure 4-2). Compared with $MgCl_2$ films, $CaCl_2$ films were clearer, less rough, and the polymer solutions could be used for more layers before producing less uniform results because the solutions themselves were also more stable. Interestingly the growth rates, while varying with salt concentration, differed very little between films made with $MgCl_2$ and $CaCl_2$, indicating that for film growth and deposition, the valency of the ion matters much more than the ion identity and its affinity to the polymer.

a)

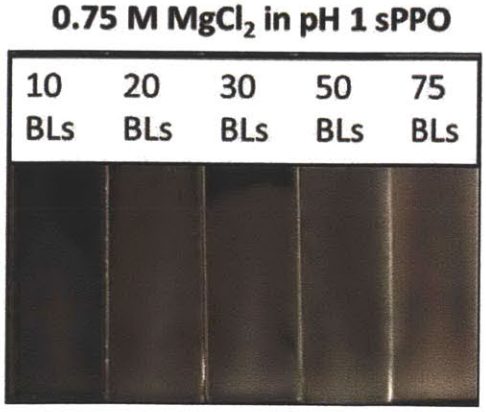

b)

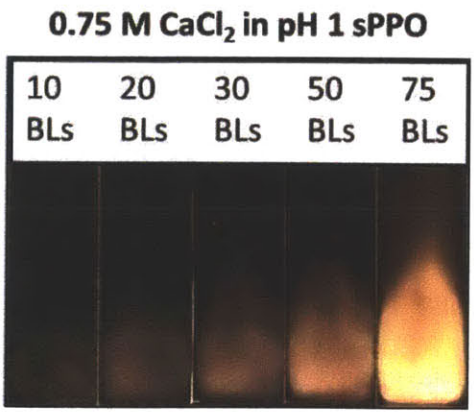

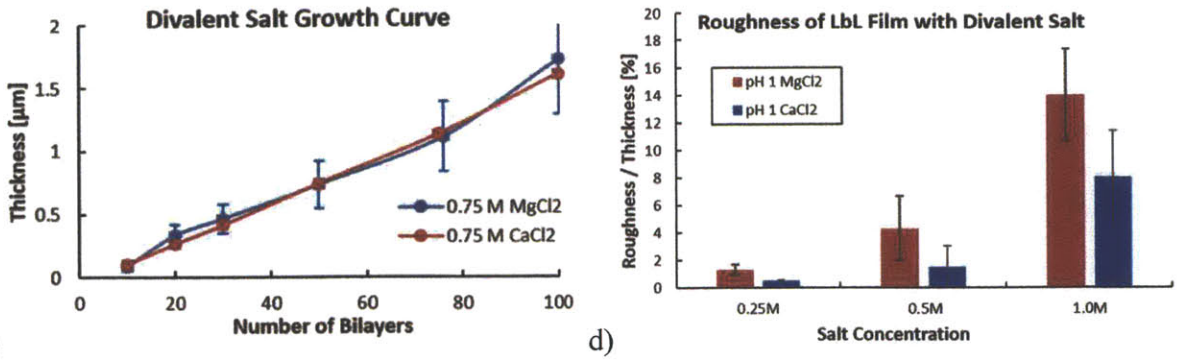

c) d)

Figure 4-2. (a) and (b) are pictures of PDAC/sPPO films deposited on glass of increasing number of bilayers (BLs) with 0.75 M $MgCl_2$ and 0.75 M $CaCl_2$ salt in the sPPO solution respectively. (c) LbL growth curves of representative PDAC/sPPO films with two different divalent salts. (d) Bar graph showing the normalized roughness of the LbL films with different salts and salt concentrations.

4.3.3 Ionic Conductivity

Protonic conductivity was measured for the LbL films mentioned above. As a result of the films being more stable, the conductivities of the LbL films made in pH 1 had less error and these results are shown in figure 4-3. The films were all soaked in 0.1 M HCl solution overnight and then rinsed in DI water before drying. Therefore the ionic conductivity measured is the conductivity of the free sulfonic acid protons of the film and not from any other salt ions or dopants. The goal of using multivalent salts was that the multivalent ions would better shield the sulfonate groups from the positively charged amine groups during LbL deposition and that the non-amine bound sulfonate groups would also be better connected to each other due to the ion-bridging affect. The free and connected sulfonate groups would then provide a low energy

pathway for protons to hop through leading to higher conductivity. The assumption was that this effect would be linear, the higher the salt concentration, the higher the conductivity, as was seen previously when using monovalent salts. However, it turned out that the divalent salt effect is not linear.

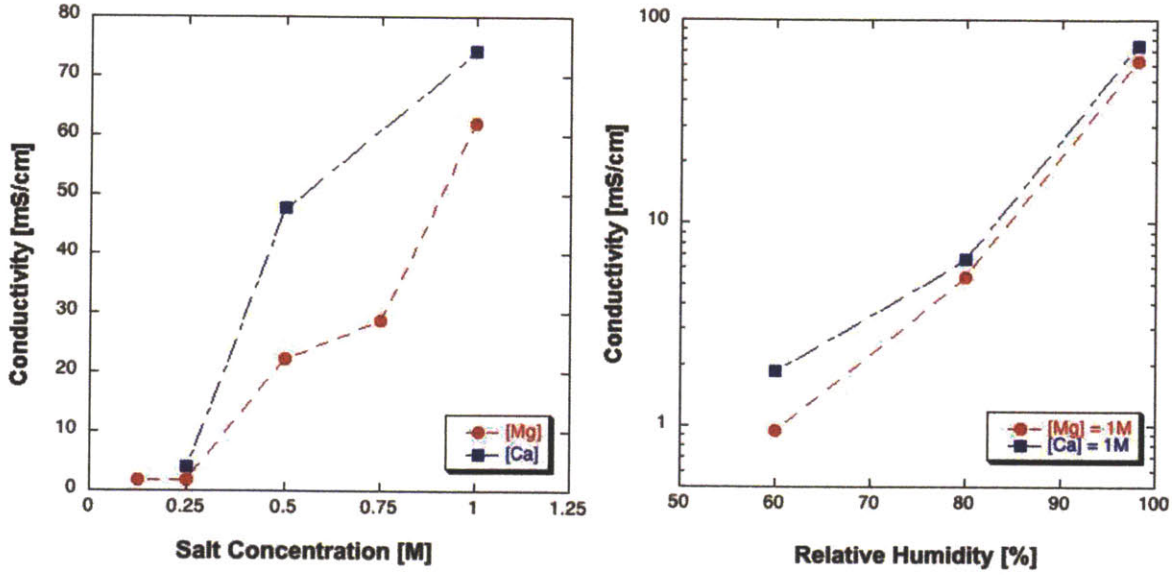

Figure 4-3. (A) Comparison of the proton conductivity measured at 98% RH of PDAC/sPPO film made with different concentrations of $MgCl_2$ and $CaCl_2$ in the sPPO solution. (B) Comparison of the proton conductivity at different relative humidities of PDAC/sPPO films made with 1.0 M $MgCl_2$ or $CaCl_2$ in the sPPO solutions.

For both the divalent and trivalent salts, there is a critical salt concentration (between 0.25M and 0.5M for divalent salts and between 0.125 M and 0.2 M for trivalent salts) below which the conductivity of the films made were not measurable and the presence of multivalent salt harmed the proton conductivity. Above this critical salt concentration, the conductivity of

the films increased dramatically and was higher than any films made with NaCl at any concentration (10 - 15 mS/cm). For the trivalent salt, sPPO was only soluble up to 0.2 M $CeCl_3$ and thus no further points could be taken. For the divalent salts, the conductivity of the films increased further with increasing salt, up to 1.0 M. At 1.0 M salt concentration, the conductivities of the LbL films made with $MgCl_2$ and $CaCl_2$ were the highest observed – 62 ± 4 mS/cm and 74 ± 4 mS/cm respectively at 98% RH. For $MgCl_2$, the sPPO solution precipitated above 1.0 M concentration and no films were able to be made; for $CaCl_2$, solutions were stable and films were made until 2.0 M concentration, but the conductivity plateaued. In addition to the conductivity increasing overall with the use of divalent salts, the relative humidity (RH) dependence of the conductivity also decreased with use of the divalent salts, with the increase of conductivity at low RHs greater for $CaCl_2$ films than for $MgCl_2$ films (Figure 4-3b). This indicates that apart from just increasing the number of free protons in the LbL films, the divalent salts, particularly $CaCl_2$, also increase the mobility of the free protons, in low RH conditions.

In sulfonated PEMs, proton conduction is generally accepted to be through the Grotthuss mechanism, where the protons hop between ionized sulfonate groups, with proton mobility defined as the hopping rate. The temperature dependence of the conductivity of an LbL film allows the energy of activation for proton conduction in that film to be calculated. The highly conducting $CaCl_2$ films had an energy of activation of 23 kJ/mol, compared with 28 kJ/mol for the $MgCl_2$ films, and 36 kJ/mol for the NaCl films. The lower energy of activation suggests the proton hopping is more favorable for $CaCl_2$ than $MgCl_2$ films further confirming that the use of divalent salts increases the proton mobility in these films.

4.3.4 Bulk Film Characterization

To observe the films' composition changes as a result of the different divalent salt concentrations and rinse steps, XPS and EDS was performed on the films. Surface XPS and EDS were taken of the $MgCl_2$ and $CaCl_2$ films before and after the rinse step to verify that all the salt cations were indeed removed or exchanged with protons both on the surface and throughout the film. In addition, XPS could be used to determine the chemical composition of the LbL films. Surface XPS was taken of films directly removed after the final sPPO dip step, before the final rinse, and rinsed in DI water and dried (figure 4-4). The DI water removed any excess sPPO and salt present in the film but preserved any Mg or Ca ions that were bound to the film. As the Mg or Ca ions would later be exchanged with protons, this measurement affords us a way to "observe" the free protons as a function of salt type and concentration. For $MgCl_2$, the Mg/S ratio was 0.22 ± 0.02 for 0.75 M $MgCl_2$ and 0.15 ± 0.01 for 0.25 M $MgCl_2$. For $CaCl_2$, the Ca/S ratio was 0.23 ± 0.02 for 1.0 M $CaCl_2$ and 0.15 ± 0.01 for 0.25 M $CaCl_2$. These results follow the general trend observed for the conductivity that increased salt concentration increases the number of free ion groups but would also suggest that even though films made with 0.25 M $MgCl_2$ and $CaCl_2$ had very little measurable conductivity, they did in fact still have free ion groups. Perhaps there just were not enough of them or they were in isolated clusters. In addition, the S/N ratio could be calculated for the films to get an estimate of the film's polymer composition. However, XPS, while quantitative, only penetrates 10 nm into the film and the chemical composition of the film at the surface may not reflect the chemical composition in the bulk.

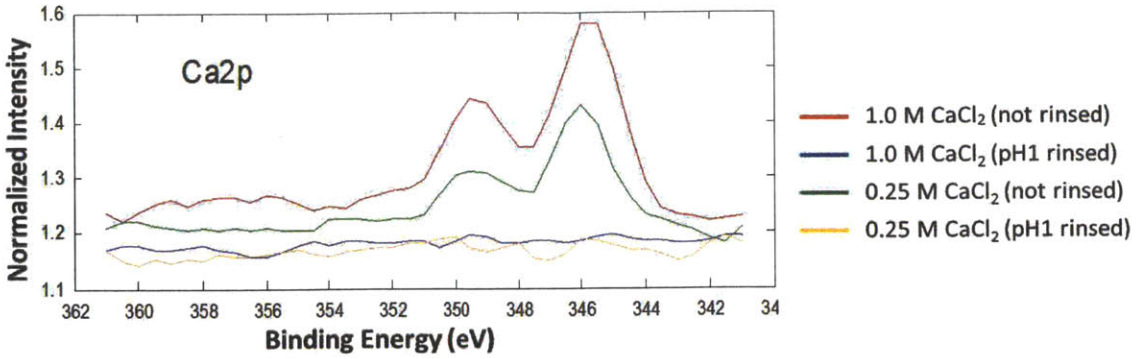

Figure 4-4. X-ray photoelectron spectrometry (XPS) of PDAC/sPPO films made with 1.0 M or 0.25 M $CaCl_2$ salt conditions with and without the final pH 1 (0.1 M HCl) rinse step. All the films were still rinsed in DI water to remove excess ions and polymers. It is clear that the final rinse step is sufficient to remove the Ca^{2+} ion from the film and that the presence of the ion indicates the presence of sulfonic acid groups in sPPO not bound to PDAC.

To analyze the LbL film's polymer composition within the bulk of the film, a C_{60}^{+} ion source was used to etch away a set amount of film from the surface multiple times and an in depth XPS scan was used to measure the chemical composition of the exposed surface after each etching step, giving the chemical composition of the film as a function of depth (see figure 4-5 of a representative film). The choice of ion beam, the length of time for the etching, and the scanning parameters were chosen to minimize chemical degradation of the unetched part of the film. Since the LbL films are actually a controlled blend, there was no discernable difference, beyond error, in the chemical compositions of the films after the surface was removed. The remaining scans were averaged, and the resulting composition was indicative of the bulk film's

chemical composition. This allowed us to definitively quantify the sPPO and PDAC content in the LBL films for the first time.

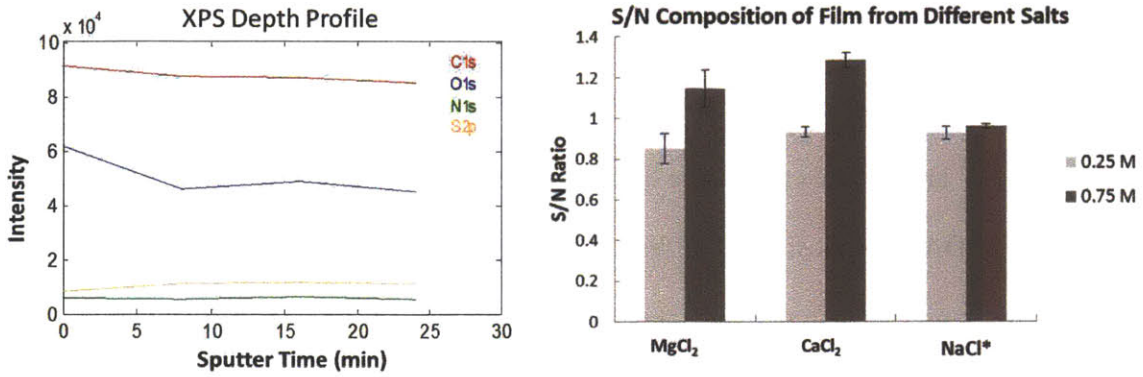

*The NaCl concentration was doubled to match the ionic strength of the divalent salts.

Figure 4-5. (a) XPS depth profile of a representative film, 0.75 M $MgCl_2$ in sPPO. The sputter rate was aproximately 8 nm/min, so the sputter time indicated depth of the film. Note how the chemical composition stabilized after the surface has been removed. (b) A bar graph displaying the atomic sulfur to nitrogen (S/N) ratios from the depth profiles of LbL films made with $MgCl_2$, $CaCl_2$, and NaCl at a low and high salt concentration. Since sulfur is unique to sPPO and nitrogen to PDAC, the S/N ratio is also the ratio of sPPO to PDAC in the film.

Figure 4-5b plots the sPPO / PDAC ratio for each film as a function of the type of salt used and the salt concentration. The sPPO/PDAC ratio varied the most for the divalent salt solutions, with the difference in sPPO content of the film between the low salt and high salt films being 35%, indicating that the divalent salts are very good at controlling the sPPO/PDAC ratio

(both decreasing and increasing it above 1:1), most likely because of the ion-bridging effect as previously mentioned. This large difference in sPPO content also corresponds well to the large increases in film conductivity measured. In contrast there is only a small difference (4%) between the sPPO content of the films made with different NaCl concentrations, corresponding to the more gradual change in conductivity of the films made with different concentrations of monovalent salt. This would explain the difficulty previous researchers encountered in detecting sPPO/PDAC compositional differences as a function of NaCl concentrations.[19] A sPPO/PDAC ratio greater than one indicates an excess amount of sPPO to PDAC, with the excess sPPO necessarily free to conduct protons, thus explaining the high proton conductivity observed for $CaCl_2$ films. The inverse statement, however, is not necessarily true as there can be free sPPO groups (matched with free PDAC groups) even as the ratio is less than one, but in general, a higher sPPO to PDAC ratio would indicate increased free protons and conducting pathways.

It is possible to measure the number of free protons present in a film by measuring the film's ion exchange capacity (IEC). Though due to the very thin dimensions of the LbL films, the IEC calculated is prone to error and is best used as just an approximation. The IEC was measured for the films made with $CaCl_2$ at high and low salt conditions. The IEC was 0.44 mmol/g (equivalent to 16% of the sulfur groups being free) for the membranes made with 0.75 M salt and 0.25 mmol/g for the membranes made with 0.25 M salt. Note that the difference in free protons of the films was not as large as the difference in conductivity numbers would suggest, indicating that the main reason the LbL films of low divalent salt concentrations had very poor conductivity was the lack of conducting pathways connecting the free protons, and

likewise that the highly conducting films benefited from not just increased free protons but also improved conducting pathways.

4.4 Conclusion

PDAC/sPPO films fabricated with multivalent salts at various salt concentrations in the polyanion solution were studied to understand the effect multivalent salts have on the LbL process and the resulting film's conductivity and composition. Multivalent salts can form ion bridges connecting the charged groups of a polymer to another charged group of the same polymer or a different polymer, further impacting the film formation and its properties. The solution properties, film growth, morphology, composition, and conducting mechanism were investigated with different multivalent salts in the polyanion solution. Multivalent salts can cause the sPPO to precipitate from the solution and 0.1 M HCl was added to help stabilize the solutions and form more stable films.

The protonic conductivities of PDAC/sPPO films are highly dependent on the concentration of salt in the sPPO solution during the LbL assembly process. At low concentrations (below 0.5M for divalent salts and below 0.2 M for trivalent salts), the LbL films have negligible conductivities. Above that concentration, the films are very conductive and their conductivity increases further with increasing salt concentrations, to 62 mS/cm and 74 mS/cm at humified conditions for $MgCl_2$ and $CaCl_2$ respectively. At 60% RH, the LbL film made in $CaCl_2$ significantly outperformed that made in $MgCl_2$ and both outperform films made in NaCl, indicating the use of multivalent salts increases the number of free charge carriers and increases the ion mobility. This is verified by measuring the energy of activation for the ion transport of the LbL films.

XPS with a C_{60}^+ ion source was used to quantify the chemical composition of these films, showing that the use of divalent salts in the assembly baths can significantly change the sPPO to PDAC ratio in the films as compared with the use of monovalent salts. The IEC was measured for PDAC/sPPO membranes made with $CaCl_2$ at low and high salt concentrations, showing that effect of divalent salts is as much about incorporating more sPPO in the LbL film as it is about how the free conducting groups are connected. The divalent salt effect for LbL films appears to be a very promising and easy to apply tool for controlling and manipulating the morphology of two strong polyelectrolytes in an LbL film. This effect could be used to increase the percent incorporation of a particularly desirable functional polymer in LbL systems for other applications, for example increasing the Li ion conductivity in solid polymer electrolytes for batteries, or increasing the binding sites for loading metal ions or charged small molecule drugs into LbL films.

4.5 References

[1] De Brujin, F. *Green Chemistry* **2005**, *7*, 132.

[2] Khaligh, A., Li, Z., *Vehicular Technology, IEEE Transactions on*, **2010**, *59*, 2806-2814.

[3] Hickner M.A., Ghassemi H., Kim Y.S., Einsla B.R., McGrath J.E., *Chem. Rev.*, **2004**, *104*, 4587.

[4] Chalk, S.G., Miller, J.F., *J. Power Sources*, **2006**, *159*, 73-80.

[5] Kreuer, K.D., *Chem. Mater.*, **2013**, *159*, 73-80.

[6] Li, Q., He, R., Jensen, J.O., Bjerrum, N.J., *Chem. Mater.*, **2003**, *15*, 4896-4915.

[7] Moore, R. B., Mauritz, K. A., *Chem Rev.*, **2004**, *104*, 4535-4585.

[8] Peckham, T.J., Holdcroft, S., *Advanced Materials*, **2010**, *42*, 4667-4690.

[9] Zhang, J., Xie, Z., Zhang, J., Tang, Y., Song, C., Navessin, T., Shi, Z., Song, D., Wang, H., Wilkinson, D.P., Liu, Z.S., Holdcroft, S., *J. Power Sources*, **2006**, *160*, 872-891.

[10] Lin, J., Wu, P.H., Wycisk, R., Pintauro, P.N., Shi, Z., *Macromolecules*, **2008**, *41*, 4284-4289.

[11] Kwon, O., Wu, S., Zhu, D.M., *J. Phys. Chem. B*, **2010**, *114*, 14989-14994

[12] Decher, G., *Science*, **1997**, *277*, 1232-1237.

[13] Hammond, P. T., *Adv. Mater.*, **2004**, *16*, 1271-1293.

[14] Lee, D., Rubner, M.F., Cohen, R.E. *Nano Lett.*, **2006**, *6*, 2305-2312.

[15] Krogman, K.C., Lowery, J.L., Zacharia, N.S., Rutledge, G.C., Hammond, P.T., *Nat. Mater.*, **2008**, *8*, 512-518.

[16] Lutkenhaus, J.L., Hammond, P.T., *Soft Matter*, **2007**, *3*, 804-816.

[17] Lee, S.W., Kim, B.S., Chen, S., Shao-Horn, Y., Hammond, P.T., *J. Am. Chem. Soc.*, **2009**, *2*, 617-679.

[18] Argun, A.A., Ashcraft, J.N., Hammond, P.T., *Adv. Mater.* **2008**, *20*, 1539.

[19] Ashcraft, J.N., Argun, A.A., Hammond, P.T., *J. Mater. Chem.*, **2010**, *20*, 6250-6257.

[20] Liu, D.S., Ashcraft, J.N., Mannarino, M.M., Silberstein, M.N., Argun, A.A., Rutledge, G.C., Boyce, M.C., Hammond, P.T., *Adv. Funct. Mater.*, **2013**, *23*, 3087-3095.

[21] Mannarino, M.M., Liu, D.S., Hammond, P.T., Rutledge, G.C., *ACS Appl. Mat. Interfaces*, **2013**, *5*, 8155-8164.

[22] Dubas, S.T., Schlenoff, J.B., *Macromolecules*, **1999**, *32*, 8153-8160.

[23] Shiratori, S.S., Rubner, M.F., *Macromolecules*, **2000**, *33*, 4213-4219.

[24] Zhulina, E.B., Rubinstein, M., *Soft Matter*, **2012**,*8*, 9376-9383.

[25] Schlenoff, J.B., Rmaile, A.H., Bucur, C.B., *J. Am. Chem. Soc.*, **2008**, *130*, 13589-13597.

[26] Dressick, W.J., Wahl, K.J., Bassim, N.D., Stroud, R.M., Petrovykh, D.Y., Langmuir, 2012, 28, 15831-15843.

[27] Kundagrami, A., Muthukumar, M.J., *Chem. Phys.*, **2008**, *128*, 244901.

[28] Kumar, R., Kundagrami, A., Muthukumar, M., *Macromolecules*, **2009**, *42*, 1370-1379.

[29] Nobuta, T., Ogawa, T., J. Mater. Sci., **2009**, *44*, 1800–1812.

[30] Hollander, A., Haupt, M., Oehr, C., Plasma Process Polym., **2007**, *4*, 773–776.

[31] Mahoney, C.M., *Mass Spectrom. Rev.*, **2010**, *29*, 247–293.

[32] Gilbert, J.B., Rubner, M.F., Cohen, R.E., *PNAS*, **2012**, *110*, 6651-6656.

[33] Smith, A.L., Ashcraft, J.N., Hammond, P.T, *Thermochimica Acta*, **2006**, *450*, 118-125.

5. Incorporating Phosphoric Acid into Layer-by-Layer Assembled Sulfonic Acid Based Proton Exchange Membranes for Higher Conductivity at Lower Relative Humidities

Abstract

Polymer electrolyte films composed of both sulfonic acid and phosphoric acid were fabricated using layer-by-layer (LbL) assembly and their ionic conductivity was tested. These LbL films consist of a phosphoric-acid-doped polymer, poly(2-vinyl pyridine) (P2VP), which has been shown to have moderate conductivity at 0% RH at 150^0 C and a sulfonic acid functionalized polymer, sulfonated poly(2,6-dimethyl 1,4-phenylene oxide) (sPPO) which has been shown to be conductive at high relative humidities in an LbL film. The phosphoric acid concentration in the LbL film and the number of free sulfonic acid groups can be controlled post film fabrication by changing the concentration of the phosphoric acid the film is exposed to before drying – thereby doping the film to different levels. Under mild doping conditions (0.1 M phosphoric acid), the P2VP/sPPO films have improved conductivity at 50% RH by an order of magnitude compared with LbL films made without phosphoric acid. Under stronger doping conditions (0.4 M – 1.0 M phosphoric acid), the film's conductivity increases by two more orders of magnitude, and its RH dependence decreases further (110 mS/cm at 25 °C and 50% RH under just 0.4 M phosphoric acid doping). These phosphoric acid doped films are over two orders of magnitude more conductive than Nafion and have higher conductivities than either component of the film by itself due to a recently reported new proton transport pathway between

phosphoric acid and sulfonic acid. These large increases in conductivity were achieved under much more mild doping conditions (0.4 M vs 85% phosphoric acid) than previously reported.

5.1 Introduction

Hydrogen fuel cells have attracted considerable attention for their possible role in a more carbon neutral future.[1-6] Of particular interest is the use of hydrogen fuel cells in place of internal combustion engines for transportation purposes due to the high energy density of hydrogen; thus enabling zero carbon emission vehicles to travel over a similar range as current internal combustion engine vehicles.[3,4] To keep the cost of the overall fuel cell system low, it is desirable to operate the fuel cell at higher temperatures (> 100 ^{0}C) to take advantage of improved catalyst kinetics at higher temperature, minimize catalyst poisoning and allow the use of less pure fuel streams.[5,6] However, at the higher temperatures, it is no longer practical to run the fuel cell fully humidified and thus the development of a thin proton exchange membrane with sustained performance up to 120^{0} C and down to 50% relative humidity (RH) is desired. Nafion, the industrial standard for proton exchange membranes, begins to deform and lose its mechanical stability near this temperature and, like other sulfonic acid based membranes, loses conductivity significantly as the relative humidity decreases.[6-8] It is therefore necessary to find an alternative proton exchange membrane that is stable at higher temperatures and can better conduct protons under lower relative humidity conditions.

Conventionally, proton-exchange membranes used in fuel cells have mostly been perflourinated sulfonic acid aliphatic polymers such as Nafion. These polymers have been

favored for their high conductivity and chemical stability, although they also present a set of difficulties.[8-11] Namely, proton conduction in these membranes is based off the Grotthuss "hopping" mechanism, which consists of the "hopping" of a proton between adjacent water molecules.[12,13] It is a very efficient proton transport mechanism, but its dependence on water limits the operational temperatures of the membrane to a 100°C range, above which it is extremely difficult to keep the membrane completely hydrated.[14] Several attempts have been made to address this problem; specifically, additives have been introduced in the membrane to aid in water retention, and the perfluorinated ionomers have been chemically modified with new side-chain groups in an effort to improve conductivity.[15,16] The main issue with all of these membranes is that they utilize sulfonic acids as their proton conducting group with which the main proton conducting mechanisms are highly dependent on water content. Alternatively, phosphoric acids have been used in anhydrous proton-exchange membranes due to a proton conduction mechanism that relies on the phosphoric acid itself to accept and donate protons. However, the phosphoric acid conducting pathway typically needs higher temperatures (>150 °C) to activate.[13,17] Phosphoric acid doped poly(benzimidazole) (PBI) based membranes have been used for anhydrous hydrogen fuel cells at higher temperatures (150-200 ^{0}C), but this material is not conductive enough at lower temperatures and has issues with retaining the phosphoric acid.[9-10]

Recently, there has been very promising work from the Kawakami group showing increased membrane conductivity if both phosphoric acid and sulfonic acid groups are present in a membrane.[18,19] They explain this phenomenon by proposing a modified Grotthuss mechanism whereby the phosphoric acid replaces water in the proton hoping mechanism. Kawakami *et al.*, reported high conductivity values for novel phosphoric acid-doped sulfonated

polyimide and polybenzimidazole blend membranes at low relative humidities and a range of temperatures (30 – 120 °C).[18] Herein we use "doped" to indicate the incorporation of a dopant, phosphoric acid in this case, into a membrane, that results in increased conductivity of the membrane. In the case of phosphoric acid, the doping is not permanent and the dopant can diffuse or be removed from the system. These conductivities at low relative humidities (0.5 S/cm at 120 °C and 45% RH) were approximately two orders of magnitude higher than those of Nafion and were attributed to a new proton transport pathway between the phosphoric acid and the sulfonic acid in the blend membrane. The conductivity of the blend was much higher than the conductivity of either sulfonated polyimide or phosphoric acid doped polybenzimidazole alone.[19] However, the high doping conditions the membranes were subjected to (85% concentrated phosphoric acid) are somewhat alarming, as they indicate an extremely high and possibly unsustainable doping level, and a more conductive sulfonated polymer (and a different amine based polymer) could further enhance the film conductivity. An alternative method using more conductive polymers and a more controlled blending method could be quite promising and provide confirmation to the observed trends as well as shed more light on the proposed mechanism.

Layer-by-layer (LbL) assembly is a versatile thin-film fabrication technique that allows the use of water soluble polymers possessing complementary interactions, such as oppositely charged functional groups, to form a stable polymer blend whose composition, morphology, and transport properties can be controlled through the adjustment of assembly parameters such as pH, salt, and post-treatment steps.[20-22] The tunability, environmentally-benign water processing, and nanoscale blending of materials which would otherwise phase separate make this technique very promising for solid state electrolyte and electrochemical energy applications.[23,24] A

particularly promising LbL system for use in fuel cells was introduced by Argun, Ashcraft, et. al whereby highly conductive but water soluble sulfonated poly(2,6-dimethyl 1,4-phenylene oxide) (sPPO) was combined with poly(diallyl dimethyl ammonium chloride) (PDAC) to create a highly conducting, methanol blocking, thermally stable, albeit mechanically weak film.[25,26] Subsequently Liu, Mannario, et.al showed the versatility of this LbL system by spraying the PDAC/sPPO film on electrospun mats to make mechanically robust proton exchange membranes.[27,28]

However, for use in a high temperature, low relative humidity hydrogen fuel cell, there was a need to replace PDAC with a phosphoric acid doped polymer. Poly(2-vinylphyridinium) (P2VP) was chosen because the doped poly(2-vinylpyridinium dihydrogenphosphate) (P2VP-DHP) was shown to have better ionic conductivities at low RHs compared to other polypyridine and amine groups.[29] In this report we manipulate the P2VP/sPPO system by changing the fabrication parameters and doping conditions to investigate their effect on ionic conductivity and phosphoric acid content in the film.(figure 5-1) The ionic conductivity of P2VP/sPPO films doped with phosphoric acid were compared with similarly doped PDAC/sPPO films. The LbL blend films were also compared with pristine P2VP films with various concentrations of phosphoric acid. The mechanism for conductivity and the effect of higher doping conditions on these systems were further explored.

5.2 Experimental Section

Chemicals. Poly(2,6-dimethyl 1,4-phenylene oxide) (PPO) (Mw = 23,000) and ortho-phosphoric acid 99%, were obtained from Sigma-Aldrich, Inc. Poly(diallyl dimethyl ammonium chloride) (PDAC) (Mw = 240,000) and poly (2-vinylpyridine) (P2VP) (Mw = 200,000 – 400,000) was obtained from Polysciences, Inc. Sodium chloride salt, methanol, and reagent grade hydrochloric acid, concentrated, was purchased from VWR and used as received. PPO was sulfonated as previously reported to yield highly sulfonated sPPO.[25] Poly (2- vinylpyridinium dihydrogenphosphate) (P2VP-DHP) salt was made as previously published.[29] All polymers, sPPO, PDAC, and P2VP-DHP, were weighed and diluted to the desired concentration using Millipore MilliQ deionized water (18.2 MΩ cm filtered through a 0.22 μm membrane) and the specified acid and/or salt.

LbL Dip Assembly (Dip-LbL). Assembly of the LbL films was completed by using a programmable ZEISS DS50 slide stainer. To construct LbL films, substrates (glass, silicon wafers) were first cleaned and plasma treated in oxygen to impart an initial negative charge to the substrates. The substrates were then immersed in PDAC or P2VP solution for 10 minutes, followed by three one minute rinses in water, and then placed in sPPO solution for 10 minutes, followed by three one minute rinses in water; the process was repeated numerous times to yield the specified number of bilayers. The PDAC, P2VP-DHP, and sPPO solutions were all 10 mM based on the molecular weight of repeat units. The sPPO and PDAC polymer and rinse solutions were adjusted to pH 1 with HCl. Phosphoric acid was added to the P2VP polymer and rinse solutions. The LbL films were rinsed briefly in DI water after assembly to remove excess ions from the films and then placed in various concentrations of phosphoric acid solutions overnight and then dried. The concentration of the phosphoric acid solution in this post-treatment step determined the final film's phosphoric acid doping level.

Bulk Film Characterization. Ionic conductivity was measured in-plane using a custom machined PEEK electrode with two platinum wires spaced 1 cm apart. The electrode was placed above the center of the LbL film and clamped down to ensure good continuous connection between the wires and the film. Humidity was controlled using a chamber from electro-tech Systems, Inc. Impedance values were determined by electrochemical impedance spectroscopy with a Solartron 1260 impedance analyzer, measuring from 1 MHz down to 1 Hz at room temperature. The films were allowed to come to equilibrium at each relative humidity point. The impedance measures the movement of all ions which in the P2VP/sPPO films includes the dihydrogen phosphate ion. However, due to the size of the dihydrogen phosphate being much larger than a proton, the majority of the measured ionic conductivity is contributed by the proton. Literature reports over 95% of the measured conductivity of phosphoric acid is contributed from the proton.[30] The thickness of the films was measured by scoring the films with a razor blade and measuring the step change in the height between the film and the substrate with a Dektak 150 profilometer. LbL films were fabricated on cut silicon wafer, soaked in the specified phosphoric acid solution and allowed to dry overnight. The dried films were then tested by EDS to get a phosphoric acid to amine to sulfur ratio for the specific post-treatment level. Using that ratio, the P2VP to sPPO ratio of the films and the phosphoric acid content of the film by weight were calculated.

5.3 Results and Discussion

5.3.1 Layer-by-Layer Film Growth

The LbL assembly of the polymers P2VP and sPPO is achieved by utilizing the electrostatic charge interaction between the positively charged ammonium onthe phosphoric acid doped P2VP and the negatively charged sulfonic acid of sPPO (Figure 5-1). P2VP/sPPO films were made with varying concentrations of phosphoric acid in the P2VP solution (from 0.05 M to 0.6 M) and P2VP rinse solution (from 0.1 M to 0.4 M) while the sPPO solution was kept at pH 1 and 0.5 M NaCl and the sPPO rinse solution was kept at pH 1 with either no salt or 0.5 M NaCl salt. The films exhibited linear growth, with the growth rate varying from 4 – 6 nm per bilayer (BL) depending on the fabrication conditions. The resultant films were visually transparent.

Top:

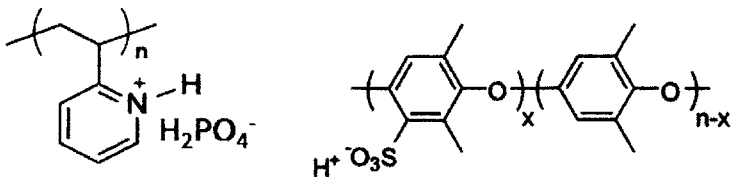

P2VP **sPPO**

Bottom:

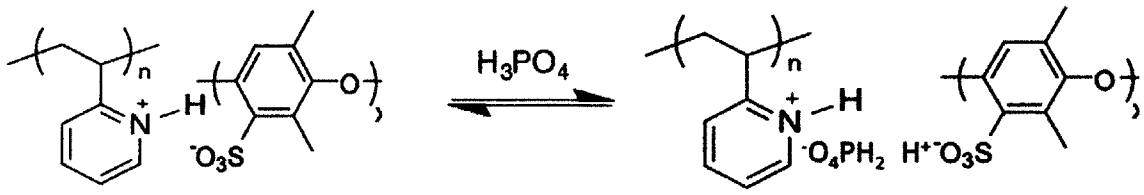

Figure 5-1. Top: chemical structures of poly-2-vinylpyridinium dihydrogenphosphate (phosphate doped P2VP) (P2VP-DHP) and sulfonated poly(2,6-dimethyl 1,4-phenylene oxide)

(sPPO). LbL films are made by opposite charge interactions between the positively ammonium ion from doped P2VP and the negatively charged sulfonate in sPPO. Bottom: schematic showing the two states in which the P2VP/sPPO system could reside. The left side is the de-doped state where the proton is bound and the right is the fully doped state where the proton is free. Depending on the post-treatment conditions, the ratio of the two states changed, with increasing phosphoric acid concentration leading to an increased percentage of doped state.

Although the P2VP-DHP salt is fully ionized as a solid, once dissolved in water, the phosphoric acid is free to dissociate from P2VP, changing the degree of ionization of P2VP in water. The degree of ionization of P2VP can thus be controlled by the concentration of phosphoric acid added to the polymer solution. The additional phosphoric acid can also shield the charged amine group, causing the P2VP to have a smaller radius of hydration in solution, affecting the LbL assembly. The sPPO polymer is a strong acid, so its degree of ionization in water remains constant, but its deposition onto the LbL films may be increased by adding salt in the polymer solution, which shields the charged functional groups and thus causing the sPPO polymer to deposited more "loopily" on the LbL film, typically increasing the number of free sPPO groups in the final film.[26]

5.3.2 Comparing Ionic Conductivity of Lightly Doped Films

The ionic conductivities of the above films were measured at different relative humidities at 25 °C. Despite the different conditions under which the P2VP/sPPO films were made, and the fact that the thicknesses varied over three-fold, the conductivities of the films did not vary much when subjected to the same post-treatment. Instead the conductivities were much more

dependent on the post-treatment. Across the different film fabrication conditions, if the films were soaked in DI water before drying, the films had negligible conductivities under 90% RH. If the films were soaked in phosphoric acid solution before drying, the films had measureable conductivities: with the conductivities increasing many fold with increasing concentration of phosphoric acid in the final soak step (post-treatment step). Thus, instead of further exploring the effect of different fabrication conditions, we chose to look at the effect of the post-treatment step, settling on one fabrication condition to look at – 0.4 M phosphoric acid in P2VP solution, 0.2 M phosphoric acid in the cation rinse solution, 0.1 M HCl and 0.5 M NaCl in sPPO solution, and 0.1 M HCl in anion rinse solution.

Films made under the identical assembly conditions were soaked in different phosphoric acid solutions (DI water, 0.05M, 0.1M, 0.2M, 0.4M, 0.7M, 1.0M) as the post-treatment step, dried, and then their conductivities were measured (Figure 5-2). As previously mentioned, when the P2VP/sPPO film was post-treated in DI water, de-doping all P2VP polymers, there was no noticeable conductivity below 90% RH. This indicates that the free sulfonate groups in these films were too low in number, possibly due to the flexibility of the P2VP backbone, and too far separated for there to be a viable proton pathways through the film relying solely on free sulfonate groups. Instead, the film's conductivity is aided by the presence of phosphoric acid groups scattered throughout the film, as a result of the post-treatment steps. Thus, increasing the phosphoric acid concentrations in the post-treatment step increases the phosphoric acid in the film in the dried state, increasing the film's conductivity.

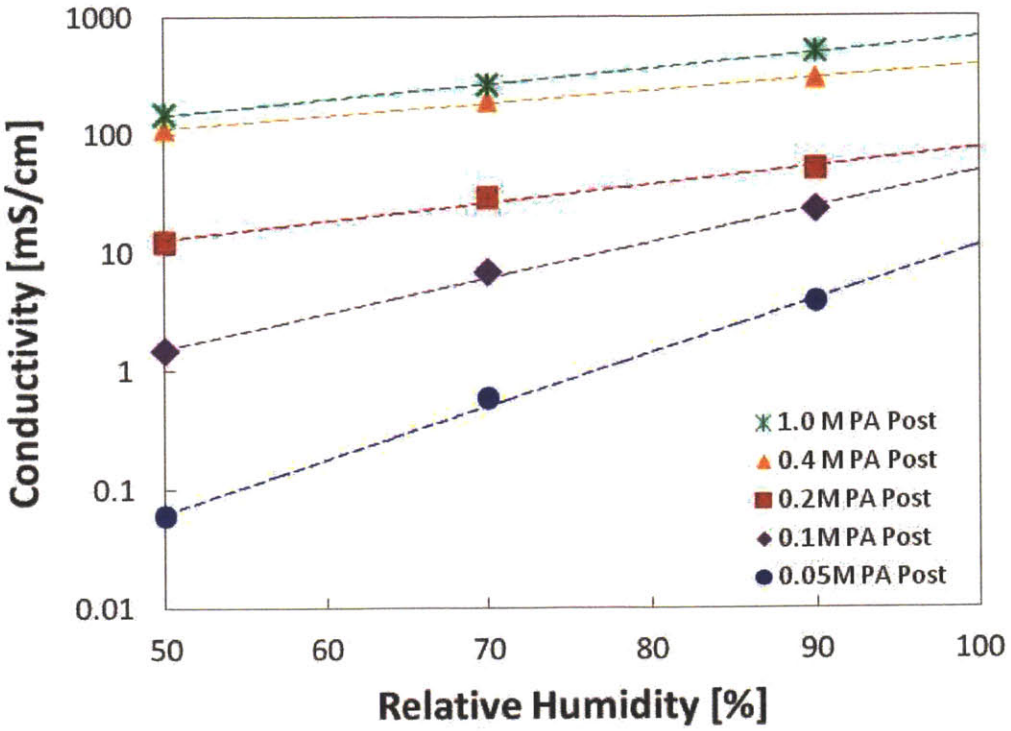

Figure 5-2. The ionic conductivity of P2VP/sPPO films made under the same conditions (0.4 M H_3PO_4 in P2VP solution, 0.2 M H_3PO_4 in the cation rinse solution, 0.1 M HCl and 0.5 M NaCl in sPPO solution, and 0.1 M HCl in anion rinse solution) with different phosphoric acid post treatment across a range of relative humidities. Note the change in RH dependence of the P2VP/sPPO films from 0.05 M to 0.2 M phosphoric acid doping levels.

It is anticipated that the presence of phosphoric acid, if it is properly incorporated throughout the film, would change the relative humidity dependence of the film's conductivity. Specifically we anticipate increased conductivity at lower relative humidities as the phosphoric acid provides alternative hoping sites for the protons to move. What we see is that as the post-

treatment increases, from 0.05M to 0.2M phosphoric acid, for the P2VP/sPPO films, there is an increase in the overall conductivity and a decrease in the conductivity's relative humidity dependence (Figure 5-3a). There is about an order of magnitude difference in conductivity at 90% RH but two orders of magnitude difference in conductivity at 50% RH. The changes can be explained as increasing the overall number of free protons in the film and increasing the mobility of the protons at lower relative humidities due to the presence of phosphoric acid throughout the film.

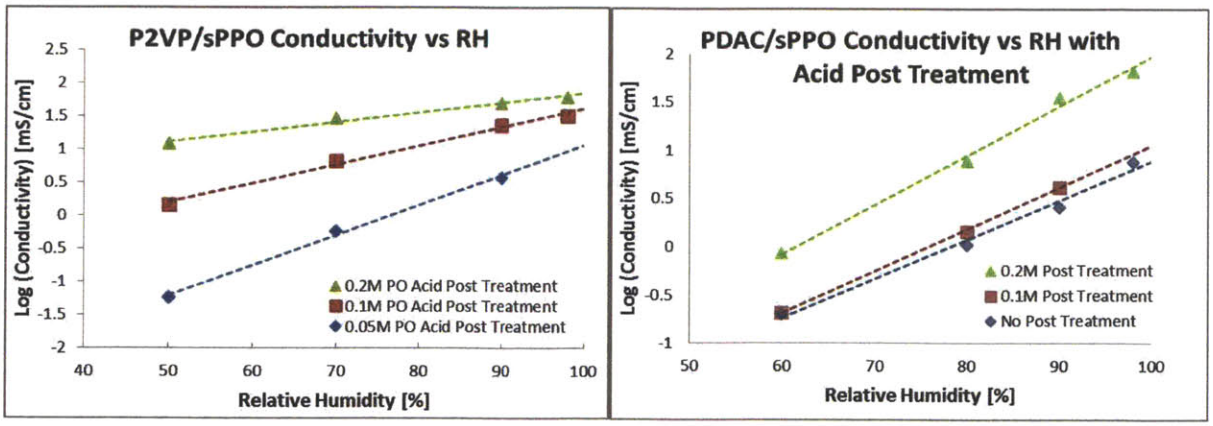

Figure 5-3. The ionic conductivity of P2VP/sPPO films made under the same conditions with different phosphoric acid post treatment at different relative humidities (left). The ionic conductivity of PDAC/sPPO films (right) with the same phosphoric acid post treatment as the P2VP/sPPO films at different relative humidities. Note the change in humidity dependence of the P2VP/sPPO films with respect to the post treatment steps versus the lack of the change in humidity dependence of the PDAC/sPPO films.

To see how this behavior would compare to an LbL film that has the same sulfonic acid functional group but without a basic nitrogen to complex with phosphoric acid, PDAC/sPPO films (made in 0.1M HCl in all solution with 0.5M NaCl in the sPPO solution) were doped at the same phosphoric acid concentrations and their conductivity was measured (figure 5-3b). In contrast to the P2VP/sPPO films, the PDAC/sPPO films exhibited little change in the relative humidity dependence of proton conductivity, only exhibiting an increase in the overall conductivity of the films at higher doping levels. At 0.1 M phosphoric acid post treatment, there was very little difference in the film's conductivity compared with a DI rinsed film, indicating that at this low phosphoric acid concentration, the number of free protons added from the phosphoric acid was small compared to the number of free protons already in the PDAC/sPPO film. With 0.2 M phosphoric acid post treatment, the PDAC/sPPO films saw an average increase of 5 times conductivity across all relative humidities. However, the relative humidity dependence of the films' conductivities remained relatively unchanged with increased phosphoric acid treatment. This indicates that although the phosphoric acid was introduced into the PDAC/sPPO film, the phosphoric acid did not affect the proton transport mechanism of the film. It is also unclear how much phosphoric acid was actually incorporated into the PDAC/sPPO film. We hypothesize that the basic amine group of P2VP helps distribute the phosphoric acid evenly throughout the film and particularly next to sPPO groups to which it is electrostatically bound. Therefore, to gain the full benefits of the phosphoric acid, the membrane needs to have an amine group present capable of being doped by the phosphoric acid.

5.3.3 Comparing LbL Films with Pristine Polymer Films

To isolate the effect of the change in proton conduction mechanism from the effect of increased phosphoric acid content, we compared phosphoric acid doped LbL films with spin cast P2VP film containing a similar amount of excess phosphoric acid (figure 5-4). The phosphoric acid content of the films under different post-treatment concentrations was estimated by EDS and the excess phosphoric acid of the film by weight was calculated. Films with various ratios of phosphoric acid to P2VP (from 1:1 to 2.5:1) were spun cast and their conductivities were tested. Note that because the LbL films were approximately only half composed of P2VP, at the same excess phosphoric acid %, the LbL films would have significantly lower total phosphoric acid content. In comparing similar excess phosphoric acid contents, the P2VP/sPPO films were consistently more conductive than the equivalently doped P2VP film. In addition, the difference was greater at lower relative humidities, as the P2VP/sPPO films' conductivity were half to one order of magnitude greater than the equivalent P2VP films' conductivity. This shows that the presence of sulfonic acid groups next to phosphoric acid groups significantly increases the conductivity despite having a reduced phosphoric acid content overall.

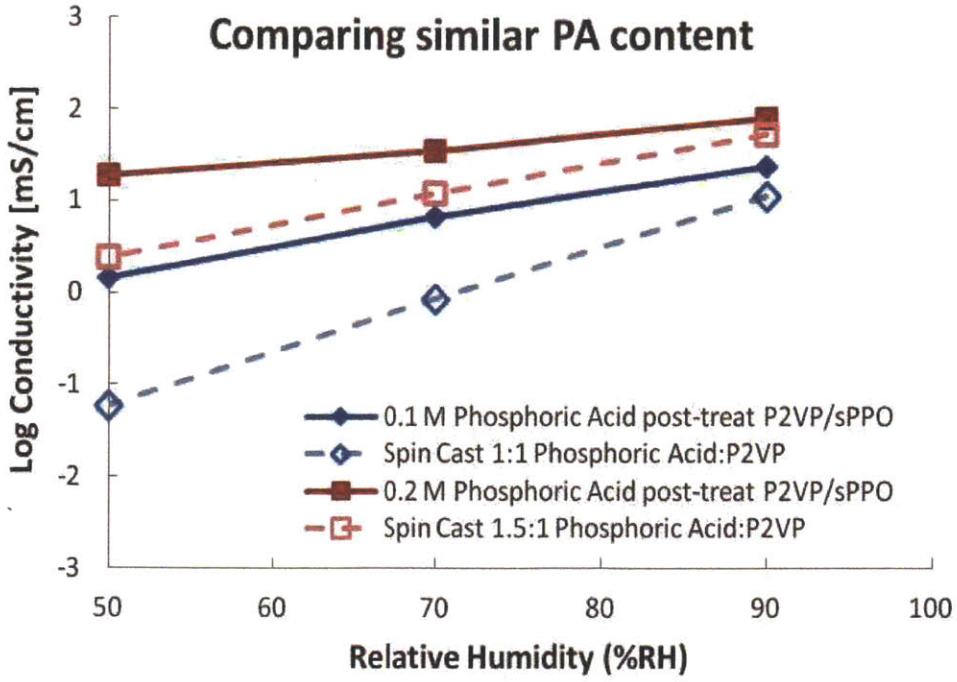

Figure 5-4. The ionic conductivity of P2VP/sPPO films made under the same conditions with different phosphoric acid post treatment compared with spin cast films of P2VP-DHP films doped to a similar phosphoric acid content (as measured by EDS) at different relative humidities. The 0.1 M H_3PO_4 doped LbL film and the spin cast 1:1 H_3PO_4 to P2VP film had approximately no excess phosphoric acid. The 0.2 M H_3PO_4 doped LbL film and the spin cast 1.5:1 H_3PO_4 to P2VP film had approximately 20% by weight phosphoric acid excess.

At higher doping levels (phosphoric acid $\geq$ 0.4 M), the overall conductivity of the P2VP/sPPO films increases further, over one order of magnitude above the conductivity of the 0.2M phosphoric acid doped films. These doping conditions result in some of the highest conductivity values for PEMs at 50% RH and 25 °C ever reported (110 ± 8 mS/cm with 0.4M

post-treatment and 148 ± 12 mS/cm with 1.0 M post-treatment) and are over one order of magnitude more conductive than Nafion (N112) at 50% RH and 25 °C (10.2 ± 0.5 mS/cm). The LbL films are also much more conductive than similarly doped P2VP films (figure 5-5). We hypothesize that the large increase of overall conductivity from 0.2M to 0.4M post-treatment is a result of a shift in the equilibrium shown in figure 5-1 due to increased dopant, whereby the electrostatic cross-link between the ammonium and the sulfonate was interrupted by the phosphoric acid and as a result a large majority of sulfonic acid groups became free to participate in the modified Grotthuss mechanism. Below 0.2 M post-treatment, the phosphoric acid was interspersed throughout the film but there were still nitrogen groups waiting to be doped; hence changing phosphoric acid concentrations had a large effect on the overall conductivity. Above 0.4 M post-treatment, most of the P2VP groups are now doped and hence further increase in phosphoric acid post-treatment only had an incremental increase in conductivity.

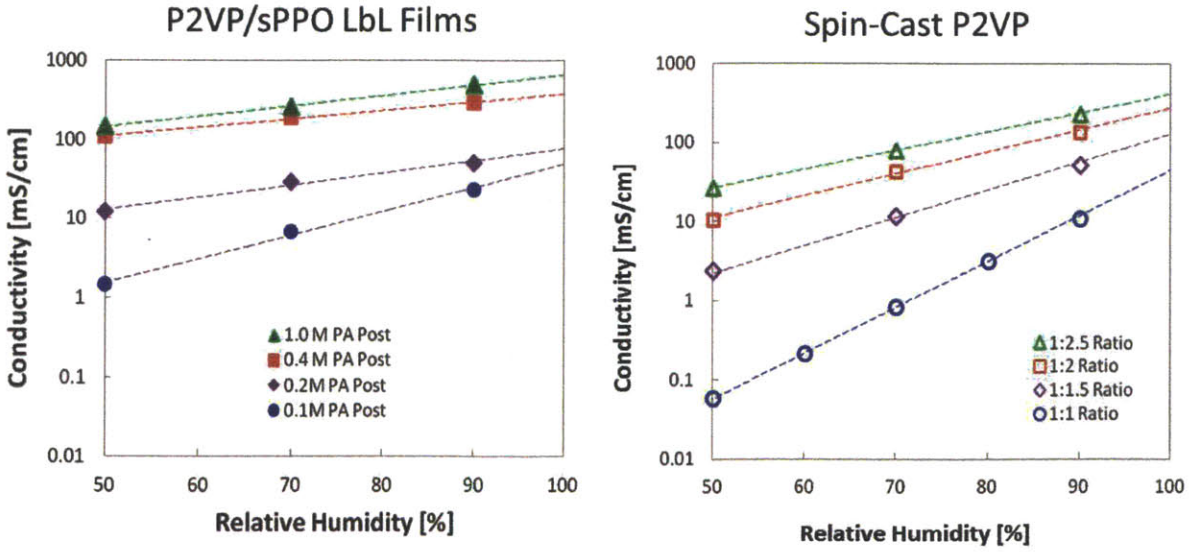

Figure 5-5. The relative humidity dependence of ionic conductivity of P2VP/sPPO films with different phosphoric acid post treatment (left) compared with spin cast films of P2VP-DHP films doped to similar phosphoric acid contents (right).

At these higher (≥0.2 M) doping conditions it was observed that the conductivity of the LbL films would decrease over time if the film was humidified above 90% RH, which is a known problem for phosphoric acid doped polymers and a similar phenomenon was also observed for the phosphoric acid doped P2VP films.[10] After such a process one would notice phosphoric acid crystals form on the top of the films, indicating a rearrangement of the phosphoric acid under these conditions and that the water condensate (with no ions present) on the surface of the films has the effect of drawing out the more concentrated phosphoric acid from the bulk of the film. Hence in order to maintain the high conductivities of these films, the films cannot be hydrated, unlike sulfonic acid based PEMs, since increased humidity increases the mobility of the phosphoric acid. For the equivalently doped P2VP films, the acid rearrangement phenomenon is significantly worse and the conductivity decreases significantly more indicating that the P2VP/sPPO system helps stabilize the excess phosphoric acid better than just P2VP by itself. Thus, utilizing a controlled sulfonic acid, phosphoric acid polymer blend not only increases conductivity over the phosphoric acid doped polymer alone but also helps stabilize the phosphoric acid, keeping it in the film longer.

5.4 Conclusion

LbL films consisting of P2VP/sPPO were fabricated and their film properties measured and compared to variously doped P2VP and a sulfonic acid only based LbL system. The P2VP/sPPO films were most affected by the final rinse step. DI water soaked P2VP/sPPO films are not conductive. Increasing phosphoric acid concentration in the final rinse step (from 0.05M to 0.2M) increases the overall film conductivity and decreases the RH dependence of the conductivity significantly. This was in contrast to phosphoric acid doped PDAC/sPPO films which only showed increases in overall conductivity but showed no change in RH dependance. P2VP/sPPO's conductivity was greater than P2VP's under the same wt% of excess phosphoric acid, further confirming the existence of an alternative proton conducting pathway that utilizes both phosphoric and sulfonic acid groups and that is favored – particularly at low relative humidities – compared to the pathways utilizing just one of the acid groups. At higher phosphoric acid doping conditions P2VP/sPPO films exhibited extremely high conductivities at 50% RH and 25 °C (110 mS/cm with 0.4M post-treatment and 148 mS/cm with 1.0 M post-treatment), much higher than either P2VP or sPPO alone. Electrolyte rearrangement was noticed in the highly doped LbL films, but this rearrangement was much less severe than in the pristine P2VP, indicating that the LbL technique resulted in a more stable doped film. Membranes using this modified conduction mechanism are very promising for use in fuel cells designed to operate at lower relative humidities. Further studies to look at additional ways to leverage this mechanism into other existing proton exchange membrane systems is warranted. In addition some computational or theoretical study into this very promising phenomenon would help firm up this fledgling field of conducting mixed acids.

5.5 References

[1] De Brujin, F. *Green Chemistry* **2005**, *7*, 132.

[2] Chalk, S.G., Miller, J.F., *J. Power Sources*, **2006**, *159*, 73-80.

[3] Khaligh, A., Li, Z., *Vehicular Technology, IEEE Transactions on*, **2010**, *59*, 2806-2814.

[4] Winter, M., Brodd, R. J.,*Chemical reviews*, **2004**, *104*, 4245-4270.

[5] Zhang, J., Xie, Z., Zhang, J., Tang, Y., Song, C., Navessin, T., Shi, Z., Song, D., Wang, H., Wilkinson, D.P., Liu, Z.S., Holdcroft, S., *J. Power Sources*, **2006**, *160*, 872-891.

[6] Peckham, T.J., Holdcroft, S., *Advanced Materials*, **2010**, *42*, 4667-4690.

[7] Alberti, G., Casciola, M., Massinelli, L., Bauer, B., *J. Mem. Sci.*, **2001**, *185*, 73-81.

[8] Casciola, M., Alberti, G., Sganappa, M., Narducci, R., *J. Power Sources*, **2006**, *162*, 141-145.

[9] He, R., Li, Q., Xiao, G., Bjerrum, N.J., *J. Mem. Sci.*, **2003**, *226*, 169-184.

[10] Mamlouk, M., Scott, K., *Int. Hydrogen Energy*, **2010**, *35*, 784-793.

[11] Mauritz, K. A.; Moore, R. B. *Chem. Rev.* **2004**, *104*, 4535-4585.

[12] Paddison, S.J., *Annu. Rev. Mater. Res.*, **2003**, *33*, 289-319.

[13] Peighambardoust, S.J., Rowshanzamir, S., Amjadi, M., *Int. Hydrogen Energy*, **2010**, *35*, 9349-9384.

[14] Dupuis, A.C., *Prog. Mater. Sci.*, **2011**, *56*, 289-327.

[15] Li, Q., He, R., Jensen, J.O., Bjerrum, N.J., *Chem. Mater.*, **2003**, *15*, 4896-4915.

[16] Bose, S., Kuila, T., Nguyen, T.X.H., Kim, N.H., Lau, K.T., Lee, J.H., *Prog. Polym. Sci.*, **2011**, *36*, 813-843.

[17] Pu, H., Meyer, W.H., Wegner, G., *J. Poly. Sci. B*, **2002**, *40*, 663-669.

[18] Suzuki, K., Iizuka, Y., Tanaka, M., Kawakami, H., *J. Mater. Chem.*, **2012**, *22*, 23767-23772.

[19] Iizuka, Y., Tanaka, M., Kawakami, H., *Polym. Int.*, **2013**, *62*, 703-708.

[20] Decher, G., *Science*, **1997**, *277*, 1232-1237.

[21] Hammond, P.T., *Adv. Mater.*, **2004**, *16*, 1271-1293.

[22] Hammond, P.T., *J. AIChE*, **2011**, *57*, 2928-2940.

[23] Lutkenhaus, J.L., Hammond, P.T., *Soft Matter*, **2007**, *3*, 804-816.

[24] Taylor, A.D., Michel, M., Sekol, R.C., Kizuka, J.M., Kotov, N.A., Thompson, L.T., *Adv. Funct. Mater.*, **2008**, *19*, 3003-3009.

[25] Argun, A.A., Ashcraft, J.N., Hammond, P.T., *Adv. Mater.* **2008**, *20*, 1539.

[26] Ashcraft, J.N., Argun, A.A., Hammond, P.T., *J. Mater. Chem.*, **2010**, *20*, 6250-6257

[27] Liu, D.S., Ashcraft, J.N., Mannarino, M.M., Silberstein, M.N., Argun, A.A., Rutledge, G.C., Boyce, M.C., Hammond, P.T., *Adv. Funct. Mater.*, **2013,** *23,* 3087-3095.

[28] Mannarino, M.M., Liu, D.S., Hammond, P.T., Rutledge, G.C., *ACS Appl. Mat. Interfaces*, **2013**, *5*, 8155-8164.

[29] Yang, B., Manohar, A., Prakash, G.K.S., Chen, W., Narayana, S.R., *J. Phys. Chem.*, **2011**, *115*, 14462-14468.

[30] Vilciauskas, L., Tuckerman, M.E, Bester, G., Paddison, S.J., Kreuer, K.D., *Nat. Chem.*, **2012**, *4*, 461-466.

6. Conclusions and Future Work

6.1 Research Conclusions

In this thesis work, the mechanical and transport properties of LbL films and composite membranes were substantially improved while structure-property relationships both in the micro and macro scale were studied through the use of a novel spray-LbL technique, charge shielding, and an alternate transport mechanism. Two main areas were targeted for improvement: the mechanical properties of the composite mats to make a viable fuel cell membrane from an LbL film and the conductive properties of the LbL films themselves for broader applications, such as hydrogen fuel cells. In addition to improving PEM properties, new stability factors were proposed, an alternative proton transport mechanism was examined, real fuel cell devices for testing were assembled, a more complete characterization of LbL films was carried out, and new approaches to reduce methanol breakthrough in composite membranes and to selectively incorporate more of a charged polymer in an LbL film were proposed and examined.

6.1.1 Composite Layer-by-Layer Electrospun Proton Exchange Membrane

The first objective of this thesis was to mechanically strengthen the LbL films through the use of a supporting substrate and to make a functioning DMFC with the composite membrane. This was accomplished in chapters two and three through the use of electrospun mats with the LbL films assembled onto the mats through both the dip- and spray-LbL methods. In chapter two, three different LbL assembly methods were examined for their ability to coat an electrospun mat: dip-LbL, spray-LbL with vacuum assist, and spray-LbL without vacuum assist. Each assembly method resulted in a different film morphology; the spray-LbL with vacuum

assist method resulted in conformal coating of the individual fibers throughout the bulk of the mat, and the spray-LbL without vacuum method resulted in a continuous fuel-blocking layer on the surface of the electrospun mats with similar properties as the free-standing LbL film by itself. The mechanical properties of the spray-coated electrospun mats were shown to be superior to the LbL-only system, particularly at hydrated conditions.

In chapter three, the properties of the composite membranes were further improved and optimized through the heat-treatment of the electrospun mats before coating, and the tuning of the spray-LbL with vacuum assist parameters. The result was a composite membrane whose proton conductivity, methanol permeability, and mechanical strength could be largely controlled independently of each other – the proton conductivity of the membrane controlled by the LbL system and spray conditions, the methanol permeability of the membrane controlled by the number of layers spray coated on the surface of the membrane, and the mechanical strength controlled by the heat-treatment of the underlying electrospun mat. An optimized composite membrane with methanol permeability twenty times lower than Nafion and through-plane proton selectivity five times greater than Nafion was fabricated. A methanol fuel cell was created with this composite membrane, with similar OCVs and comparable membrane resistances to Nafion, demonstrating the membrane's viability. In addition, the composite membranes saw a fourfold reduction in linear swelling due to the electrostatic interactions of the LbL film and the underlying electrospun mats, resulting in improved stability factors which indicate the ability of the membranes to withstand hydration cycling. A new stability factor, hydration yield factor, was introduced to better evaluate the irreversible deformation a membrane experiences with each swelling cycle.

6.1.2 Use of Multivalent Cation Salts in Layer-by-Layer Proton Exchange Membranes

The second objective was to increase the proton conductivity of the PDAC/sPPO system through increasing the number of free protons in the LbL film and to explore the effect multivalent cation salts have when introduced in the polyanion solution during the LbL assembly process. This was accomplished in chapter four through the use of a couple representative divalent salts and a trivalent salt with the same anion ($CaCl_2$, $MgCl_2$, and $CeCl_3$) in place of NaCl in the sPPO solution during the LbL assembly process. Multivalent salts have been shown in literature to form ion-bridging across multiple charge groups both inter and intramolecularly in solution resulting in different polymer solution properties than polymer solutions with just monovalent salts. However, the effect of multivalent salts in LbL assembly as a function of concentration had never been studied. Through varying the concentration of the multivalent salts in the LbL assembly, it was observed that the protonic conductivity of the resulting films, compared with the film made with NaCl, decreased significantly at low salt concentrations and increased significantly at higher salt concentrations (from 15 mS/cm with 1 M NaCl to 62 mS/cm and 74 mS/cm at humified conditions for 1.0 M $MgCl_2$ and $CaCl_2$ in pH 1 respectively). The molecular composition of the films was measured for the first time using XPS with depth profiling and the sulfur to nitrogen ratio of the films made with divalent salts was observed to increase with increasing salt concentration, indicating an increase in sPPO incorporation relative to PDAC. In addition, the divalent salts were shown to be able to decrease the film's energy of activation for proton transport, indicating that the divalent salts weren't just able to incorporate more of the desired polymer, hence more free protons, but that under the right conditions, the salts were able to make the desired free polymer groups better connected. The combined result was an LbL film made from the same two polymers but over five times more conductive.

6.1.3 Effect of Incorporating Phosphoric Acid into Layer-by-Layer Assembled Sulfonic Acid Based Proton Exchange Membranes

The third objective was to increase the proton conductivity of an LbL system at low relative humidity (50% RH) through the incorporation of an additional proton conducting group, phosphoric acid doped pyridine, and to explore and utilize a proton conducting mechanism that is less susceptible to relative humidity than sulfonic acid based PEM's proton conducting mechanism. This was accomplished in chapter five by replacing the polycation in the previous LbL system (PDAC) with a polymer (P2VP) that can be doped by an electrolyte that can function like water at low relative humidities – phosphoric acid. The films made with P2VP were subjected to different concentrations of phosphoric acid before drying – thereby doping the P2VP/sPPO films. The resulting P2VP/sPPO films exhibited greater conductivity than similarly doped P2VP films and under stronger doping conditions (0.4 M phosphoric acid versus 0.1 M) whereby a large percentage of the P2VP group became doped and the associated sulfonate groups became free, the film's conductivity further increased seventy-fivefold (110 mS/cm at 50% RH at room temperature), resulting in a conductivity an order of magnitude greater than Nafion® and the proposed target for this objective (10 mS/cm) and the highest reported conductivity in literature. The conductivity of higher doped (>0.2 M) P2VP/sPPO films also exhibited much lower RH dependence than other sulfonic acid based PEMs (loss of conductivity only half an order of magnitude when RH is reduced by 40% compared with over two orders of magnitude for hydrocarbon based PEMs and over one order of magnitude for fluorocarbon based PEMs), indicating an alternative proton conducting mechanism that utilizes both sulfonic and phosphoric acid in proton conduction and is less dependent on the presence of water.

6.2 Unanswered Questions / Recommendations for Future Work

6.2.1 Composite Layer-by-Layer Electrospun Proton Exchange Membrane

A platform technology was shown with composite membranes of highly conductive LbL films and electrospun fiber mats that were fabricated, characterized for mechanical strength and selectivity, and tested in an operational direct methanol fuel cell. As a platform technology, other LbL systems could be incorporated and a composite mat made with that system could be produced. Specifically, the two systems studied in chapters four and five could be incorporated into a composite mat with the improved properties of those systems (higher conductivity overall and at lower RH conditions) potentially improving the composite membranes. One unknown is whether those other systems could be adapted to a spray LbL assembly method (adsorption time changing from minutes to seconds) and how might the presence of fibers affect either the adsorption of the LbL system (with divalent salts) or the adsorption of the phosphoric acid (with the pore spaces possibly acting as electrolyte sinks).

Overall, the biggest hinderance to using an LbL membrane in a fuel cell is the contact resistance between the catalyst layers, with its Nafion based binders, and the LbL composite membranes as evidenced by the high cell resistance (>3 $\Omega \cdot cm^2$) compared to the membrane resistance (0.4 $\Omega \cdot cm^2$). Because the LbL films do not flow or melt with temperature, it is particularly difficult to adhere them well to another surface. One possible solution to this issue is to remove the use of the binder all together and just spray a thin layer of catalyst directly onto the membrane – possible for hydrogen fuel cells which do not require as much catalyst. For a direct methanol fuel cell, the most promising solution would be to form an all-LbL membrane electrode

system whereby the catalyst layers are deposited onto the PEM through an LbL method. There was work started in the Hammond Lab that deposited Pt/Ru nanoparticles on polyaniline fibers which can then be LbL assembled with carbon nanotubes on a porous substrate to form an LbL catalyst network.

6.2.2 Use of Multivalent Cation Salts in Layer-by-Layer Proton Exchange Membranes

The use of divalent salts allowed for the assembly of a PDAC/sPPO system that was composed of a greater percentage of sPPO and was more conductive than the previously studied PDAC/sPPO system used in the composite membrane work. It is not known if (and by how much) the use of divalent salts would affect the fuel blocking capabilities of the PDAC/sPPO system. In addition, the films studied in chapter four were made by the dip-LbL method and it is unknown whether the observed effects of utilizing divalent salts would be the same under the spray-LbL method, whereby the adsorption time changes from minutes to seconds. Before this system could be tested in a fuel cell, the fuel crossover and the spray-LbL parameters would have to be optimized.

Further research can also be done to explore the effect the use of multivalent salts has in LbL assembly both for the PDAC/sPPO system in particular and for a general LbL system. For the PDAC/sPPO system, it is not clear why there is a critical concentration of salt below which the sPPO polymer is being negatively selected against – i.e. a lower percentage of sPPO polymer is incorporated with multivalent salt than without. Even a small addition of salt should increase shielding and result in more of the polymer being incorporated, not less. Is this a universal effect of utilizing divalent salts in LbL assembly thus reflecting some effect of ion-bridging that is not

yet known or just a particular quirk of the PDAC/sPPO system? To further study the effect of multivalent salts in LbL systems in general, one would need to use a polymer that wouldn't precipitate upon the addition of the multivalent salts – one that would have a strongly charged group but would be extremely water soluble. In this way, more salts could be studied and the effect of divalent versus trivalent salts could be examined.

6.2.3 Effect of Incorporating Phosphoric Acid into Layer-by-Layer Assembled Sulfonic Acid Based Proton Exchange Membranes

The use of phosphoric acid as a dopant for a basic amine / sulfonic acid LbL system was shown to result in multiple orders of magnitude improvements in conductivity at low relative humidities and was a confirmation of a proposed modified proton conducting mechanism that utilized phosphoric acid in place of water in the grotthuss mechanism. One issue with this system was that film grew very thinly (~ 4nm/BL), and thus the films tested were also relatively thin (~ 200 – 300 nm). For conductivity, this was fine as the films were very conductive, but for use in a fuel cell, this growth rate would make making a viable membrane cost and time prohibitive. Finding the parameters to allow for a larger LbL growth per bilayer while maintaining similar conductivity values would be necessary. This could be done through the use of salt in the sPPO rinse baths as well as the sPPO solution bath. To do a preliminary test of this system in a fuel cell, one could LbL-assemble Nafion with this system in the same way PDAC/sPPO was assembled with Nafion in the early works of PDAC/sPPO. This would serve two purposes: one, Nafion would provide vital mechanical support for the P2VP/sPPO system (as long as the test is carried out at less than 100 °C), and two, it could be observed whether the coating of Nafion is enough to dope Nafion and improve its conductivity at low RH. In addition,

other amine based polymers could be tested (like linear poly(ethylene imine) (LPEI), poly(allylamine hydrochloride) (PAH), and poly(4-vinylpyridine) (P4VP)) to discern what effect the different backbones and side chains would have on the conductivity of the system.

The proposed modified grotthuss mechanism is very promising because it is widely applicable and has the potential to improve the conductivity of commercially available sulfonic acid PEMs which have long had issues with maintaining conductivity at low RH conditions. However, the mechanism isn't very well understood as there has been no modeling of this mechanism. For example, how much of an effect does this mechanism have and how important is the blending of the polymers and the proximity of the acids? It was observed that just adding phosphoric acid into a sulfonic acid based LbL film (PDAC/sPPO) did not have the same effect as utilizing a basic amine group in the LbL film. In addition, the LbL systems were more easily doped (treated to much more dilute phosphoric acid concentrations prior to drying) than the previously reported blend of sulfonated polyimide and polybenzimidazole. Finally, the biggest challenge utilizing this modified mechanism in a fuel cell is the fact that the phosphoric acid is not permanently bonded to the membrane and can, in the presence of water, diffuse out of the membrane, thus reducing the membrane's conductivity over time. Work looking at ways to better stabilize the phosphoric acid in the membrane – either with a crosslinking post-treatment or with excess "dry" air flow – would be invaluable in allowing this promising technology to be implemented commercially.